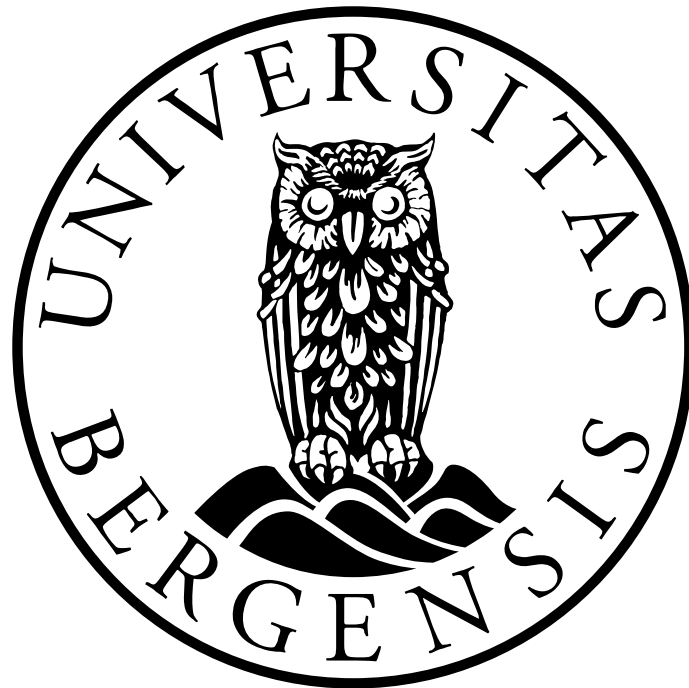# Foam Generation and Flow in Fractures with Different Aperture

Master Thesis in Petroleum Technology - Reservoir Physics

By

Andreas Grøteide Polden

Department of Physics and Technology

University of Bergen

June 2017

Summary

This experimental thesis investigate foam generation and flow properties in real, rough-walled fractures, through impermeable marble core plugs. A range of fracture apertures was investigated, denoted open, partially open or tight, and represents a variation is system permeability. The foam evaluation was performed by co-injection of N_2 gas and surfactant solution and measuring the differential pressure at different boundary conditions.

A comprehensive experimental investigation of foam generation and behavior in fractures was conducted with a total of 42 co-injections for a range of conditions. Differential pressure and visual observations of produced fluids, combined with calculation of mobility reduction factor (MRF) and apparent viscosity, confirmed that foam generated and reduced gas mobility in rough-walled fractures. In fracture systems with smooth surfaces, without foam generation sites, foam generation was not observed for the same conditions and system dimensions.

Local changes in sweep efficiency were visualized *in-situ* during co-injections with positron emission tomography (PET) combined with computed tomography (CT). An aqueous tracer was added to the co-injections to determine local aqueous phase saturations. Direct comparison between co-injections with or without a foaming agents demonstrated a significant sweep efficiency increase with foam, combined with a local reduction in liquid saturation.

A critical superficial velocity for foam generation was determined in the fracture system, below which foam was not observed. Foam behavior in partially open fractures was similar to foam in porous media, with a notable exception: high-quality foam behaved similarly in fractures as in porous media, but low-quality foam, however, deviated from porous media observations. Low-quality foam was dependent on both liquid and gas velocities in fractures, compared with porous media, where low-quality foam only depends on gas velocities.

A significant hysteresis effect is observed in experiments with varying gas fraction. Different pressure trends are seen when comparing results performed from gas fraction 1 to 0 with experiments conducted from gas fraction 0 to 1.

Acknowledgement

Andreas G. Palden

Table of Content

Part I – Introduction and Background

1. Introduction

The world energy demand has steadily increased over the last century, and is expected to continue increasing in the years to come. Renewable resources are being developed to contribute to energy production; however, fossil fuels are still predicted to be the main energy source in the next decades. Because new field discoveries and developments are declining, enhanced oil recovery (EOR) is necessary to maintain the level of energy supplied from oil and gas. Several predictions of peak-oil have has been made, perhaps the most famous by Hubbert (1956), who predicted maximum oil production rate in year 2000. Oil production has, however, continued to increase after 2000, due to innovation, new technology and new solutions.

60% of all known oil reserves are contained in carbonate reservoirs, which often exhibit significant reservoir heterogeneities, therein fractures (Roehl and Choquette, 1985). Fractures combined with oil-wet or mixed-wet reservoir characteristics, often present in carbonate rocks, may cause primary and secondary recovery methods to recover less oil than expected. During water or gas floods, the injected phase will often prefer to flow through the fractures rather than entering into the matrix to displace oil, resulting in poor macroscopic and microscopic sweep, and early breakthrough of the injected phase in production wells. Foam injection represents a possibility to reduce mobility and remedy fracture flow during gas floods. Foam increases the apparent gas viscosity to improve sweep efficiency and oil recovery, and has recently been suggested to provide mobility control in fractures and systems featuring large permeability contrasts (Kovscek et al., 1995, Haugen et al., 2012, Seethepalli et al., 2004), with a factor of up to 600 (Buchgraber et al., 2012). Foam flow is often studied in micromodels or other artificial models of fractured or porous media, and less investigated in conjunction with real rock fractures.

In this thesis, experimental work was performed to investigate foam flow in fracture networks of varying aperture. Marble core material was used, and provided a calcite surface similar to carbonate reservoirs. A special fracturing technique was adapted to create controlled fractures through the core material, with a surface roughness comparable to real reservoirs. The results were compared to foam flow in smooth fractures, to investigate the effect of fracture roughness on foam generation. Surfactant solution and gas were co-injected into seven different fracture networks, constituting open, partially open and tight fractures. Foam flow was monitored by differential pressure and visual observations of the produced effluents in most experiments. In one fracture network, PET-CT imaging was utilized to monitor foam flow *in-situ*.

2. Fractured reservoirs

The definition of a fractured reservoir is: "a reservoir in which naturally occurring fractures may have a significant effect on reservoir fluid flow either in the form of increased reservoir permeability and/or reserves or increased permeability anisotropy (Nelson, 2001)".

Fractures present in a hydrocarbon reservoir may significantly impact fluid flow, and cause an early water breakthrough. Resulting in rapid decline curves and difficulties to predict the outcome of secondary recovery (Ahr, 2011). These challenges can result in wrong economical estimates on both expenses and income.

Fractured reservoirs can be divided into four different types (Nelson, 2001)

Type 1: Fractures provide essential porosity and permeability

Type 2: Fractures provide the essential reservoir permeability

Type 3: Fractures exist in an already recoverable reservoir

Type 4: Fractures exist, but instead of creating additional porosity or permeability, they function as significant reservoir barriers

The aim of this thesis is improvement of oil recovery in (type 2 and) type 3 reservoirs, by the use of foams. The experiments in this thesis, however, are performed using a type 1 system: fractured marble rock, where the marble does not provide any porosity or permeability, to thoroughly study foam flow in fractures.

Reservoirs with low permeability, which often is the case for carbonates, can practically be unrecoverable without fractures (van Golf-Racht, 1982), which will work as flow paths from the matrix to the producing wells.

3. Recovery Methods

Uren (1946) defined an oil reservoir as: "a body of porous and permeable rock containing hydrocarbons which may move towards recovery openings under the pressure that exist or that can be applied". After formation in the source rock, hydrocarbons (oil and/or gas) migrate upwards until they either reach the surface or settle in a trap. There are several forces which will make the oil migrate upwards, including gas pressure, gravity (buoyancy) and compaction of sediments. Considering more recent recovery methods such as water and/or gas flooding, chemical flooding and fracturing one may say that Uren's definition is outdated. Several new recovery techniques have made reservoirs that would not fulfill Uren's definition producible, such as shale gas and heavy oil reservoirs (Holditch, 2003).

3.1. Primary Recovery

In most oil and gas reservoirs the initial pressure is sufficient to produce some of the hydrocarbon reserves. Depleting the reservoir pressure over time to produce the hydrocarbons is a form of primary recovery. Artificial lift, such as pumps or gas lift, can be used to continue production when the reservoir pressure is insufficient to produce hydrocarbons. As long as there is sufficient pressure to force hydrocarbons into the wellbore it is possible to recover hydrocarbons by pressure depletion (Speight, 2009). There could be several disadvantages by producing a reservoir by pressure depletion, depending on the reservoir. The worst conditions for primary recovery are in live oil reservoirs with dissolved gas. As the pressure is depleted, gas will come out of solutions making the remaining oil heavier and reducing the relative permeability by the introduction of a third phase, gas. The recovery by solution gas drive is usually below 25% (Lyons and Plisga, 2006). If a large gas cap is present above the oil, primary recovery could be the best method of recovery. The gas cap expansion will maintain the pressure when recovering the oil, and the total recovery can be high.

3.2. Secondary Recovery

Secondary recovery is necessary to continue production when the pressure in a primary recovery becomes too low, or the pressure depletion method results in low recovery. Secondary recovery can be defined as introduction of energy to a reservoir to produce more oil (Speight, 2009), e.g. injecting gas or water. Injecting water and/or gas can result in pressure support, gas/water drive, or both, depending on the injection method. Maintaining the reservoir pressure gives the reservoir energy to force hydrocarbons to the surface and inhibit free gas. The second

effect is to force the oil from the injection well to the producing well, called sweep (Donaldson et al., 1989).

The mobility ratio, M, heavily influence the effect of injections in a reservoir. The mobility ratio is the ratio between the mobility of the injected fluid behind the front, λ_j, and the mobility of the reservoir fluid ahead of the front, λ_k, defined as:

$$M = \frac{\lambda_j}{\lambda_k} = \frac{k_{rj}/\mu_j}{k_{rk}/\mu_k} = \frac{k_{rj}\mu_k}{k_{rk}\mu_j} \tag{1}$$

where k_r is the end-point relative permeability, μ is the viscosity and the denotation j and k are the injected and displaced fluid respectively (Zolotukhin and Ursin, 2000).

Unfavorable mobility ratios will result in an unstable displacement where channels of the injecting fluid may form, known as viscous fingering, see **Figure 3-1** (Chen and Wilkinson, 1985). Viscous fingering result in early breakthrough and poor areal sweep of the reservoir. Due to the low viscosity of gas, viscous fingering represents a challenge during gas injections, but also for water injections in medium to heavy oils.
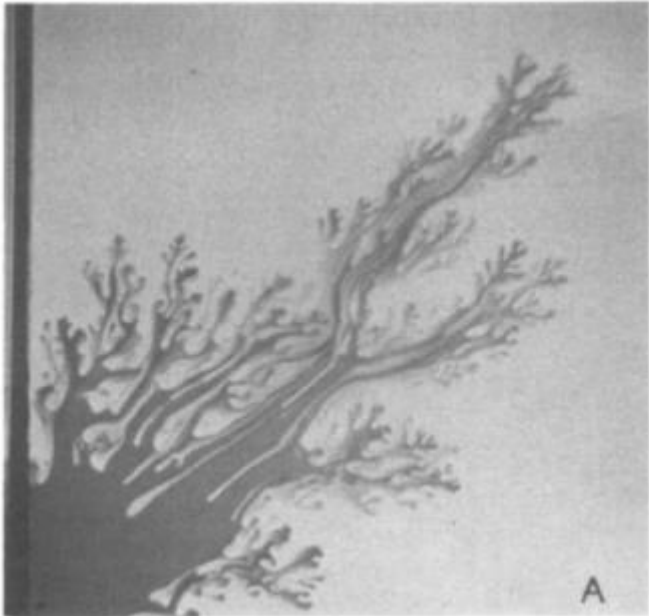
Figure 3-1: Example of viscous fingering during water displacement of glycerin in a five-spot pattern. The injector is placed in the lower left corner and the producer is in the upper right corner (Homsy, 1987).

Due to the high conductivity of fractures, secondary recovery can be challenging in fractured reservoirs. The injected fluid will easily flow through the fractures too the producer. This result is poor sweep and low recovery rates. For gas injections this is an especially large challenge due to the low viscosity of the gas. This thesis focuses on reducing the mobility of gasses in fractures by generating foam in fractures; this could potentially increase the effect of gas injections is fractured reservoirs significantly.

3.3.   Tertiary Recovery

Tertiary or enhanced oil recovery (EOR) is oil recovery by injection of fluids or chemicals not normally present in the reservoir (Lake, 2010). The ultimate goal of EOR processes is to increase the overall displacement efficiency, which is divided into microscopic displacement and macroscopic displacement (Romero-Zerón, 2012). The macroscopic displacement is the area of the reservoir contacted by the EOR method, and the microscopic displacement dictates how much residual oil there is in an area flooded by the EOR method. EOR methods can generally be divided into four different groups: thermal, solvent, chemical and other, shown in **Figure 3-2**.
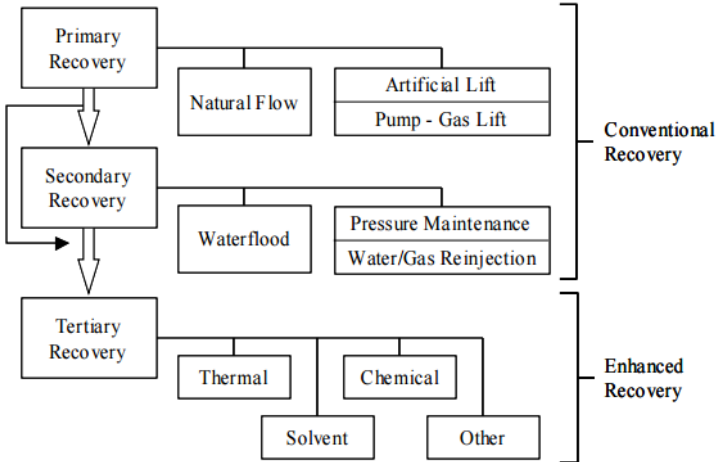
Figure 3-2: An overview of different recovery techniques and which classification they belong to (Lake, 2010)

Thermal methods enhance oil mobility by reducing oil viscosity and/or vaporize the crude oil (Speight, 2009). The most common method of thermal stimulation of oil fields is vapor injections, but *in-situ* combustion can also be used. Thermal methods are most commonly used in reservoirs with heavy oil. Solvent methods are injection of liquids or chemicals which is miscible with the crude oil. Commonly used fluids are organic alcohols, ketones, refined hydrocarbons and CO_2 (Lake, 2010). Thermal and solvent methods will not be further discussed

in this thesis, the focus is on foam, which is a chemical method. The most common chemicals used in flooding are polymers and surfactants. Polymers increase the viscosity of injected water, hence reducing its mobility and improving the mobility ratio resulting in increased sweep. Surfactants are injected to reduce the surface tension between water and oil increasing the microscopic displacement (Zolotukhin and Ursin, 2000). For surfactants, there is also a second option which is to reduce the mobility of gas by generating foam. Foam can reduce gas mobility by several orders of magnitude (Fernø et al., 2015a). The most common reason for failed enhanced oil recovery projects is reservoir heterogeneity, which results in the injected material bypassing the oil bearing layers in the reservoir (Donaldson et al., 1989). Another method for reducing gas mobility is by water alternating gas (WAG) injection. This method reduce the relative gas permeability by the presence of mobile water, however not as significant as the presence of foam. This thesis will focus on foams, and the use of foam to reduce heterogeneous flow in fractured reservoirs.

4. The Fundamentals of Foam

Foams are gas bubbles dispersed in a continuous aqueous phase separated by thin liquid films known as lamellae (Yan et al., 2006). Foams can be divided into two main groups; bulk foams and foams in porous media. Both types of foams are used in the oil industry. Foams in porous media are used to enhance oil productions, whereas bulk foams can be used during drilling, fracturing and cementing (Martinez, 1998). The effect of foam in fractured reservoirs is not well understood. Foam could potentially be an effective mobility reduction agent for gasses in fractures. Foam in fractures is believed to behave as bulk foams (Sheng, 2013), however this might not apply to tight fractures.

Foam has much higher viscosity than pure gas, which will increase the mobility ratio and enhance sweep efficiency. In pure gas injections, viscous fingering and gravitational override is a major challenge. Foam has been found to greatly reduce the mobility of gas flooding and increasing the sweep. The foaming agent also preferentially went into the more permeable zone previously flushed by gas. This generates foam in the regions with the largest permeability and redirect gas to less permeable zones (Yan et al., 2006, Ransohoff and Radke, 1988, Casteel and Djabbarah, 1988).

To further discuss foam, foam generation and foam behavior some general knowledge affecting foam is necessary. The most important parameters for foam generation are surfactants, interfacial tension and capillary pressure. Relative permeability and wetting are also important factors for foam generation and stabilization, and will also be discussed.

4.1. Surfactants

Surfactants consist of two parts, a hydrophilic *body* and a hydrophobic *tail*. Due to this construction surfactants will have a tendency to accumulate in the interface between two immiscible fluids (e.g. water/oil or water/gas). This results in a dramatic decrease in the interfacial tension between the two fluids. The reduction in interfacial tension can result in production of the previous capillary trapped oil. Capillary trapped oil can frequently present more than half of the residual oil (Zolotukhin and Ursin, 2000).

To generate foam two essential ingredients is needed, gas and surfactant. A surfactant solution will significantly change the properties of gas dispersion. The reduced interfacial tension between the gas and the liquid will facilitate the dispersion of gas, reduce the size of the generated bubbles and lower the work needed to generate foam (Exerowa and Kruglyakov,

1998). A surfactant or surfactant solution is necessary to generate stable foam in a liquid; without surfactant present the formation of stable foams is impossible.

4.1.1. Interfacial Tension

Interfacial tension, σ (or IFT), can be considered as a membrane-like equilibrium between two immiscible fluids. The interfacial tension is a result of how large the intra- and interfluid cohesive forces are. The interfacial tension is, in reality, interfacial energy. The greater the interfluid forces are, the greater the work needed to bring a molecule to the surface, resulting in a greater interfacial tension (Zolotukhin and Ursin, 2000). The value of the interfacial tension between two fluids will tell us how the different fluids will react. This can be divided into three different categories.

- Interfacial tension greater than zero, $(\sigma > 0)$: The intrafluid forces are greater than the interfluid forces; hence the molecules prefer their own kind. In other words if the interfacial tension is positive the fluids are immiscible.
- Interfacial tension equals zero, $(\sigma \approx 0)$: The intrafluid and interfluid forces are equal. Fluid with zero interfacial tension is miscible, but will not spontaneously mix. With time diffusion will eventually lead to full mixing.
- Interfacial tension less than zero, $(\sigma < 0)$: The interfluid forces are greater than the intrafluid forces; hence the fluids will spontaneously mix. This kind of miscibility is called dissolution.

4.2. Mobility Reduction Factor (MRF)

The main objective of foam is to reduce the gas mobility, and the mobility reduction factor is often used to evaluate foam, as defined by equation (2):

$$MRF = \frac{\Delta P_f}{\Delta P_g} \tag{2}$$

ΔP_f and ΔP_g are the pressure drops across a porous medium or fracture for gas and foam respectively. The subscript *f* stands for foam, and *g* for single phase gas (Buchgraber et al., 2012). There are mainly two mechanisms that reduce gas mobility during flow in porous media and fractures. The first mechanism is significant drag from viscous and capillary forces due to

constant deformation of bubbles (Hirasaki and Lawson, 1985). The second mechanism is the reduced area of flow due to stationary lamellae blocking flow paths (Falls et al., 1989).

4.3. Bulk Foams

Bulk foams are several gas bubbles separated by a continuous liquid film. When looking at bulk foam in one plane the bubbles will meet two possible ways: in a crossing point between three or four bubbles, shown in **Figure 4-1**.
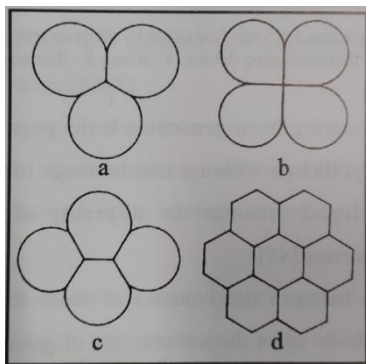
Figure 4-1: Different foam structures. (a), (c), and (d) are stable equilibriums for three, four or several bubbles. Common for these three situations is that there is never a point where four or more bubbles meet. Structure (b) is an unstable equilibrium of four bubbles, where the slightest disturbance will make the formation switch in to (c) (Exerowa and Kruglyakov, 1998).
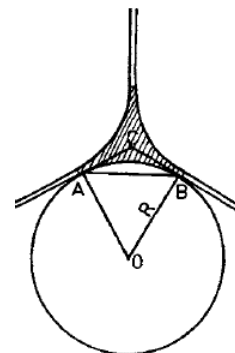
Figure 4-2: Cross-section of a Plateau border where three bubbles meet. Film tension, $\gamma = 2\sigma$ (where σ equals surface tension), are equal for all three borders and therefore the forces will balance each other out when the three angels between the borders are equal (first law of Plateau) i.e. $\angle ACB = 120^o$ (Exerowa and Kruglyakov, 1998).

The meeting point between three bubbles, called a Plateau border, form a stable structure and is illustrated in **Figure 4-2**(Exerowa and Kruglyakov, 1998).

4.4. Capillary Pressure

The capillary pressure is of significant importance in a reservoir because it largely controls the distribution of the fluids in the reservoir (together with gravitational forces). The capillary pressure influences both the mobility of the different fluids and how the fluids will move during production of a reservoir (Brown, 1951). From equation (3) the relation between the capillary pressure, P_c, and radius, r, of a pore is given; the capillary pressure increase as the radius decrease. i.e. less force is required to move fluids in larger pores.

If the two immiscible fluids are in a narrow glass, pipe or a rock pore channel the stronger adhesive forces of the wetting fluid will make the meniscus to curve, illustrated in **Figure 4-3**(Zolotukhin and Ursin, 2000).
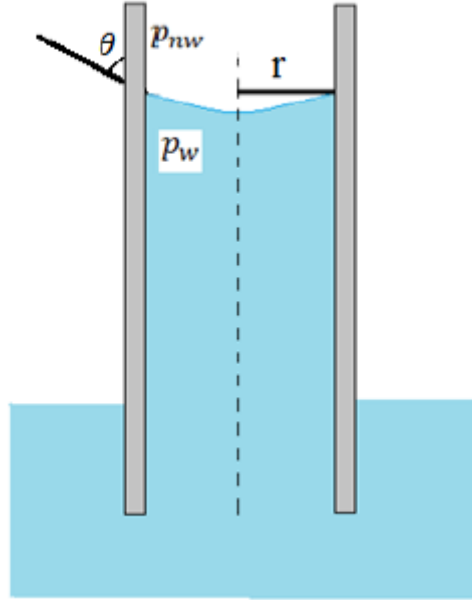
Figure 4-3: Illustration of water and air in a water-wet capillary tube. The contact angle between wetting fluid and solid is given by θ. The water rises in the tube due to capillary forces (Lien et al., 2011).

By using the Young-Laplace equation, the capillary forces in a tube can be written as equation (3):

$$P_c = P_{nw} - P_w = \frac{2\sigma * cos\theta}{r} \qquad (3)$$

P_c is the capillary force, P_{nw} and P_w are the internal pressure in the wetting and non-wetting fluid respectively, σ is the interfacial tension between the wetting and non-wetting fluid, θ is the contact angle between the wetting fluid and the solid and r is the radius of the tube (Lake, 2010). Capillary pressure is an important factor for foam generation in fractures, as will be discussed in **4.5 Foam Generation**. The importance is further investigated by studying foam generation in smooth versus rough-walled fractures.

4.5. Foam Generation

In experimental studies pre-generated foam is often used as an injection strategy. However, this is usually not the case in field scale. In field scale injection either simultaneous surfactant-CO_2 injection or SAG (surfactant alternating gas) is used. Both methods require foam generation *in-situ* (Sheng, 2013). This thesis will, therefore, use co-injection of gas and surfactant to investigate foam generation and behavior in fractures.

There are three mechanisms generating foam a porous media: leave-behind, snap-off and lamella division (Dicksen et al., 2002). There is a critical velocity involved in foam generation. Below the critical velocity generated bubbles are stagnant; above critical velocity already generated bubbles will flow. If the velocity is above or below this critical velocity will dictate the dominant mechanism for foam generation (Ransohoff and Radke, 1988).

4.5.1. Leave-behind

The leave-behind mechanism is the main mechanism for producing lamellae below the critical velocity. When gas invades an area previously saturated with liquid, some of the liquid is displaced, while some will be left behind. When two gas fronts enter the same pore space, the liquid will be squeezed between them. If there is sufficient surfactant present in the liquid, the liquid film can be stable and a lamella is made, illustrated in **Figure 4-4**. The gas invasion can occur simultaneously or one at a time (Ransohoff and Radke, 1988). The leave-behind effect will reduce the gas mobility by forming dead ends and closing off potential flow paths. Foam formed by leave-behind reduces gas mobility less than other mechanisms, and is therefore considered as a weak foam (Ransohoff and Radke, 1988). The leave-behind mechanism blocks flow paths, but does not generate any new gas bubbles.
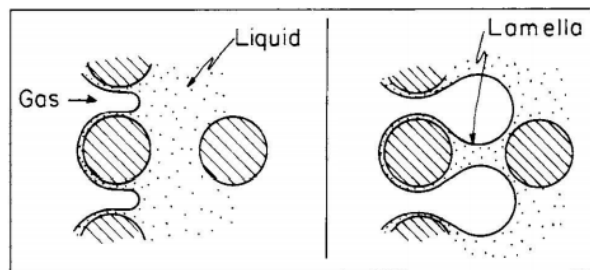
Figure 4-4: An illustration of how the leave-behind mechanism generate lamellae which will reduce flow path but not generate new bubbles (Ransohoff and Radke, 1988)

4.5.2. Snap-off

The snap-off mechanism will generate new bubbles when above a critical velocity. When gas enters a pore space previously filled with liquid, the capillary pressure decrease, as the size of the gas bubble increase. This results in liquid being forced to the throat of the pore. If the capillary pressure drops below a critical value, the liquid will snap-off a gas bubble as shown in **Figure 4-5**. The result of this effect is several new gas bubbles which greatly reduce the mobility of gas, hence making a strong foam (Ransohoff and Radke, 1988). The new bubbles can continue flowing through the formation, or block flow paths. A discontinuous gas phase (such as foam) have higher resistance to flow than pure gas, hence the relative permeability of gas has been greatly reduced (Hirasaki and Lawson, 1985).
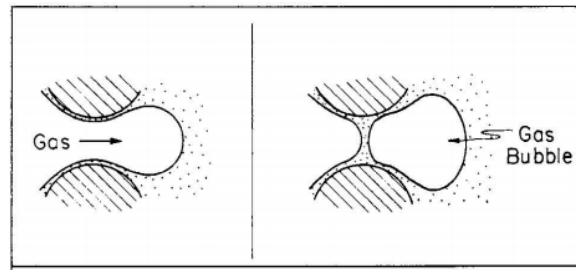
Figure 4-5: Snap-off will generate new bubbles due to the reduced capillary pressure when gas invades a pore space. The liquid films at the pore throat will thicken until they meet and "snap off" the bubble inside the pore space (Ransohoff and Radke, 1988)

4.5.3. Lamella-division

Lamella-division is the third mechanism for foam generation in porous media. This mechanism differs from leave behind and snap-off because it requires a moving lamella. Hence foam generation must already have taken place. When a gas bubble meets a branch it can start moving in two directions, as shown in **Figure 4-6**. When this occurs one gas bubble can be separated into two. This method is very similar to snap-off, but requires a flowing bubble. Lamella-division also requires flow velocity to be above a critical value (Ransohoff and Radke, 1988).
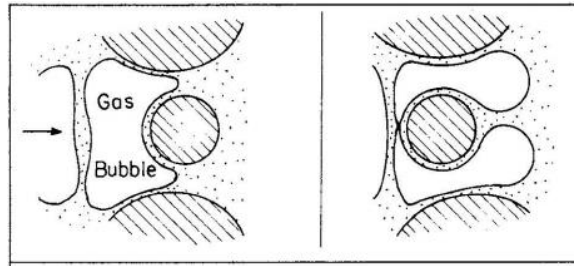
Figure 4-6: Lamella-division splits already generated bubbles into two smaller bubbles (Ransohoff and Radke, 1988)

4.6.   Relative Permeability and Wettability

Relative permeability is the ability a porous media has to conduct one fluid when two or more fluids are present (Craig, 1971). When more than one fluid is present there will be an internal fluid distribution, depend on core wettability. Wetting fluid will distribute along the surface while the non-wetting fluid will tend to accumulate in the center of large pore spaces. This distribution occurs because different fluids will experience different adhesive forces to the same solid. The situation where one fluid spread on the surface is, therefore, the most energetically favorable distribution (Anderson, 1987, Exerowa and Kruglyakov, 1998). This distribution will cause the flow path for each fluid to be reduced, compared to a situation where there is only one fluid present. This blocking of flow paths is the reason behind the reduction in conductivity of the porous medium. When performing foam flooding the relative permeability of gas is greatly reduced, hence reduce the gas mobility.

4.7.   Foam Quality

Foam quality is defined as the volume fraction of gas per volume of foam, also known as gas fraction, f_g (Martins et al., 2001). For qualities below 50% gas it is no longer called foam, but gas dispersion in liquid. Because gas is highly compressible, changes in pressure will alter the quality of foams. Pressure behavior is therefore important when discussing foam quality (Martins et al., 2001). The foam quality has a significant impact of the apparent viscosity of foams, as illustrated in **Figure 4-7**.
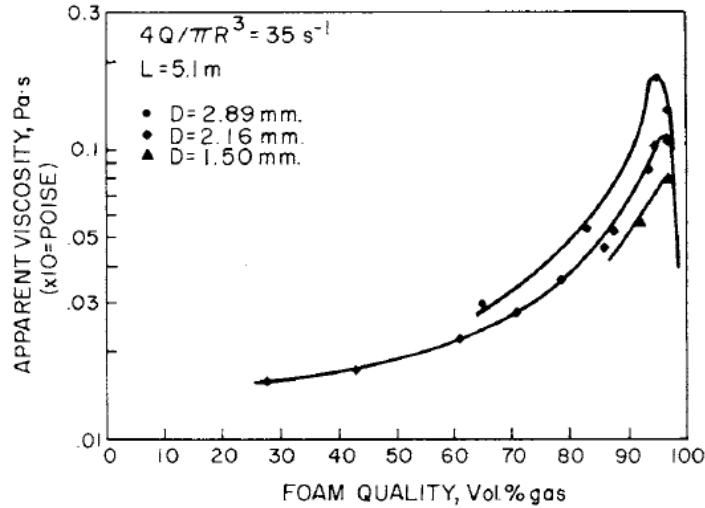
Figure 4-7: The apparent viscosity measured in three capillary tubes of different size plotted against the foam quality (Patton et al., 1983).

The apparent viscosity is calculated using Darcy's law, solved for viscosity. By treating foam as a single phase, its apparent viscosity is found by equation (4) (Farajzadeh et al., 2015):

$$\mu_f^{app} \equiv \frac{K\nabla P}{q} \tag{4}$$

where

$$\nabla P = \frac{\Delta P}{L} \tag{5}$$

Here μ_f^{app} [cP] is the apparent viscosity at a given gas fraction, K [D] the absolute permeability or fracture conductivity, ∇P [atm/cm] the pressure gradient, q [cm/s] the flux, ΔP [bar] the pressure drop across the sample and L [cm] the length of the sample. Permeability have been used to describe fracture conductivity throughout this thesis, although it might not be technically correct. In permeability calculations the cross sectional area of flow is used, in porous cores this is easily calculated by measuring the radius of the core sample. However, when using marble, as in this thesis, all flow go through the fracture. The cross sectional area of the fracture could be used, but it is not easily found, and is expected to vary through the sample.

16

4.8. Foam Stability

Foam life time is often used to measure foam stability (Exerowa and Kruglyakov, 1998). Foam lifetime can be measured by filling a cylinder or pipette with a bulk foam and measure the decay with time. Foams are thermodynamically unstable, and over time the thin liquid films will rupture (Schramm, 2000). All foams degrade over time, and the term "stable" therefore refers to relatively stable in a kinetic sense. There are several factors involved in the stability of foam, and they can be divided into interfacial and bulk solution properties. These factors include gravity drainage, capillary suction, surface elasticity, viscosity, electric double-layer repulsion, dispersion force attraction and steric repulsion (Schramm, 2000). The most important processes which destabilize foams are film thinning, liquid drainage due to gravity, gas diffusion through film-flow from smaller bubbles to bigger bubbles, and rupture of films (Exerowa and Kruglyakov, 1998).

The stability of foam lamella depends on the capillary pressure, and a limiting capillary pressure, P_c^*, has been defined where lamellae are stable. If the gas fraction is increased after reaching the limiting capillary pressure, the lamellae become unstable and coalescence (lamella rupture) will coarsen the foam, illustrated in **Figure 4-8**. Coarser foam increase gas mobility, and relative gas mobility becomes proportional to the ratio of gas-to-liquid fractional flow (Khatib et al., 1988). There are several factors which control the limiting capillary pressure, including surfactant type, surfactant concentration and permeability. Experiments have shown that in high permeable media there is not one liquid saturation in which foam coalescence occur, but rather a range of saturation where coalescence occur gradually (Farajzadeh et al., 2015).
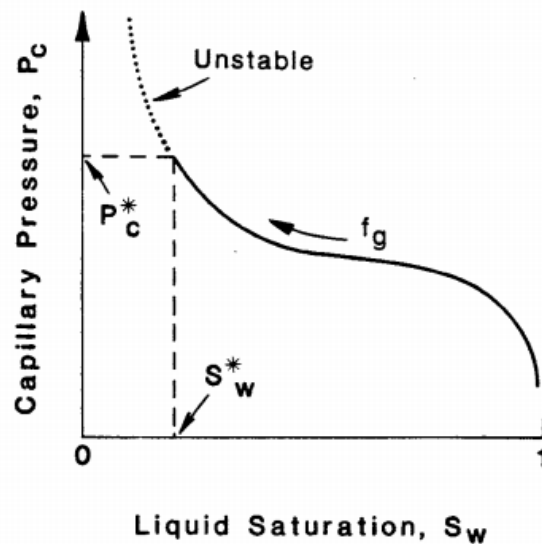
Figure 4-8: The correlation between gas saturation, capillary pressure and lamella stability (Khatib et al., 1988)

4.9. Flow Regimes

Foam inside a porous medium is either stagnant or moving. Experiments have shown that there is a minimum pressure gradient necessary to mobilize foam (Rossen, 1990, Falls et al., 1989). The pressure gradient needed to mobilize foam is found to be approximately 10 to 20% larger than the pressure gradient necessary to keep mobilized foam to continue flowing. This can lead to some areas being blocked by foam, while other areas flow. In the flowing areas the flow is described as "bubble trains" where bubbles flow in a single path of least resistance (Kovscek et al., 1995).

Two different flow regimes in foam flooding are investigated (Osterloh and Jante, 1992): the high-quality regime and the low-quality regime. The two regions are divided by a given gas fraction f_g^*. The region above f_g^* is the high-quality foam region and the low-quality foam region is below f_g^*. In the strong foam region the flow pressure gradient is dependent on the liquid velocity only and below f_g^* the pressure gradient is dependent on the gas velocity only, illustrated in **Figure 4-9** (Alvarez et al., 2001); this plot is known as an "L-plot" due to the characteristic shape of the pressure contours. This is caused by the bubble size; which is fixed at roughly pore size in the low-quality foam region. This theory is based on smaller bubbles disappearing due to diffusion (Alvarez et al., 2001).
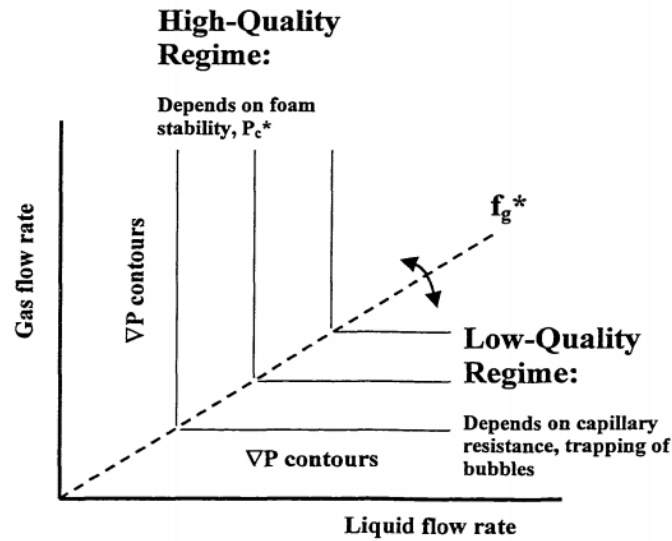
Figure 4-9: Pressure gradient in foams depending on liquid and gas flow rate (Martinez, 1998). The illustration shows how the pressure gradient of foam only depends on liquid or gas velocity on either side of the f_g^*. f_g^* is a certain gas fraction, found to be between 0.94 and 0.96 in porous media (Osterloh and Jante, 1992)

In the high-quality foam region (i.e. above f_g^*), the foam quality is dictated by the limiting capillary pressure. Above P_c^* the foam will become coarser, and the gas mobility will increase. This will result in an increase in the liquid saturation and P_c will decrease. If P_c is below P_c^* it will generate stronger foam and the gas saturation will increase, resulting in increased P_c towards P_c^* (Martinez, 1998).

In experiments Osterloh and Jante (1992) found the gas fraction for the limiting capillary pressure, f_g^*, to be approximately 0.94 in porous media. In fractures, however, it is estimated that the gas fraction for the limiting capillary pressure is as high as 0.99 (Pancharoen et al., 2012)

4.10. Foam Hysteresis

Hysteresis is the state of a system's dependency on its historical state. In reservoirs, this is experienced by the fact that field and experimental results are depending on previous conditions and the production history. A single velocity can experience two different foam states

19

depending on the previous state, shown in **Figure 4-10** (Lotfollahi et al., 2017). Ransohoff and Radke (1988) reported that there is a minimum velocity, known as critical velocity, necessary to generate foam. The hysteresis effect on foam indicates that after foam is generated, it can be sustained with a lower velocity than the critical velocity (**Figure 4-10**). This can be an important property on full field foam injections, where velocities are reduced as the foam propagate away from the injection well.
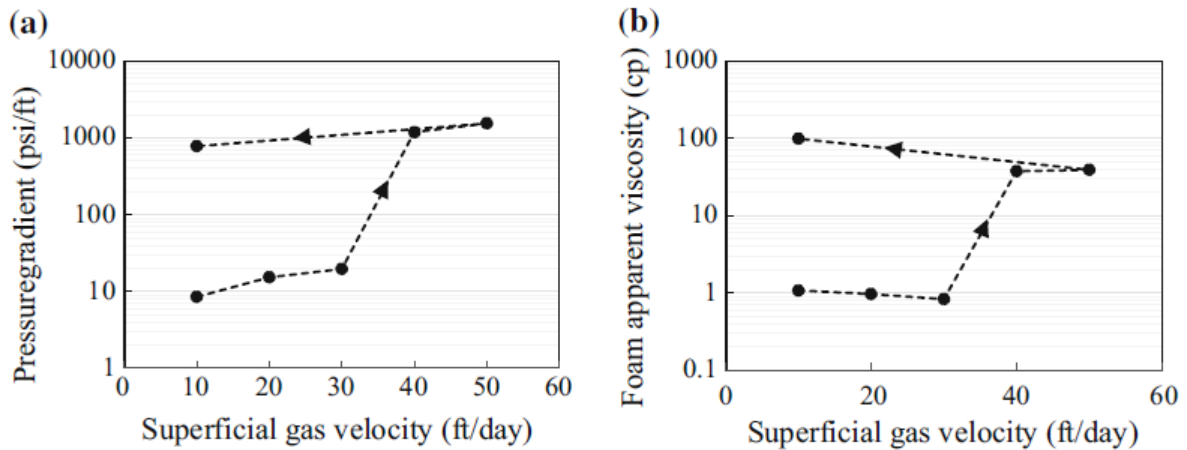
Figure 4-10: Foam (f_g 0.8) injection into on rocks of 250mD permeability show clear signs of hysteresis. The injection velocity was increased in steps and then decreased. A significant hysteresis effect is seen at low velocities. The plot is made by Lotfollahi et al. (2017) using experimental data from Chou (1991).

The hysteresis effect, in which two different foam states can occur at the same condition, is important to consider when during foam experiments and analysis. Experiments conducted by Kahrobaei et al. (2017) only experienced foam rheology at high-quality foam, i.e. hysteresis can be dependent on foam quality.

4.11. Foam Rheology

Rheology is the study of the deformation and flow of matter (Barnes et al., 1989). The rheology of foam includes shear stress, shear rate, and viscosity and is highly influenced by temperature, pressure, liquid phase properties, foam quality, foam stability and surfactant concentration (Sani et al., 2001).

Foam experiencing stress will start to deform, as illustrated in **Figure 4-11**b). When the stress exceeds a threshold stress known as "yield stress" the foam will start flowing as a pseudoplastic fluid (Stevenson, 2011). Pseudoplastic behavior is also known as shear thinning, in other words, as stress applied to foam is increased the apparent viscosity of the foam decrease (Patton et al., 1983). Another rheological property of foam is slippage between foam and solid surfaces

(Prud'homme, 1995). If the applied force on the foam is below the "yield stress" the foam will have a "stick and slip" behavior, and the measured viscosity will not be the foam viscosity, but the slippage viscosity.
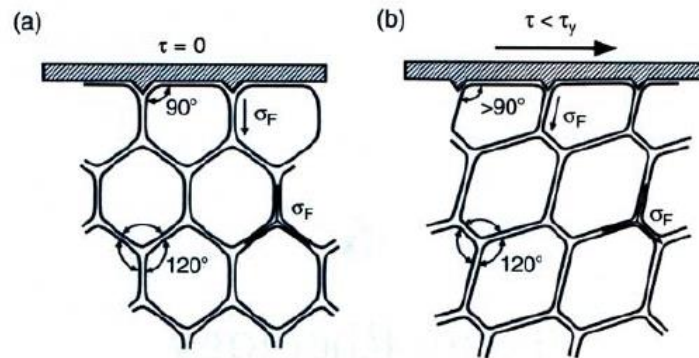
Figure 4-11: a) In stagnant foams, without any force/stress applied to it, all angels are equal. When a shear force, τ, is applied the foam will gradually start to deform, but still be stagnant, as seen in b). The foam will gradually deform with increased pressure, this is the "gel strength", until the yield stress, τ_y , is reached and the foam will start moving (Stevenson, 2011).

While flowing foams behaves like a pseudoplastic, stagnant foam have a measurable gel strength which increases with increasing foam quality (David and Marsden Jr, 1969). Hence, stagnant and moving foams exhibit different behaviors.

4.12. Foam in Fractures

The effect of pure CO_2 injections is greatly reduced when fractures occur, as the CO_2 will tend to flow through the fractures due to higher conductivity and not the matrix (Fernø et al., 2015a). Reducing the mobility of gas in fractures, by usage of foams, has potential to greatly improve gas injections in fractured reservoirs.

It has been shown that foam generation in fractures is possible (Fernø, 2015, Brattekås and Fernø, 2016). The primary mechanisms for generating foam in a fracture is believed to be the snap-off effect (shown in **Figure 4-5**), occurring at "snap-off sites" (Kovscek et al., 1995). Foam in fractures differs from foam generated in porous media by having a much larger bubble size. Kovscek et al. (1995) found that bubbles formed in fractures are roughly four times larger than bubbles in foam generated under the same conditions in Berea sandstone. This is as expected because there are fewer snap-off sites in a fracture than in a porous medium (Kovscek et al., 1995).

21

Experiments on micromodels show that in smooth fractures both surfactant solution and gas moved in a smooth and linear motion, resulting in low lamella generation. In rough-walled fractures, flow was unidirectional, and a "stick and slip" motion was observed. This resulted in higher levels of mixing and foam generation *in-situ*. A higher pressure drop in rough-walled fractures was observed at the same time (Buchgraber et al., 2012). This correlates to Kovscek's observation of foam generation at "snap-off sites".

Fernø et al. (2015a) found, through laboratory experiments, that CO_2 foam injections significantly increased the oil recovery rate compared to pure CO_2 injections. The total oil recovery was not increased because the oil recovery mechanisms on micro scale are the same for a miscible CO_2 foam flooding as for a miscible CO_2 flood. Increased oil recovery rate was explained by increased sweep efficiency, due to reduced fracture conductivity (Fernø et al., 2015a). The reduced conductivity resulted in an increased pressure drop across the fracture, which introduced a new viscous component to the recovery process in addition to diffusion – the main recovery mechanism during pure CO_2 floods.

4.13. Capillary Pressure in Fractures

Capillary pressure influence foam generation and capillary pressure in fractures must, therefore, be discussed. Capillary pressure in fractures is often ignored, and given the value zero (Firoozabadi and Hauge, 1990). Real rock fractures have a rough surface and numerous contact point (Tsang, 1989), and will, therefore, have a capillary pressure. Experimental measurements of capillary pressure within a fracture were done by Reitsma and Kueper (1994). They varied the normal pressure applied to the fracture and showed that increased normal pressure increased the measured capillary pressure (Reitsma and Kueper, 1994).

5. Imaging Techniques

During experiments on the core scale, the pressure drop across the system and produced fluid volumes are often used to account for the properties of flow. However, this might not cover all mechanisms occurring *in-situ*. Visualization of flow *in-situ* enables a close look at changes in fluid distributions, displacement efficiency etc. This chapter presents a short description of the imaging techniques used in this thesis.

5.1.   Positron Emission Tomography (PET)

Positron Emission Tomography (PET) is a nuclear medicine imaging technique which highlights metabolism in living humans or animals. This is an effective method for detecting tumors (cancer), due to the high metabolism that occurs in tumors cells. This is done by using the unstable isotope ^{18}F, which is made in a cyclotron and used to synthesize ^{18}F-fluorodeoxyglucose (FDG). The FDG is adsorbed by metabolism, hence an increased concentration will occur where high metabolism occurs. When FDG decays, it emits a positron; the anti-particle of the electron. The positron will quickly annihilate an electron, result in a pair of gamma rays traveling in opposite directions, illustrated in **Figure 5-1 a)**. By detecting these two gamma rays, the origin will be somewhere on the line between them, illustrated in **Figure 5-1 b)**. This is done by using a ring detector enclosing the patient. By measuring several detections, it is possible to make a 3D image of the patient, where the level of radiation is shown. A widely-used imaging method for detecting head and neck cancer is combining PET with CT imaging (Bailey et al., 2005, Maučec et al., 2013, Omami et al., 2014).
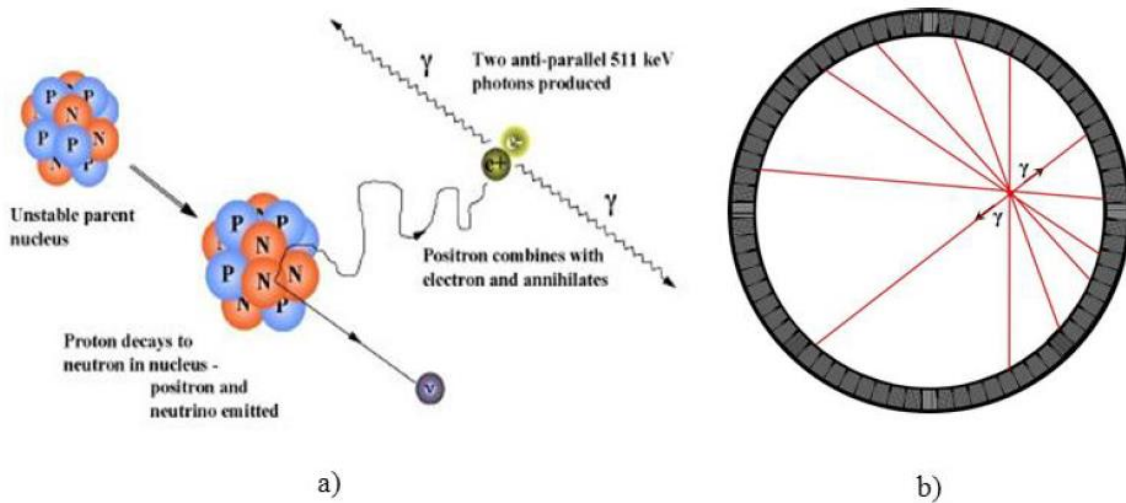
Figure 5-1: An illustration of Positron Emission Tomography (Maučec et al., 2013). a) An illustration of the decay of a positron. b) Ring detector measuring signals at 360 degrees. It is possible to locate the radiation source by measuring signals which travels in opposite direction. The measurements are then used to generate a 3D picture of the whole sample where radiation intensity is shown.

The procedure for PET imaging can be adapted to visualize liquid flow inside fractured systems. FDG is water-soluble and by mixing FDG with the injected liquid, the liquid is traceable *in-situ*. By measuring the radioactive signal throughout experiments, it is possible to generate a time-lapse of fluid saturations. In this thesis this method will be used to evaluate foam generation and propagation in fractures and fracture conductivity. PET shows the radioactive source, and do not depend on density differences, which CT does. PET is therefore found superior compared CT in determining front progression and fluid saturation *in-situ* (Fernø et al., 2015b).

5.2. X-ray Computed Tomography (CT)

X-ray computer tomography (CT) can be used to obtain several values important for hydrocarbon production strategies, such as lithology, porosity and and/or saturation (Hicks Jr, 1996). By combining PET and CT, one can get a very detailed image showing the distribution of the labeled fluid inside porous media or fracture matrix. CT scanners main components are a radioactive source and a series of radioactive detectors. The sample (or core) which is being imaged is placed between the source and the detectors. The measured X-ray value can be correlated to the density of the sample. While measuring the x-rays passing through the sample the source and receivers are rotating around the sample, illustrated in **Figure 5-2**. This is the core difference between a computed tomography and a regular x-ray. The series of images are

put together to generate what is known as a slice. A slice is a 2D section of the sample, i.e. what you would see if the sample was cut in two. By making several slices and stacking them together, one can generate a 3D image of the sample (Ketcham and Carlson, 2001). This 3D image visualize densities in the sample, which can correlate to porosity, fractures, fluids, etc.
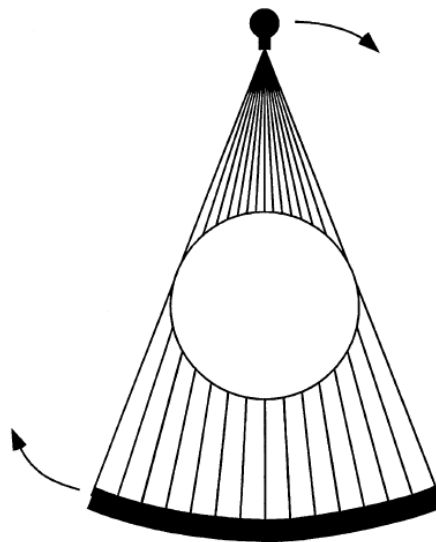
Figure 5-2: An illustration of an X-ray computed tomography. The source and the detectors placed on opposite sides of the sample. Arrows indicating the rotation during the scan (Ketcham and Carlson, 2001)

Part II – Experimental Procedure

6. Objective of Experiments

This part describes the experimental preparations, procedures, rock materials and fluids used in this thesis. The main objective of this study was investigating foam formation and behavior in fractures of different aperture. In order to investigate foam generation and behavior in fractures, fractured marble cores were used. Co-injection of gas and surfactant solution was performed with varying gas fractions, varying total rate and changing only gas or liquid velocity. This was done to investigate foam generation and behavior in the different fractured systems. Measurements of differential pressure during co-injections was conducted to evaluate the foam behavior, and compared to baseline studies of co-injection of N_2 and brine. PET/CT imaging was used to get a better understanding of foam behavior in fractures and provided *in-situ* observation of saturation during co-injection with varying gas fraction. All experiments were performed at the Department of Physics and Technology (IFT) at the University of Bergen (UoB) except for the imaging which was performed at the Molecular Imaging Center (MiC) at Haukeland University Hospital (HuH).

7. Core Material

The experimental work in this thesis was performed using fractured marble core plugs. Marble is a metamorphic rock made by regional metamorphism of carbonate sediments (Haldar, 2013), and have the same surface and mineral composition as sedimentary carbonate rocks. A significant distinguishment is, however, the lack of porosity and permeability in the marble inhibiting both storage and flow of fluids in the matrix.

The marble material was chosen for experimental work on foam flow in fractures because:

- Zero porosity and permeability inhibits foam flow in the rock matrix. Foam behavior in fractures without the influence of adjacent matrix is therefore possible.
- Fluids will behave similarly as in carbonates due to same mineral composition, surface charge, etc. hence same liquid-solid interactions.

An overview of all fractured cores used in this thesis is found in **Table 7-1**.

Table 7-1: An overview of all fractured cores used and prepared for experiments

Fracture category	Core	Length [cm] ± 0.01	Diameter [cm] ± 0.01	Bulk volume [ml]	Fracture volume [ml]	Permeability [D]
Open	2i-1	14.94	5.08	302.7±0.8	17.9±0.02	8.63±0.04
Partially open	2i-2	15.23	5.05	304.9±0.8	10.0±0.2	0.30±0.01*
	2i-3	14.52	4.95	278.8±0.7	7.9±0.1	6.8±0.3
Smooth	2i-4	14.47	5.06	290.9±0.8	12.4±0.2	7.1±0.4
	2i-5	14.56	4.95	-	-	-
Tight	1.5i-1	15.05	3.90	-	-	-
	1.5i-2	14.35	3.90	171.4±.6	6.1±0.1	0.35±0.02
	1.5i-3	14.57	3.90	174.3±0.6	6.2±0.1	0.129±0.005
	1.5i-4	14.50	3.88	171.8±0.6	6.1±0.1	0.101±0.002

* Permeability measurement were done at confinement pressure of 25 bar to investigate the effect confinement pressure had on the measurements.

Drilling, fracturing and reassembling of the cores are described in greater details in the following chapters.

7.1. Drilling of the Marble Cores

Marble cores were drilled from a single marble block by previous master students Johansen (2016) and Vasshus (2016). The marble block was washed and cleaned by soap and a pressure washer to remove growth and contaminations due to outdoor exposure. The block was brought to Statoil's facilities at Sandsli where the cores were drilled. The drilling was done by diamond

coated bits with outer diameters of 1.5 and 2 inches. The marble block was mounted to the drilling rig prior to drilling and the drilling speed (rpm) was set. Water was continuously flushing the drill bit to avoid overheating and remove cuttings. Picture of the drilling can be seen in **Figure 7-1**.
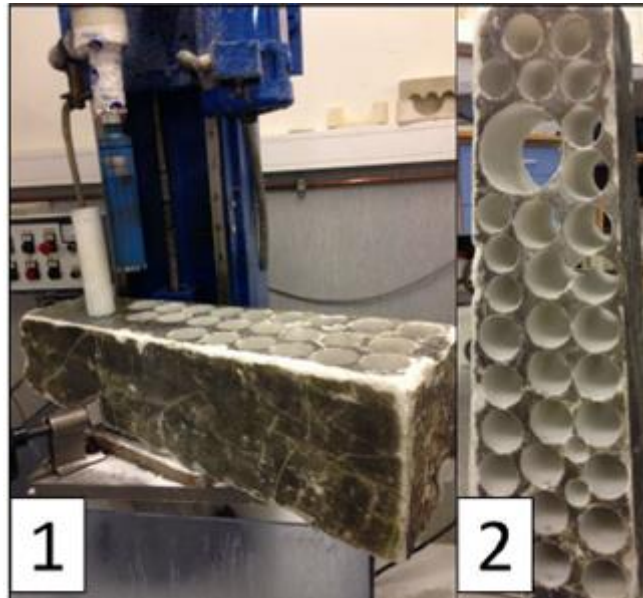
Figure 7-1: 1) Cores were drilled by an automatic drill at Statoil's facility at Sandsli, Bergen. 2) A picture of the marble block after the cores were drilled. The holes of both 4, 2 and 1.5 inches can be seen. Pictures by Johansen (2016)

7.2. Fracturing Marble Cores

Fractures were created in the marble cores using a fracturing device that was specially made by Johansen (2016) and Vasshus (2016) in collaboration with the mechanical workshop at the Department of Physics and Technology. The method was inspired by the Brazilian test described by Mellor and Hawkes (1971). The fracturing device is made up of two thick metal plates with indents to fit the circular cores. An edge was fitted in a groove which was milled in the bottom of the indents. This edge was caused very large fractures at the contact point with the cores. To reduce the fracture size, this edge was sharpened to reduce the contact area with the cores. This reduced the fracture size significantly. The cores were placed between these two sharp edges, and the whole device was put in a hydraulic press. The pressure from the hydraulic press was increased until the core fractured. Picture of the fracturing process is shown in **Figure 7-2**.
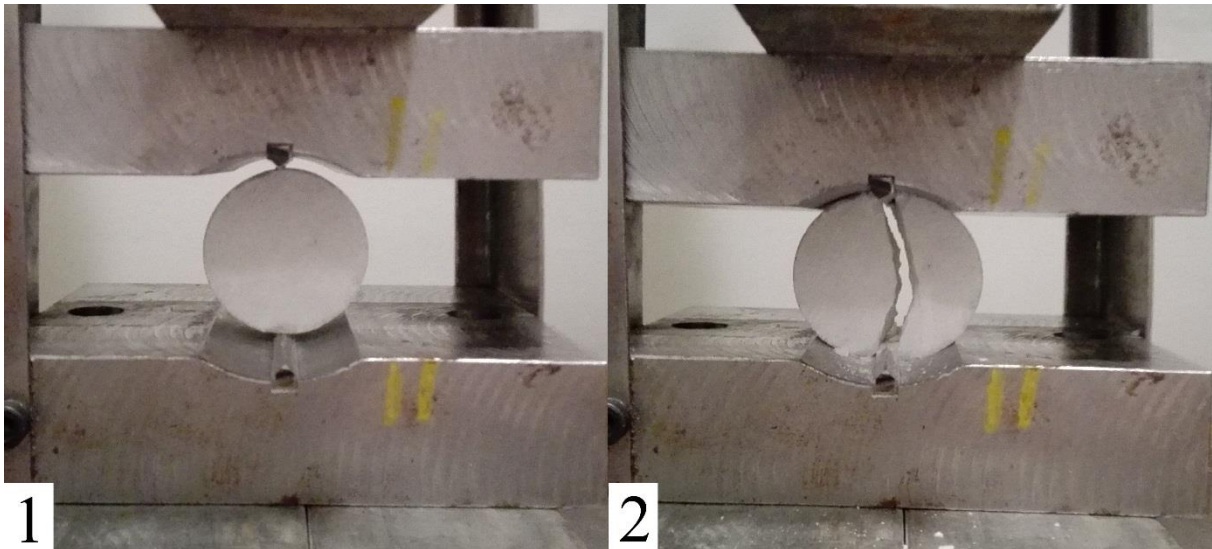
Figure 7-2: Picture of the fracturing procedure. 1 show the marble core placed inside the fracturing device before pressure is applied. On picture 2 the pressure has been applied until the fracturing occurred.

When fracturing the cores, there is a large force applied to the core from the hydraulic press. A step-by-step instruction to fracture marble cores is as follows:

1. The fracturing device was set in the hydraulic press and made sure it was at the center of the press. The marble core was then loaded into the fracturing device and carefully placed in the center, both vertically and horizontally.

2. Pressure was gradually applied. The best method to apply pressure was found to be pulse wise. The pressure was gradually increased this way until the core fractured. If the pressure was increased at a steady pace, rather than pulse wise, the chance of crushing the core more than desired was significantly higher.

3. After the core had fractured the pressure was released, and the core was carefully removed. The core segment were wrapped in plastic foil and marked to ensure the whole core was reassembled in the correct order.

The fractured cores usually got a clean fracture with some minor crush marks from the two edges that applied the force. A few cores were fractured more than desired and some even completely shattered. The problems with crush marks and shattering were reduced after the edges were sharpened, and increasing pressure was switched to pulse like manner. To generate a more complex fracture network; cores were cut into three or six segments, and each segment

fractured individually. With this method, the segments could be stacked together to form a whole core with different orientation on the individual fractures.

When fracturing marble in the manner described above the fracture is believed to be more similar to fractures found in reservoirs/nature. Using a saw to split a core in two, to simulate fractures is believed to generate fractures with smoother surfaces. Fractures in nature have rough walls and numerous contact points (Tsang, 1989). Experiments have shown that foam generation in smooth fractures is difficult due to low mixing of gas and surfactant solution (Buchgraber et al., 2012, Haugen et al., 2012). Results from PET scans performed by Johansen (2016) and Vasshus (2016) showed that fluid flow mainly occurred in the large open fractures. None or very low flow was seen in tight fractures next to open fractures. By using sharp edges in the fracturing device in addition to epoxy, fractured networks without open fractures were made. This was done to emphasize on flow in fractures of varying aperture. A more detailed description of the different fracture types is described in the assembling procedure.

7.3. Assembling the Fractured Network

After being fractured, wrapping was necessary to keep the fractures and core segment together. Three different methods were used to assemble the cores, depending on the fractured system, resulting in open, partially open, smooth and tight fractures respectively. A more detailed overview is listed below:

- Open fractures: Core 2i-1 had two main fractures on opposite sides that were open and highly conductive. The two open fractures were connected by a tight fracture. It is estimated that all flow appears in these two main fractures, verified by PET/CT scans performed by Vasshus (2016).

- Partially open fractures: Four cores (2i-2 – 2i-5) had partially open fractures. Each core consisted of three segments (~5 cm), each individually fractured. The longitudinal fractures were alternately oriented vertically or horizontally during stacking, as illustrated in **Figure 7-3**. The longitudinal fractures are wider at the edges (compared to the middle) due to the fracturing device, but not as significant as core 2i-1.

- Tight fractures: Four cores only contained tight fractures (core 1.5i-1 – 1.5i-4). Each core is made up of 6 segments of approximately 2.5 cm each. Each segment is stacked with fracture directions perpendicular to each other.

Because the cores were designed by stacking several fractured segments together with different fracture orientation the orientation of the core was believed to be insignificant. However, when a new core was used for the first time, it was marked to indicate which direction it was used. Further experiments on the same core would always be performed in the same orientation to ensure consistency during experiments.
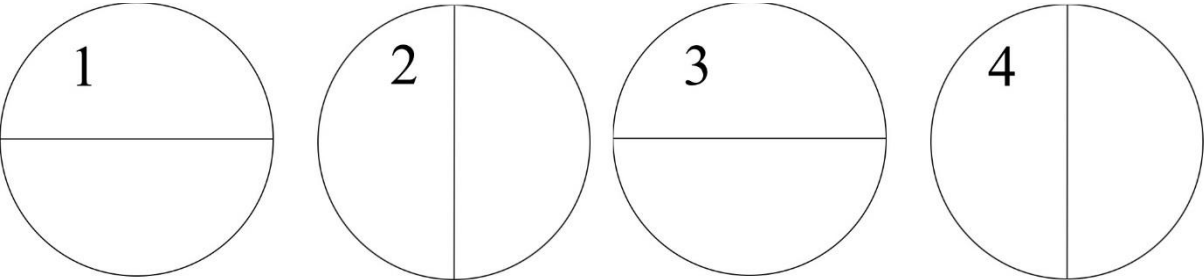
Figure 7-3: Fractured systems of several core segments were stacked with alternating fracture direction. Every second longitudinal fracture were either horizontal or vertical, as shown above.

Open and Partially Open Fractures

To keep the fractured segments of the 2 inch cores together, shrink-sleeve was used. Shrink-sleeve is a plastic tube designed to shrink when exposed to heat. The shrink-sleeve was cut to a length a few centimeters longer than the core itself. The core segments were carefully placed inside the shrink-sleeve. When the core segments were placed as desired within the shrink-sleeve, they were held in place while the shrink-sleeve was heated with a hot air gun. The core segments were held through the ends of the shrink-sleeve. The core and shrink-sleeve were rotated while heat was applied to avoid folding and bubbles, and ensure even distribution of shrinking. After the shrink-sleeve was tightly fitted around the core, the plastic ends were cut to fit the length of the core. An overview of the process can be seen in **Figure 7-4**. These cores were then placed inside a hassler core holder to conduct experiments.

Figure 7-4: 1) The fractured segments of marble next to each other. 2) The segments placed inside the shrink-sleeve 3) Top view of the finished and reassembled core. The fracture is oriented horizontally on this picture between the "I" and "2i-3".

Other cores were designed in such a way that they should be able to fit inside the animal PET/CT-scanner at the Molecular Imaging Center. Both intensity, weight and size limitations make it impossible to use Hassler core holder during scanning. If the intensity of the source is too weak and/or the diameter of the core is too large, the image will be of poor quality. To visualize fractures images of high-quality and resolution is necessary. The PET/CT-scanner is designed for small animals (rats and mice), and in addition to intensity there is a weight limitation of 2kg; a hassler core holder weighs significantly more than 2kg. To make fractured networks within size and weight limitations, the cores were fitted with an end-piece made of POM (polyoxymethylene), shown in **Figure 7-5**. The end of the shrink-sleeve was rubbed by sand paper and covered with epoxy. The end-piece made from POM was then carefully placed over the epoxy. It was made sure that there were no air pockets between the shrink-sleeve and end-piece. POM is a stiff and solid plastic, an ideal material to use as end-pieces. The POM was shaped to the desired design at the mechanical workshop at the Department of Physics and Technology.

Figure 7-5: The top end-pieces are attached with epoxy, and the bottom end-pieces are ready to be attached to core 2i-4 and 2i-5. 1) Top view where the inside and top of the end-piece can be seen. 2) Side view where the epoxy attaching the end-piece to the core is seen. The black lines mark the overlap of the end-pieces on the bottom core segment.

Tight Fractures

The 1.5 inch cores were made for imaging at the animal-PET machine at the Molecular Imaging Center. Generating fractured networks from 2 inch cores within weight limitations was difficult, and therefore cores of 1.5 inches were made. Narrower cores will also result in reduced beam hardening and better resolution in images. The cores were made up of 6 segments which were approximately 2.5 cm each. To ensure all liquid flow went through the fractures these cores were reassembled by the use of epoxy resin. This was done in several steps:

1. Each fractured core segment was assembled separately, using a clear and viscous epoxy with short cure time. The epoxy was smeared on the outside of the core segment, whilst the fracture was held tight with an f-clamp, see **Figure 7-6**.

2. The outside of the joints, between the different segments, were covered the same epoxy to keep the segments together. To ensure the epoxy stayed on the outside of the fracture network, a fine nylon mesh was placed over the joints before the epoxy was applied. Each core segment were oriented with alternating horizontal and vertical direction in the longitudinal fractures, as illustrated in **Figure 7-3**.

3. All remaining segments were assembled to form one complete core. Each remaining joint was covered with epoxy. The same method as described in step 2 was used. An image of this step is shown in **Figure 7-7**.

4. The end-pieces were attached. This was done by a different (blue) epoxy, with greater viscosity and slow curing time, to ensure a higher pressure resistance.

36

5. The core was placed in a lathe. The viscous (blue) epoxy was applied as core turned around in the lathe. When the epoxy had cured, a new layer was applied. The epoxy surface was roughed before application of a new layer for improved adhesion. This was done to further strengthen the core, enabling sufficient pressure resistance during imaging.
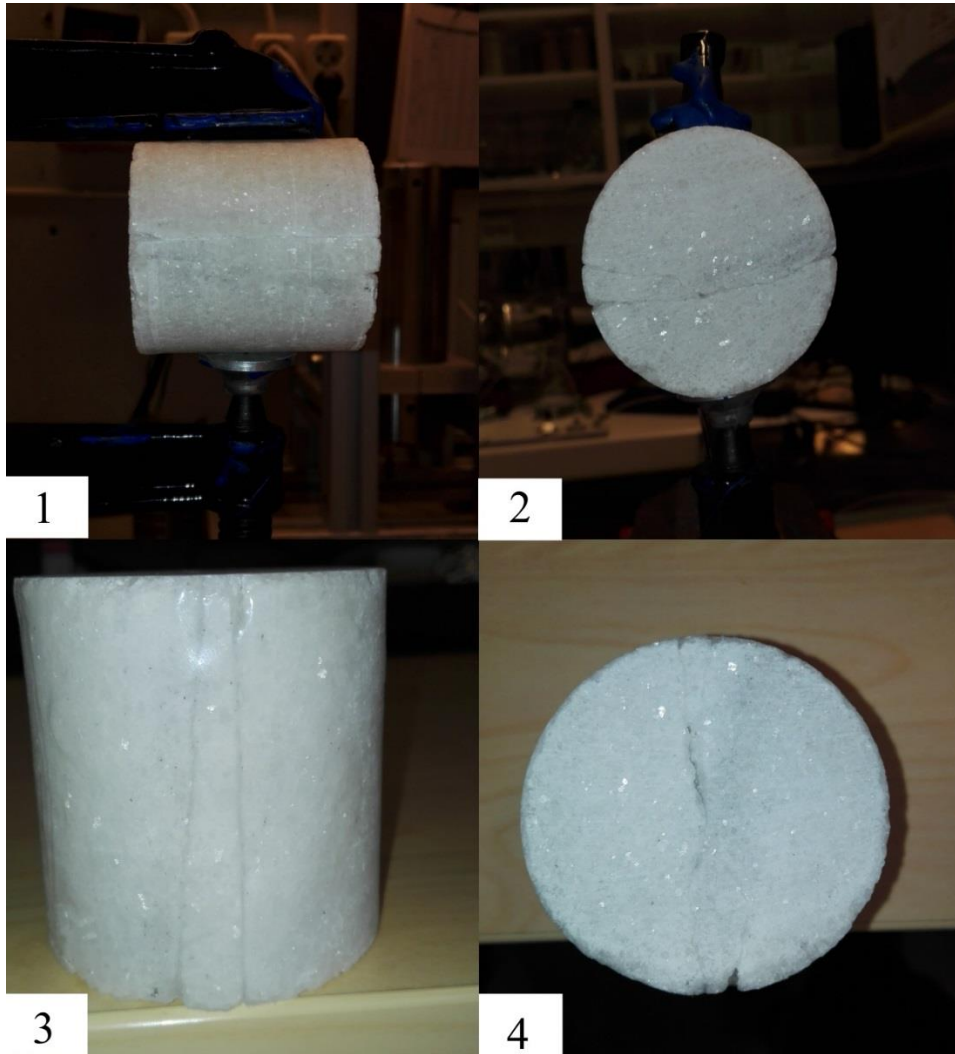
Figure 7-6: Assembling of a core segment. In picture 1 and 2 the core is placed in an f-clamp ready to apply epoxy on the outside. In picture 3 and 4 the epoxy has been applied to the outside of the fracture. Picture 4 show that no epoxy is covering the end of the segment.

During the first step described above, shown in **Figure 7-6**, an important criterion is that there is no intrusion of epoxy into the tight fractures. A test sample was fractured and reassembled with the epoxy, as described above. After the epoxy was completely solidified, it was cracked open to investigating possible epoxy intrusion. There was no significant epoxy intrusion, and this method was therefore chosen for all other samples.
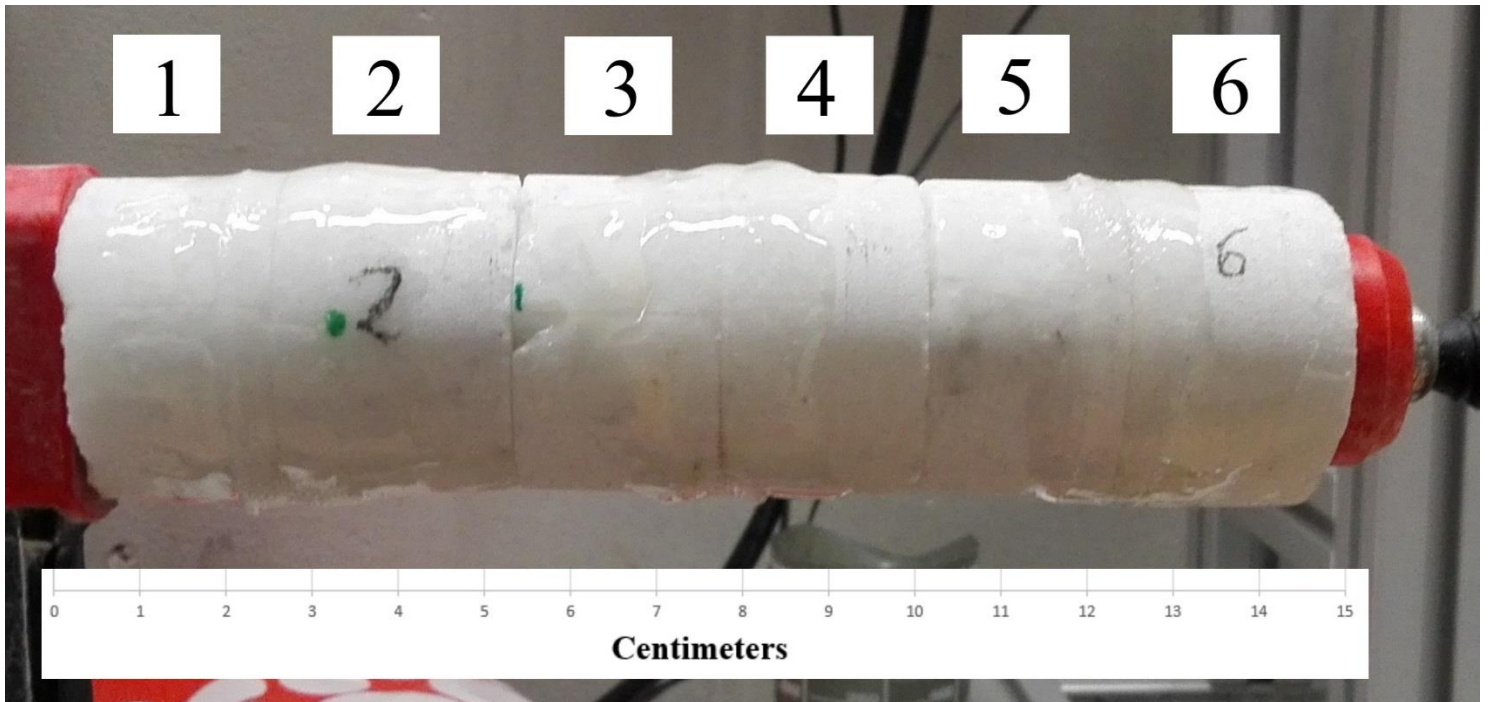
Figure 7-7: Assembling of the fractured marble core. Each segment (1-6) is approximately 2.5 cm long and the whole core is 15 cm long. This picture was taken when the joint between segment 1-2, 3-4 and 5-6 had been attached as described in paragraph 2 above. The joints between segment 2-3 and 4-5 are ready to be glued.

The different assembling methods can be divided into three groups, where different setups were used: Hassler core holder, shrink-sleeve, and epoxy. Each has its own positive and challenging aspects.

- Hassler core holder: all open and partially open fractures were used in a hassler core holder. Hassler core holders are made of metal and can therefore not be used during PET/CT scans. The overburden pressure is adjusted by a hand pump; this can result in difficulties in performing all experiments at the same overburden pressure. The overburden pressure ensures all flow going through the core, and do not bypass in any way.

- Shrink-sleeve: No metal, and can therefore be used during PET/CT scanning. There is, however, no overburden pressure with the shrink-sleeve. This can result in changes in capillary pressure in the fractures, and flow outside the core.

- Epoxy: Epoxy can be used to block wide fractures, i.e. generating tight fractures. The epoxy can contain higher pressures (8 bar was tested without any leakage). No metal, can therefore be used in the PET/CT scanner. Flow bypassing the fracture network is highly unlikely.

38

8. Fluids

An overview of all fluids used in this thesis is shown in **Table 8-1**. Two brines were used, a sandstone brine with 1wt% NaCl and a chalk brine with 5wt% NaCL and 5wt% $CaCl_2*2H_2O$. The surfactant solution was a mixture of 1wt% Huntsman SURFONIC® L24-22 surfactant in the brine used during baseline. The University of Bergen has field pilot in East Seminole, Texas, USA. This is a carbonate reservoir, and the decision to use Huntsman SURFONIC® L24-22 in the pilot have already been taken. To maximize the possibility of using result or conclusions from this thesis in the field pilot the same surfactant was therefore used in all experiments.

All experiments were performed at room temperature (20-22°C) and at elevated pressures between 1 and 6 bar. The gas used in all experiments was N_2, because the experiments were done below supercritical condition for CO_2. Below supercritical conditions N_2 will behave as CO_2. This thesis focuses on foam generation and foam properties, and CO_2 is therefore not necessary.

Table 8-1: An overview of the different liquids used in this thesis

Fluid	Composition
Sandstone Brine	1wt% NaCl in distilled water
Chalk Brine	5wt% NaCl, 5wt% $CaCl_2*2H_2O$ in distilled water
Sandstone surfactant solution	1wt% Huntsman SURFONIC® L24-22 in sandstone brine
Chalk surfactant solution	1wt% Huntsman SURFONIC® L24-22 in chalk brine
Gas	Nitrogen, N_2

The L24-22 surfactant is stored as a wax like substance and does not easily mix with water. A magnetic stirrer was therefore used to stir the mixture for approximately 12 hours to make sure all surfactant were dissolved.

9. Preparations

Before baseline or foam experiments were conducted essential fracture values where obtained. The bulk volume, fracture volume and fracture conductivity (permeability) were measured.

9.1. Saturating the Fracture Network

To measure fracture volume and conductivity, the fracture network must be saturated. This was done by removing the air inside the cores by a vacuum pump and then exposing the cores to brine. A step by step instruction is as follows:

1. The core was connected to the vacuum pump. When a hassler core holder was used, a confinement pressure was applied before the vacuum pump was started. The vacuum pump was run until the pressure reached 200mTorr. The valve connecting the core to the vacuum pump was closed.

2. A beaker with brine was vacuumed to remove trapped air inside the brine.

3. The vacuumed core was placed vertically. The lower end was connected to a tubing going into the brine. A syringe was used to fill the tubing with brine to avoid any air entering the fractured network, see **Figure 9-1**.

4. The beaker with brine was placed on a scale, and the valve to the core was opened. The brine flooded the core from the bottom up, and the volume of brine removed from the beaker was measured.

5. The fracture volume was determined from the weight difference. Cores utilizing POM end-pieces and epoxy/shrink-sleeve were weighted before and after saturation.
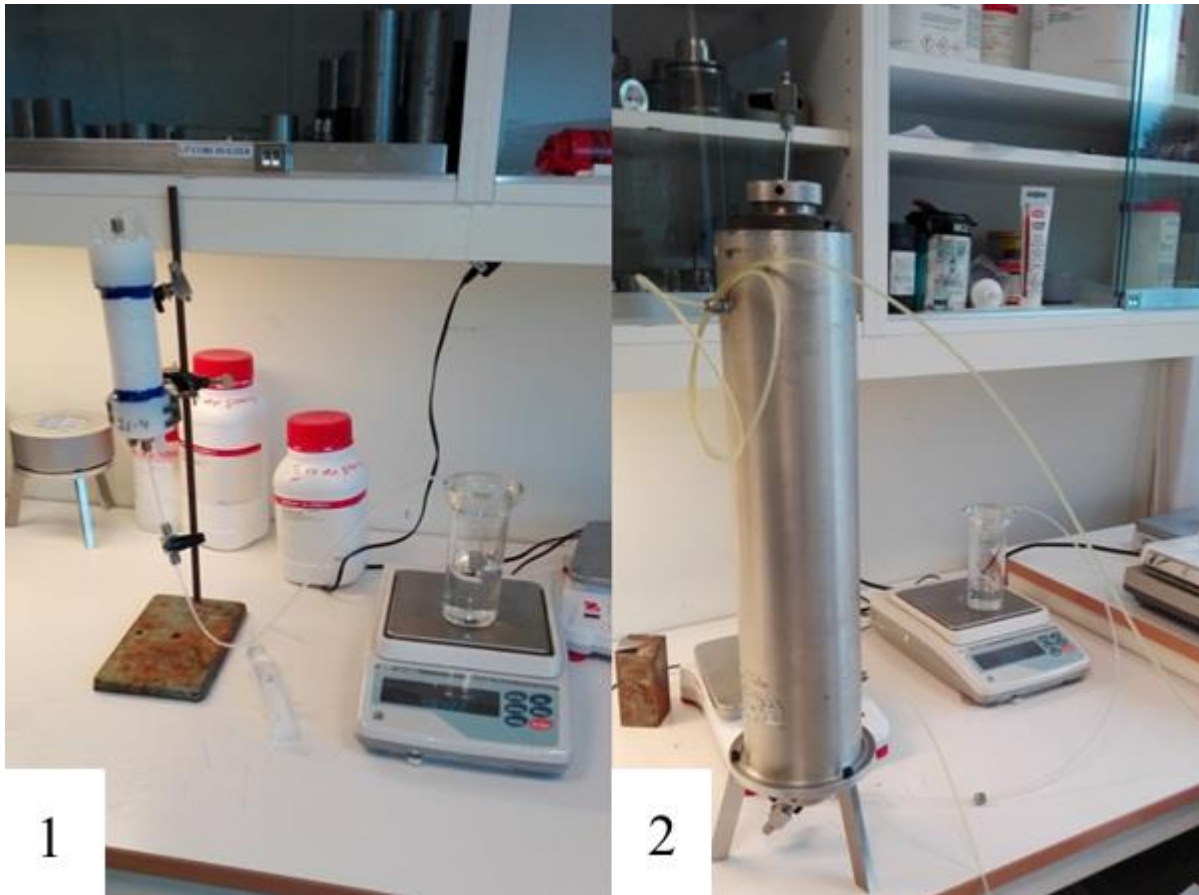
Figure 9-1: Saturating cores. 1) Saturating of a core without core holder. 2) Saturating of a core inside a core holder. Water enters the fracture network from the bottom by vacuum.

9.2. Measure Fracture Volume

The fracture volume was measured by the saturation method. By saturating the fracture network with a fluid of known density, the void-space can be found by the weight difference between a dry and saturated core. The equation used for calculating the fracture volume is equation (6):

$$V_f = \frac{w_{sat} - w_{dry}}{\rho}$$

(6)

Here V_f [ml] is the fracture volume, w_{sat} and w_{dry} [g] is the weight of the core before and after saturation, ρ [g/ml] is the density of the fluid which the core has been saturated with. The subscript *sat* and *dry* stands for saturated and dry respectively.

9.3.   Fracture Conductivity

Fracture conductivity is a measurement of the fractures ability to transport fluids. This can be compared to the permeability of porous media. The absolute permeability is a measurement of the transmissibility with only one fluid present. The conductivity of each core was measured after saturation, i.e. the fracture was totally saturated with brine. The conductivity was measured by injecting brine with a Pharmacia P-500 pump at several different liquid rates. The differential pressure was measured during the injection with two ESI pressure transducers; one at the inlet and one at the outlet. The conductivity/permeability was then calculated using Darcy's law for uncompressible fluids and horizontal flow, shown in equation (7).

$$q = -\frac{K}{\mu}\nabla P \qquad\qquad (7)$$

Where q [cm/s] is the flux, K [D] is the absolute permeability, μ [Pa ·s] is the fluid viscosity, and ∇P [Pa/cm] is the pressure gradient. To get high accuracy on the measurement the same core where measured several times with different liquid rates. Afterward, the mean value was used and uncertainties where calculated by equations in **Appendix C** . The permeability was measured with sand stone brine or chalk brine at room temperature (20℃).

10. Procedures

In this chapter, all experimental setups and procedures will be described. An overview of all experiments with details of fracture category, confinement method and injection strategy is also shown in Table 10-1 and Table 10-2.

10.1. Performing Co-Injection Into Fractured Networks

The same experimental setup was used for all core floods, with minor variations. N_2 gas was injected into the fracture network simultaneously to brine, for baseline experiment, or surfactant solution to form foam. **Figure 10-1** gives an overview of the experimental setup. The same setup was used for all cores, with the only difference being the use of core holder for in some experiments and epoxy cores/shrink-sleeve in other experiments.
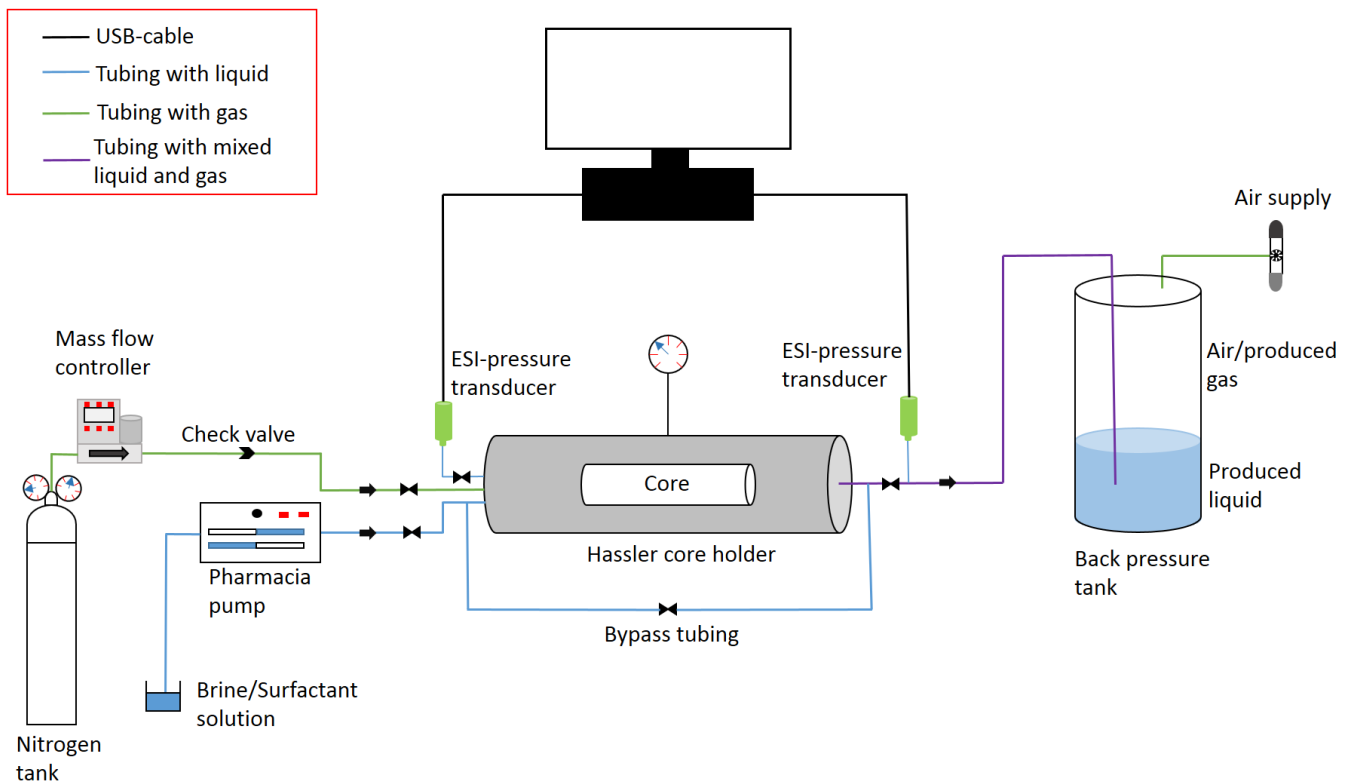

Figure 10-1: Illustration of the experimental setup used for co-injection of liquid (brine or surfactant solution) and N_2 gas. Arrows indicate the direction of flow, black crosses indicate valves and an overview of what the different colors represent is shown in the upper left corner. The Hassler core holder was substituted by cores in epoxy or shrink-sleeve.

List of equipment used

- Fractured marble core in core holder, shrink-sleeve or epoxy with different fracture apertures.
- 2 pcs ESI Digital USB pressure transducers, range 0-10 bar
- N_2 gas with gas regulator
- Air pressure supply with regulator – for back pressure
- 1/8 tubing with Swagelok fittings and Swagelok valves
- Mass flow controller (either Alicat MC Mass Flow Controller or Bronkhorst EL-FLOW Select Series Mass Flow Controller)
- Check valve (to avoid backflow into mass flow controller)
- Pharmacia LKB P-500 pump
- Back pressure tank 20L (used to contain constant back pressure)
- Computer (to measure pressure and regulate gas flow)

10.2. Description of Experimental Procedure

All tubing were saturated with water (except the tubing injecting N_2 gas). For the cores in the Hassler core holder, a confinement pressure of approximately 10 bar was applied (with some exceptions, seen in Table 10-2). This was done to prevent fluid flow bypassing the core, i.e. all injected fluids went through the fractured network. Reitsma and Kueper (1994) found that the capillary pressure inside a fracture increased as normal stress applied to the fracture increased, care was therefore taken to ensure a constant confinement pressure throughout all similar experiments. Differences in capillary pressure could potentially have large impacts on experimental results. Tubing from the Pharmacia pump and tubing from the mass flow controller was connected to the inlet end-piece separately. This was to ensure a consistent gas fraction throughout the injections. Tubing from the outlet end-piece was attached to a back pressure tank. Two ESI pressure transducers were connected, one at the inlet and one at either side of the core.

All cores were initially flushed with several fracture volumes of N_2 or surfactant solution, to establish the desired start saturation. (some experiments were performed using increasing, and some using decreasing gas fraction). This was done to ensure that the initial saturation, assumed to be either fully saturated with gas or surfactant was achieved, ensuring minor influences by hysteresis. There is a chance that there could be some connate gas or liquid at the start of experiments, however, this was estimated to be of insignificant proportions, due to the nature

of fractures. Connate gas or liquid is significant in porous media due to capillary trapping in pores, however this is not likely to occur in fractures.

The Pharmacia pump or mass flow controller was started, depending on the initial saturation of the fractured network (either gas or liquid), and the air supply to the back pressure tank was opened. The pressure in the back pressure tank was steadily increased until the desired back pressure was reached. Back pressure was used to reduce gas compressibility, which in turn make the whole system more stable and ensure control of foam quality. Without the back pressure, large velocity variation in the production tubing together with severe fluctuations in absolute pressure were observed. This is believed to be caused by gas compressibility effects (Rossen, 1990, Buchgraber et al., 2012).

When both initial saturation and desired back pressure was in place the experiment was ready to start. The experiments can be divided into four different types:

- Increasing or decreasing gas fraction
- Constant gas fraction, with increasing injection rate
- Constant liquid rate with increasing gas rate
- Constant gas rate with increasing liquid rate

The predefined injection strategy was started. Once the initial conditions were stable, i.e. stable differential pressure was measured, the gas fraction or injection rate was changed. The changes were done in pre-defined increments, and the new conditions were run until the system once again was stable. This method was performed throughout all experiments. An overview of experiments with either constant liquid rate with increasing gas rate or constant gas rate with increasing liquid rate is shown in Table 10-1. Experiments with increasing gas fraction, decreasing gas fraction and constant gas fraction can be seen in Table 10-2.

Table 10-1: An overview of experiments with either constant liquid rate with increasing gas rate or constant gas rate with increasing liquid rate

Core	Fracture category	Baseline /foam	Back pressure	Confinement	Liquid rate [ml/h]	Gas rate [ml/h]
2i-3	partially open	foam	4 bar	Core holder at 10 bar	9	3 to 900
2i-3	partially open	foam	4 bar	Core holder at 10 bar	18	3 to 300
2i-3	partially open	foam	4 bar	Core holder at 10 bar	28	3 to 900
2i-3	partially open	foam	4 bar	Core holder at 10 bar	36	3 to 900
2i-3	partially open	foam	4 bar	Core holder at 10 bar	54	3 to 900
2i-3	partially open	foam	4 bar	Core holder at 10 bar	3 to 100	18
2i-3	partially open	foam	4 bar	Core holder at 10 bar	3 to 100	42
2i-3	partially open	foam	4 bar	Core holder at 10 bar	3 to 100	84
2i-3	partially open	foam	4 bar	Core holder at 10 bar	3 to 300	114

Table 10-2: An overview of all experiments with increasing, decreasing or constant gas fraction

core	Fracture category	Baseline /foam	Back pressure	Confinement	Rate [ml/h]	Gas fraction
2i-1	open	foam	4 bar	Core holder at 10 bar	13 to 120	0.7
2i-1	open	foam	4 bar	Core holder at 10 bar	13 to 120	0.7
2i-1	open	foam	4 bar	Core holder at 10 bar	13 to 120	0.7
2i-1	open	foam	6 bar	Core holder at 10 bar	13 to 120	0.7
2i-2	partially open	baseline	6 bar	Core holder at 25 bar	180	0→1, step 0.1
2i-2	partially open	baseline	6 bar	Core holder at 25 bar	180	0→1, step 0.1
2i-2	partially open	baseline	6 bar	Core holder at 25 bar	120	0→1, step 0.1
2i-2	partially open	baseline	2 bar	Core holder at 25 bar	120	0→1, step 0.1
2i-3	partially open	foam	4 bar	Core holder at 10 bar	3.6 to 180	0.7
2i-3	partially open	foam	4 bar	Core holder at 10 bar	180 to 3.6	0.7
2i-4	smooth	baseline	1 bar	shrink-sleeve	50	0→1, step 0.1
2i-4	smooth	baseline	1 bar	shrink-sleeve	100	0→1, step 0.1
2i-4	smooth	baseline	1 bar	shrink-sleeve	150	0→1, step 0.1
2i-4	smooth	baseline	1 bar	shrink-sleeve	50	1→0, step 0.1
2i-4	smooth	baseline	1 bar	shrink-sleeve	100	1→0, step 0.1
2i-4	smooth	baseline	1 bar	shrink-sleeve	150	1→0, step 0.1
2i-4	smooth	foam	1 bar	shrink-sleeve	50	0→1, step 0.1
2i-4	smooth	foam	1 bar	shrink-sleeve	50	1→0, step 0.1
2i-4	smooth	foam	1 bar	shrink-sleeve	100	0→1, step 0.1
2i-4	smooth	foam	1 bar	shrink-sleeve	100	1→0, step 0.1
2i-4	smooth	foam	1 bar	shrink-sleeve	150	0→1, step 0.1
2i-4	smooth	foam	1 bar	shrink-sleeve	150	1→0, step 0.1
2i-4	smooth	foam	1 bar	shrink-sleeve	150	0→1, step 0.1
1.5i-2	tight	baseline	1 bar	epoxy	150	0→1, step 0.1
1.5i-2	tight	baseline	1 bar	epoxy	150	1→0, step 0.1
1.5i-2	tight	baseline	1 bar	epoxy	100	1→0, step 0.1
1.5i-3	tight	baseline	1 bar	epoxy	100	0→1, step 0.1
1.5i-3	tight	baseline	1 bar	epoxy	100	1→0, step 0.1
1.5i-3	tight	foam	1 bar	epoxy	100	0→1, step 0.1
1.5i-3	tight	foam	1 bar	epoxy	20	1→ 0, step 0.1
1.5i-4	tight	baseline	1 bar	epoxy	10	0.9→0.3
1.5i-4	tight	foam	1 bar	epoxy	10	0.9→0.3
1.5i-4	tight	foam	1 bar	epoxy	10	0→ 1, step 0.1

10.3. Visualization of Foam Flow by PET/CT

A common challenge during experiments on core samples is to quantify foam behavior *in-situ*. To visualize foam flow micromodels of visible materials is often used. This is however not on the same scale as cores, and not necessarily comparable. Another challenge with micromodels is that they are not made of the same surface material as is found in reservoirs. Fractured tile models have been used to visualize foam flow in open fractures by Brattekås and Fernø (2016). This is a good method for visual investigation of foam behavior in open fracture, but not for tight fractures. To visualize foam distribution, foam propagation and quantify *in-situ* saturations in tight fractures a PET/CT-scanner was used. A picture of the experimental set-up is shown in **Figure 10-2**.

Figure 10-2: Experiments were done inside a PET/CT -scanner. The fractured core was placed on a modified "bed" originally designed for rats. The "bed" with the fractured core was then wrapped in plastic in case of leakage. A leakage inside the PET/CT machine could potentially damage or destroy the machine. All other equipment (pump, pressure transducer, vacuum pump, mas flow controller, laptop, and liquids) was placed on a table next to the PET/CT-scanner and was connected to the core with tubing.

List of equipment used

- InterView fusion software

- Mediso nanoScan® PET/CT, small animal PET/CT scanner

- FDG (^{18}F-fluorodeoxyglucose) radioactive isotope mixed in brine/surfactant solution

- Fractured marble core

- 2 pcs ESI Digital USB pressure transducers, rage 0-10 bar

- N$_2$ gas with gas regulator

- Air pressure supply with regulator

- 1/8 tubing with Swagelok fittings and Swagelok valves

- Check valve (to avoid backflow into mass flow controller)

- Pharmacia LKB P-500 pump

- Back pressure tank 20L (used to contain constant back pressure)

- Computer (to measure pressure)

- Mass flow controller (Alicat MC Mass Flow Controller)

- Core bed

Description of experimental procedure

The experimental setup used is equal to **Figure 10-1** except a few changes. Fractured cores with epoxy as confinement were used, and the bypass was removed to avoid metal. The fractured cores where mounted on the core bed and the bed was attached to the PET/CT-scanner. Before the fractures were saturated with brine, a dry CT scan was acquired to describe the fractured network. The tube voltage was not high enough to correctly visualize the fractured network, due to poor resolution and beam hardening. Beam hardening is caused by attenuation of X-ray photons, which is particularly a problem in materials with high atomic numbers such as bone or metal (Boas and Fleischmann, 2012). The use of CT in this thesis is therefore limited to core positioning and back ground picture to PET measurements. No direct analyses of CT images were performed. The fractured core was then vacuumed and saturated with brine. A CT-scan of the saturated core was then taken.

At Haukeland University Hospital they have a cyclotron which produces ^{18}F. The ^{18}F was then used to synthesize ^{18}F-fluorodeoxyglucose (FDG). A delivery of FDG was received in an ampoule inside a lead container with an activity of 200MBq. A syringe was used to extract the FDG and mix it with the injection fluid. A liquid-liquid displacement was then preformed where

the radioactive brine displaced the regular brine. This was done to investigate the preferred liquid flow path and the liquid sweep during miscible displacement. Afterwards, the radioactive brine was displaced with regular brine, to bring the system back to the initial conditions before baseline co-injection was performed.

Both baseline and surfactant co-injection was performed with PET acquisition. Due to the short half-life of FDG, $t_{1/2} = 109min$, only a limited number of experiments could be performed. Experiments with decreasing gas fraction was chosen, where gas fraction 0.9, 0.8, 0.7, 0.5 and 0.3 were performed. The distribution of gas fraction was chosen to focus on high-quality foam, because this is most interesting on field scale.

Part III – Results and Discussion

11. Foam Behavior in Fractures with Varying Apertures

Foam is a well-known method for reducing gas mobility. However mechanisms for foam generation and reduced gas mobility in fractures is not fully understood. The following chapters investigate differences in foam generation and behavior in open, partially open, smooth and tight fractures.

The experiments focused on foam behavior at different velocities and gas fractions in the different fractures. *In-situ* imaging applying PET/CT was used to investigate foam behavior in tight fractures. Foam quality was also assessed in many experiments by visual inspection of the produced foam in the outlet tubing.

In the first sub chapter, **11.1**, co-injection of increasing total volumetric rate were conducted to investigate a possible critical velocity for foam generation in open fractures. In sub chapter **11.2** foam behavior at different gas and liquid velocities were investigated. This was done to study foam behavior in high- and low-quality foam regions. In the next two chapters **11.3** and **11.4** foam generation and behavior in smooth and tight fractures were investigated. The following chapter, **11.5**, correlates the results obtained so far. This is done by evaluating MRF and apparent viscosity in tight, open and smooth fractures. Partially open fractures were not included in this comparison. This was because the partially open system was used to evaluate flow at increasing liquid and gas velocities, and did not have sufficient data for calculation of MRF.

PET/CT results are evaluated and discussed in **11.6** and finally a general summary of results are made in chapter Error! Reference source not found..

11.1. Minimum Velocity for Foam Generation in Open Fractures

Several experiments with varying gas fractions were performed by previous master students Johansen (2016) and Vasshus (2016), who found clear indications of foam generation in open fractures. The preferred gas fraction found to generate foam in open fractures was $f_g = 0.7$.

This thesis is a continuation of the previous experiments, aimed to explain the influence of fracture aperture on foam generation and behavior. Johansen (2016) and Vasshus (2016) showed, by performing experiments on different scales, that results obtained on small fractured core samples were valid and descriptive of flow in larger fractured networks. The experiments in this thesis, therefore, used 1.5 and 2 inch fractured networks. To further investigate the results obtained by Johansen and Vasshus new experiments on the same fractured core, 2i-1, was

performed. The purpose of the new experiments was to investigate a possible minimum velocity for foam generation in open fractures. Foam formation in fractures is generated by snap-off (Kovscek et al., 1995); snap-off is reported to require a minimum velocity to occur (Ransohoff and Radke, 1988). Co-injection started at 12ml/h and was increased in pre-defined increments. Co-injection continued at each rate until a stable differential pressure was reached. The measured pressure gradients are plotted as a function of rate in **Figure 11-1**.
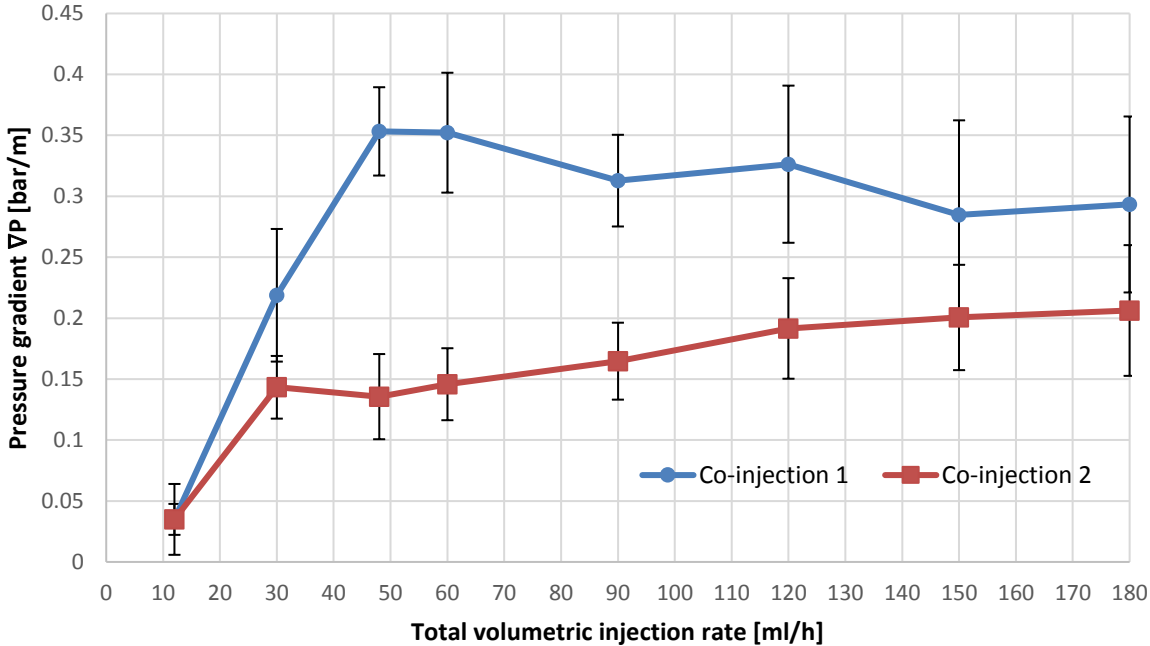

Figure 11-1: Differential pressure measured in core 2i-1 with gas fraction 0.7. Total velocity was increased in pre difened increments. These experiments were conducted at 15 bar confinement pressure, and therefore permeability 3.94 [D], which is lower than what is listed in Table 7-1. **The differences in the co-injections is not fully understood, but could occur from differences in confinement pressure and/or internal changes due to reaction between the brine and rock surface.**

A significant increase in the differential pressure was observed as the volumetric rate increased. The calculated uncertainties are the standard deviation of the pressure measurements during stable conditions, see **Appendix C** for equations. Throughout the experiments fluctuations in the pressure measurements were observed, especially prominent at flow rates above 120ml/h, resulting in relatively large uncertainties. At these rates unstable flow in the tubing was observed; flow could stop and then suddenly seem to "let go" and flow at very high velocity. Fast flowing foam in the production tubing was followed by a sudden decrease in pressure, probably caused by gas slippage effect (Prud'homme, 1995) and/or gas compressibility effects (Rossen, 1990).

There is a noticeable difference between co-injection 1 and 2. Both co-injections experience an increase in differential pressure at the first increase in volumetric rate. At volumetric rates above 30ml/h the co-injections exhibit different trends. Co-injection 1 reached its maximum differential pressure at approximately 50-60ml/h and then experienced a decreasing trend. Co-injection 2 have a slight reduction in the differential pressure at 50ml/h, but then show an increasing trend in the differential pressure. The reason behind this difference is not fully understood, but two reasons are proposed. The difference could come from differences in the confinement pressure. The confinement pressure was adjusted with a hand-pump and differences in the confinement pressure could inflict large differences in the capillary pressure in fractures. Another possibility could be differences is snap of sites. During these co-injections sandstone brine was used, in chapter **11.7** it is proven that there is a reaction between sandstone brine and the marble surface. This could result in fewer snap-off sites in the second co-injection, resulting in reduced foam generation.

By plotting the apparent viscosity, calculated by equation (4), for the same experiment (**Figure 11-2**) further indications of a critical velocity for foam generation in fractures are apparent. There is a significant increase in the apparent viscosity from low to medium rates. Above rates in the range of 30-50ml/h a decreasing apparent viscosity was observed, attributed to the shear thinning behavior of foam.
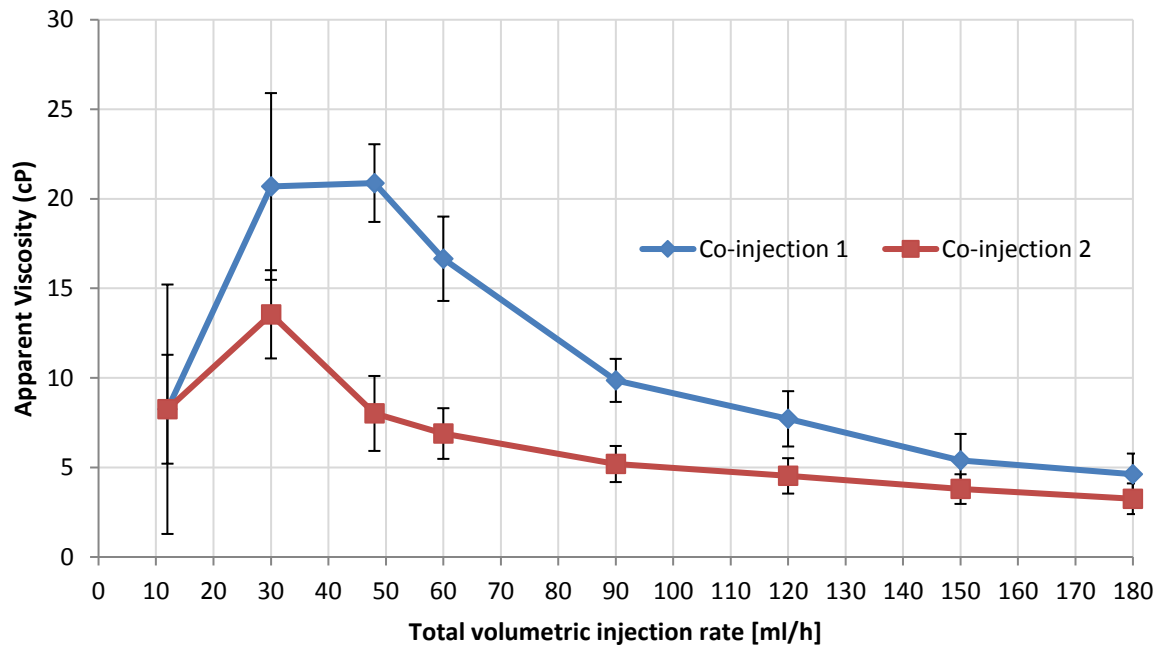
Figure 11-2: Apparent viscosity measured in core 2i-1 with f_g = 0.7. **Total volumetric velocity was increased in pre defined increments and held until stable pressures where observed. Uncertainties calculated by standard deviation through stable regions. These experiments were conducted at 15 bar confinement pressure, and therefore permeability 3.94 [D] which is lower than what sowed in** Table 7-1. **The differences in the co-injections is not fully understood, but could occur from differences in confinement pressure and/or internal changes due to reaction between the brine and rock surface.**

11.2. Gas Fraction Impact on Foam Flow in Partially Open Fractures

Experiments conducted by Osterloh and Jante (1992) found a limiting capillary pressure dictating the behavior of foams in a porous medium. By plotting the differential pressure in a contour plot, with liquid velocity and gas velocity as the x- and y-axis respectively, the characteristic "L-plot" appears. Drawing a straight line from origo through the sharp angle of the pressure contours marks the gas fraction differentiate, f_g^*, separating the weak and strong foam regions (Martinez, 1998). Experiments were performed to investigate whether foam behavior in fractures behave comparably to foam in porous media.

To investigate foam behavior in partially open fractures and generating the contour plot, core 2i-3 was used. Core 2i-3 was made by three individual core segments, which were fractured separately. The segments were stacked so that the fractures were oriented perpendicular to each other. The experiments were performed by co-injection of surfactant solution and N_2 gas. The liquid rate was held constant, and the gas volumetric rate was increased in pre-defined increments. The procedure was repeated several times using different liquid rates. **Figure 11-3** show a clear pressure trend during the co-injection; pressure increase as the gas velocity increase until it reaches a maximum differential pressure. After the maximum differential

pressure is reached the pressure decrease and stabilizes at a constant level. This tendency correlates the theory of the limiting capillary pressure (Martinez, 1998). When the gas fraction exceeds the limiting capillary pressure, coalescence will occur; coalescence will increase gas mobility, resulting in decreased gas fraction *in-situ*. The effect is described in **4.9**. Flow Regimes.
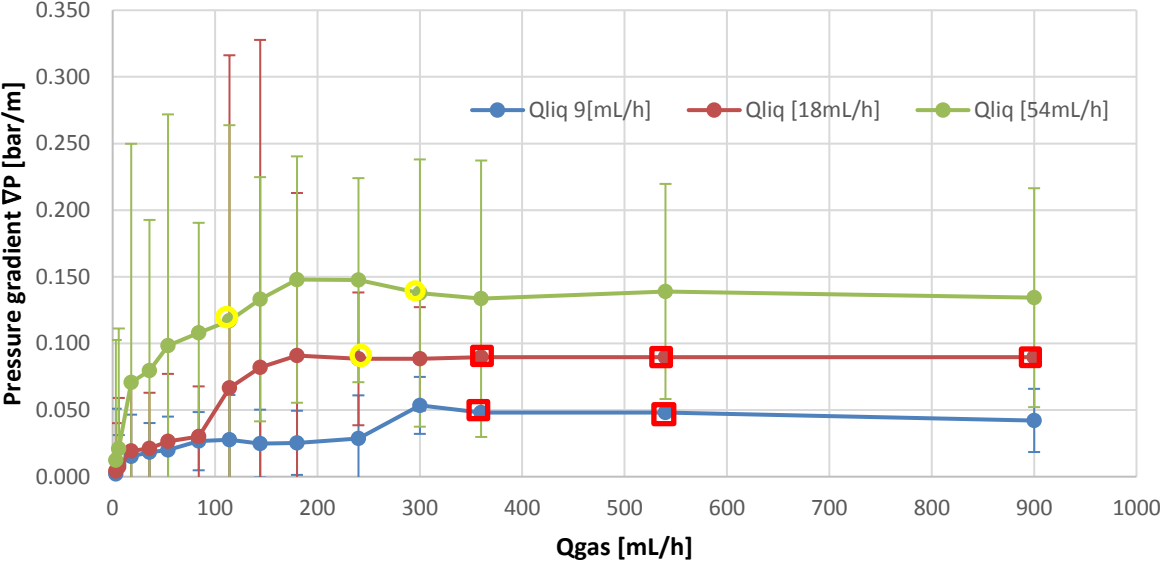

Figure 11-3: Pressure gradient [bar/m] measured with increasing gas fraction in core 2i-3. An increasing pressure gradient is observed until gas velocities reach 200-300ml/h. The pressure gradient is stable above these velocities and does not increase with increased gas velocity. The pressure measurements marked with yellow dots were smoothed to align with the overall pressure trend. This was necessary to create the L-plot. These adjustments were only made within experimental uncertainties to objects not fitting to the general trend of the plot. Five pressure readings are extrapolated from the general trend; these are marked with red squares. Uncertainties were calculated by standard deviation of several pressure measurements at stable conditions.

To generate a proper L-plot, a few pressure gradient measurements were smoothed (marked with yellow circles in **Figure 11-3**). Small deviations in the measured differential pressure in Figure 11-3 will have a significant impact when generating a contour plot form the results. The experiment with constant liquid rate 9 and 18ml/h did not contain all gas fraction between 300 and 900ml/h. Artificial pressure readings were added to generate a complete plot; these are marked with red squares in **Figure 11-3**. Raw data for the experiment can be found in **Appendix D** .

The results in **Figure 11-3** were used to generate a contour plot, shown in **Figure 11-4**. A clear and characteristic L-plot shape, as Osterloh and Jante (1992) found in sand packs was observed. The straight lines added to the plot indicates the gas fraction where the change between high- and low-quality foam occurs. The gas fraction differentiate seemed to depend on the liquid rate.

It is set at $f_g^* = 0.89$ below liquid rate 15ml/h and gradually increasing to $f_g^* = 0.82$ at liquid rate above 45ml/h. It may look as the f_g^* lines do not start in origo, however, this is because the figures start at the liquid velocity of 9ml/h. A figure of the plot with origo in the lower left corner is shown in **Appendix D**
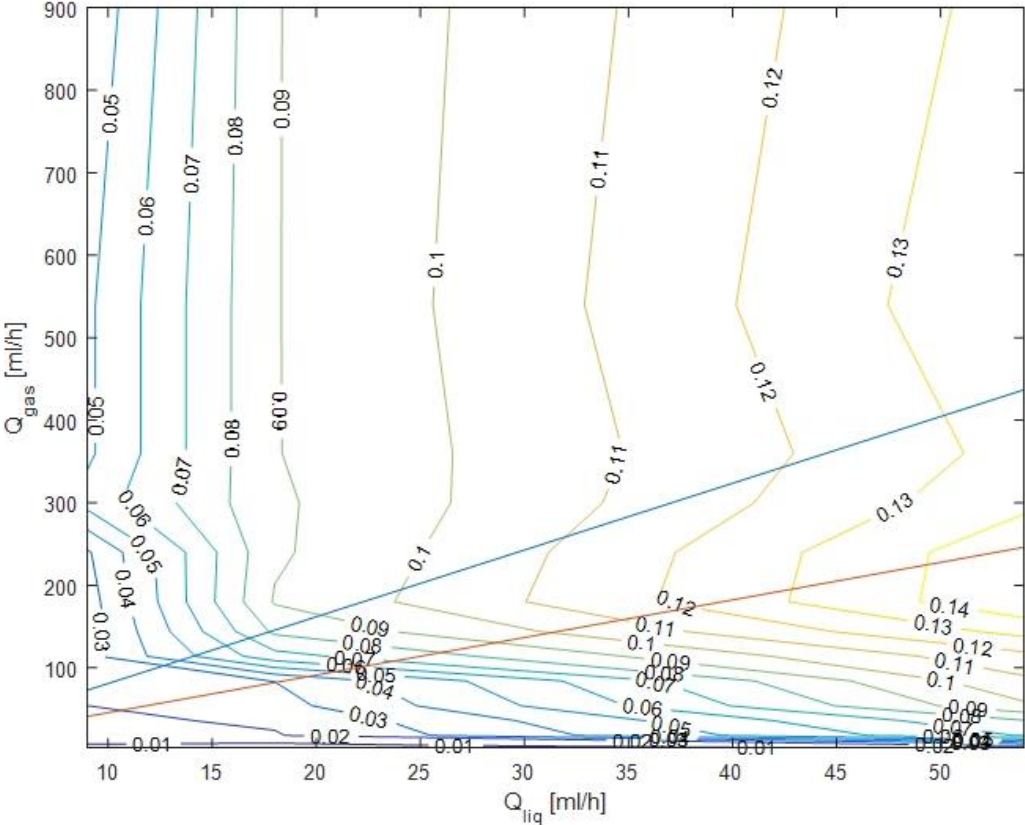

Figure 11-4: Contour plot made from measurements with constant liquid rate and increasing gas rate in core 2i-3. In the high-quality foam region the trend in the contours is similar that found in a porous media. For the low-quality foam region, however, a slightly dipping trend is observed. The contours are the pressure gradients, ∇P [bar/m]. The straight blue line is $f_g = 0.89$ and the straight brown line is $f_g = 0.82$

The contour plot generated by the measurements in **Figure 11-3**, have a clear and distinctive "L-plot" shape. The pressure trend is similar to the trend in a porous medium and is evident sign of foam generation in fractures. A clear correlation between foam flow in fractures and porous media is observed, e.g. a clear difference between high- and low-quality foam. In the high-quality foam regime (above f_g^*) the pressure trend is equal to that found in porous media; vertical pressure contours. In the low-quality foam regime (below f_g^*), the behavior of foam in fractures deviates from the accepted foam behavior in porous media (Osterloh and Jante, 1992): in sand packs, straight, strictly horizontal pressure contours were observed. In Figure 11-4, the contour lines in the low-quality foam region show a clear dipping trend. This dipping trend is

emphasized in **Figure 11-5**. In porous media, the pressure drop for low-quality foams is found to be dependent on gas velocity only, hence strictly horizontal. Dipping pressure contours illustrates a different dependency for foam formed and travelling in fractures. The trend indicates that low-quality foam behavior in fractures is dependent on both the liquid and the gas velocity. This is the most striking result in this thesis, and is to my knowledge never observed or discussed before.

The reason for horizontal pressure contours in the low-quality foam region in porous media is due to fixed bubble size at roughly pore size (Alvarez et al., 2001). This may explain why the differential pressure in the low-quality foam region is dependent on both gas and liquid velocities in fractures: without pores bubble sizes will not be fixed at pore size. Further investigation is necessary to investigate and confirm this hypothesis, and to reveal the mechanisms involved.
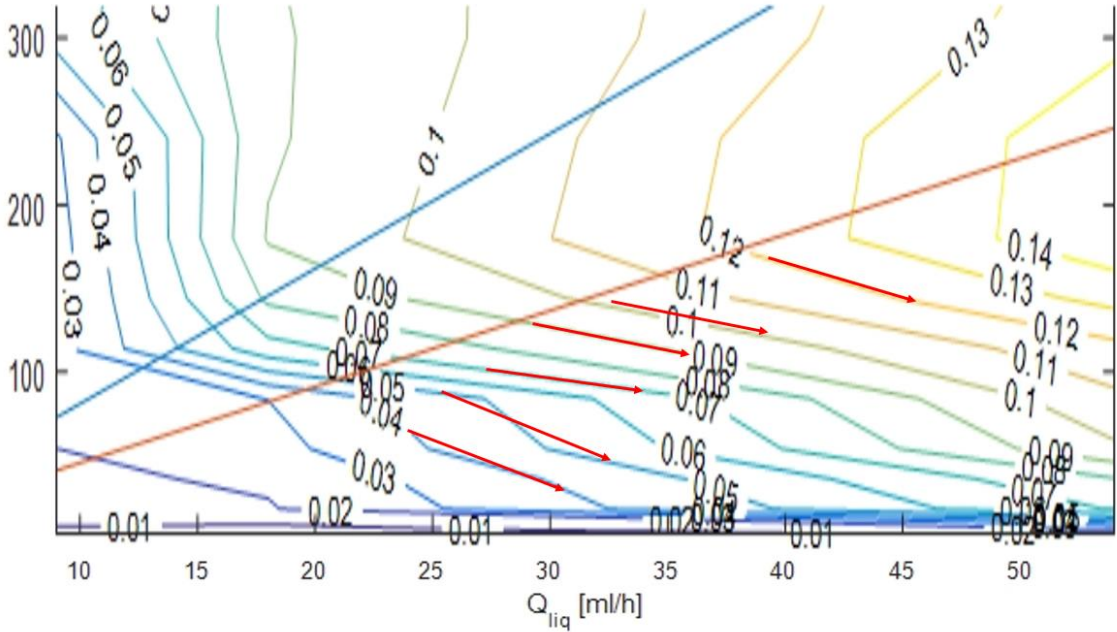
Figure 11-5: A picture of the low-quality foam region from Figure 11-4 which emphasize the dipping trend. The dipping trend of the pressure contours are indicate by the red arrows.

In **Figure 11-4**, f_g^* is found between gas fraction 0.89 and 0.82, which is lower than what Osterloh and Jante (1992) found in sand packs, where f_g^* was 0.94 to 0.96. Pancharoen et al. (2012) estimated f_g^* to be as high as 0.99 in fractures. This does not correlate to the result obtained in this thesis, but could potentially vary a lot depending on fracture characteristics. In

chapter **4.13**. it is found that the capillary pressure in fractures vary as normal stress is applied. This can possibly impact foam generation and behavior in fractures, hence inflict at which gas fraction f_g^* is found. This may result in large variation in f_g^* depending on the fracture characteristics. Further investigations of f_g^* in different fracture types is necessary to draw any conclusions.

11.3. Foam Generation in Smooth Fractures

Co-injection with varying gas fractions at constant volumetric rate was performed using core 2i-4. Core 2i-4 had the same configuration as 2i-3, and their permeabilities are equal within experimental uncertainties. Core 2i-3 was placed inside a core holder during co-injection while core 2i-4 was placed in a shrink-sleeve. The shrink-sleeve was not strong enough to withstand the internal fluid pressure. Flow of both gas and liquid was observed between the shrink-sleeve and core. The flow between the sleeve and core resulted in low to no foam generation. This is seen by the differential pressure plotted **Figure 11-6**, where no significant difference between baseline and foam flow was seen. The gap between the shrink-sleeve and marble surface still constitute a fracture. Both the outside of the core, which was drilled with diamond coated bit, and the shrink-sleeve have smooth surfaces (compared to real rock fractures). This can therefore be seen as flow in smooth fractures. Visual observation of the fractured core indicated vertical segregation. Gas flow was mainly seen in the upper part whereas liquid flow was concentrated in the lower parts of the fractured core. The areas where there were both gas and liquid flow was characterized by shifting saturation; gas displaced water and vice versa. This form of displacement did not seem to generate sufficient mixing for foam generation to take place. Previous experiments conducted by Haugen (2012) found that smooth fractures did not enable sufficient mixing to generate foam. There are also none or few foam generation sites present, which is necessary for foam generation to occur in fractures (Kovscek et al., 1995). Core 2i-4 exhibited the same behavior, and no visible foam was observed in the outlet tubing.
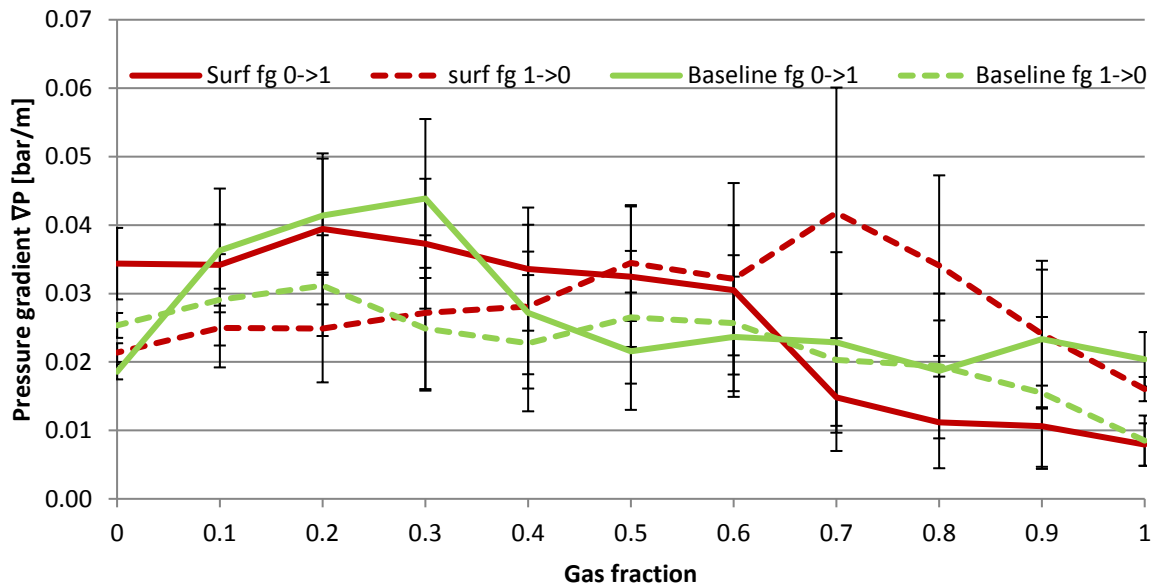
Figure 11-6: Differential pressure measured at different gas fractions for core 2i-4. The main flow occurred between the shrink-sleeve and core. No foam generation was experienced. The total volumetric rate for the experiment plotted above is 150ml/h. The reason for low or no foam generation is believed to be due to flow in smooth fractures, which lack snap-off sites.

Without confinement pressure applied to core 2i-4, it is possible that the internal pressure inflicts an equal but opposite effect of that normal stress do on fractures. Normal stress on fractures has been shown to increase the capillary pressure within fractures. An increased internal pressure and no confinement pressure may result in reduced capillary pressure inside the fractures. This could also impact the results, and be a reason why no foam generation is observed.

11.4. Foam Generation and Behavior in Tight Fractures

Foam behavior in tight fractures were investigated by co-injection in 1.5 inch fractured cores. To avoid flow outside the fractured core and limit flow along the larger fractures, caused by the fracturing method, the setup was changed. Shrink-sleeve was changed with epoxy, and the fractured core was prepared as described in chapter **7.3**. Johansen (2016) showed that experiments conducted on fractured systems of different sizes were comparable. Flow in fractures was dominated by the most conductive fracture. The fractured networks made from 1.5 inch cores should therefore be comparable with the results obtained in fractured networks made from 2 inch cores. By further using the mobility reduction factor, equation **(2)**, and apparent viscosity, equation **(4)**, results obtained in fractured system of 1.5 inch and 2 inch systems should be directly comparable. The baseline differential pressure on core 1.5i-3 is shown in **Figure 11-7**.
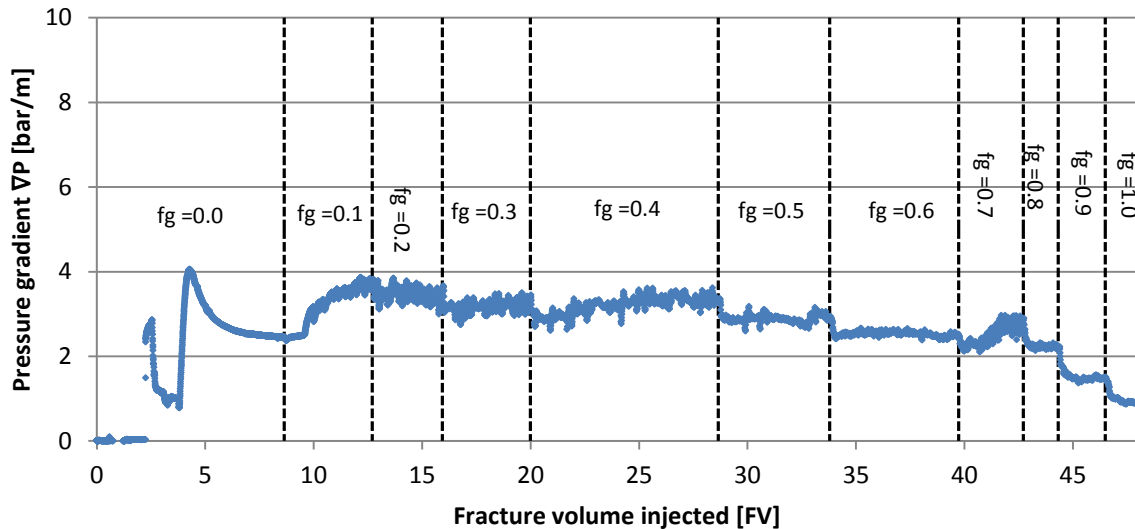
Figure 11-7: Baseline experiment performed on core 1.5i-3, total volumetric rate 100ml/h. The fractured network was first flushed with N₂ gas before baseline started. The baseline was then performed starting at 100% brine injection and increasing gas fraction until 100% gas was injected. Each gas fraction was run until stable behavior was observed.

Before the baseline started the fractured network was flushed with several fracture volumes of N₂ gas. The baseline started at gas fraction 0 (pure brine injection) with an increasing gas fraction trend. The gas fraction was increased with increments of 0.1 until gas fraction 1.0 was reached. Each gas fraction was run until stable differential pressure were observed. As the baseline goes from gas fraction 0 to 0.1 an increased pressure is observed. This correlates to the theory of relative permeability of two phase flow. An increase in differential pressure will occur when there is more than one fluid present, due to blocking of each other's flow paths. From gas fraction 0.1 until 0.4 the differential pressure is relatively stable, with minor variations. From gas fraction 0.5 to 1.0 a general decrease in differential pressure is observed. At gas fraction 0.7 a sudden increase in differential pressure was measured. The reason behand this increase is not understood, but a possible reason could be an internal re-distribution of fluids.

Co-injection of surfactant solution and N₂ was performed on the same fracture network using the same experimental conditions. A significant increase in differential pressure was observed (**Figure 11-8**), which is a clear indication of foam generation. Tiny bubbles were observed in the outlet tubing. Bubbles were not observed during any of the baseline studies, and is believed to be a strong indication of foam generation *in-situ*. Fellow master student Solberg (2017) conducted similar experiments in sand packs. The produced bubbles in the tight fractures were similar to bubbles produced in the experiments conducted by Solberg (2017). The bubbles

observed in the production tubing from open fractures were several magnitudes larger, as seen in **Figure 11-9**. During co-injection in smooth fractures no bubbles were seen.
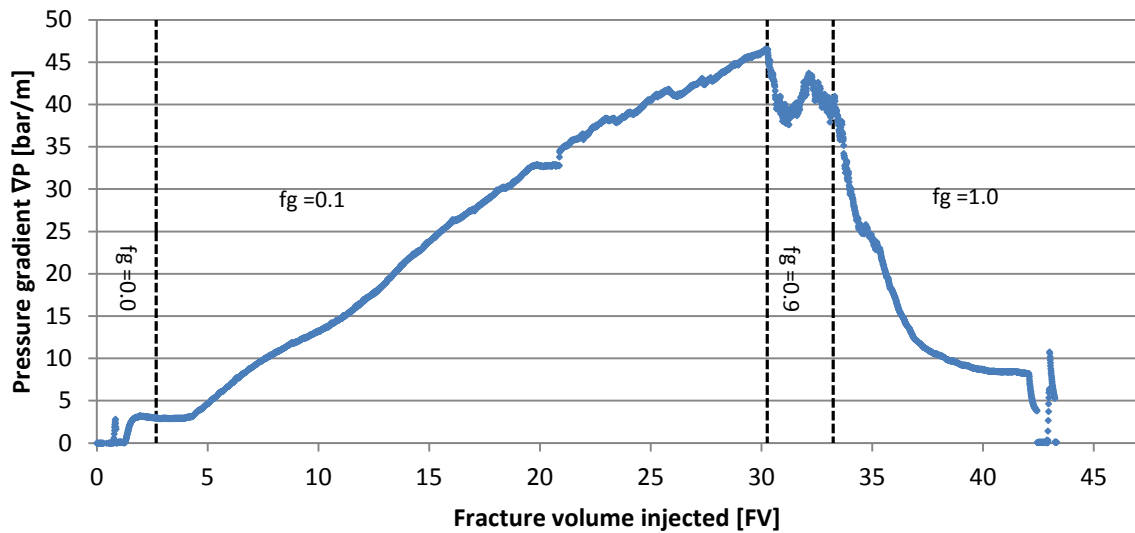

Figure 11-8: Pressure gradient measured during foam experiment in core 1.5i-3 with total volumetric rate 100ml/h. The inlet pressure increased above the limiting pressure of the mass flow controller, and the experiment had to be stopped. The gas fraction were changed directly from 0.1 to 0.9 due to this. A seemingly stable area is seen at 20FV. This is an experimental artifact due to the inlet pressure reaching the gas supply pressure, hence stopping gas flow.

The differential pressure in **Figure 11-8** increased to the maximum pressure of the mass flow controller (8 bar) without any tendency to stabilize. There is a stable region at approximately 20 fracture volumes injected. This is an experimental artifact associated with a temporary reduction in gas flow rate. The N_2 supply was set at 5 bar, when 5 bar was reached at inlet the mass flow controlled could not deliver the set rate any more. This resulted in reduced injection rate, hence the stable pressure. The N_2 supply was increased to 8 bar, which is the mass flow controller's limitation. The pressure then continued to increase. When the inlet pressure reached 8 bar (maximum pressure for the mass flow controller used), the gas fraction was changed to 0.9 to see if this resulted in reduced differential pressure. The differential pressure fell as gas fraction 0.9 was initiated, however, the continued observed pressure was rather unstable. This is presumed to be due to internal re-distribution of fluids. The fractured core was then flushed with N_2; it took more than 5 fracture volume of injected N_2 before the pressure stabilized. At gas fraction 1.0 no foam generation should occur, but the differential pressure was still significantly higher than baseline. During baseline injection at $f_g = 1.0$, gas only, a pressure gradient of approximately 1 bar/m was measured, whereas the foam experiment had approximately 8 bar/m at $f_g = 1.0$. This is a clear hysteresis effect because 100% N_2 injection should be equal at both baseline and surfactant study. A possible reason for the increased

63

differential pressure at 100% N_2 injection could be stagnant foam blocking parts of the fracture, hence reducing the possible flow paths for N_2. The 5 fracture volumes necessary to reach stable differential pressure at pure gas injection are also an indication for stagnant foam *in-situ*.
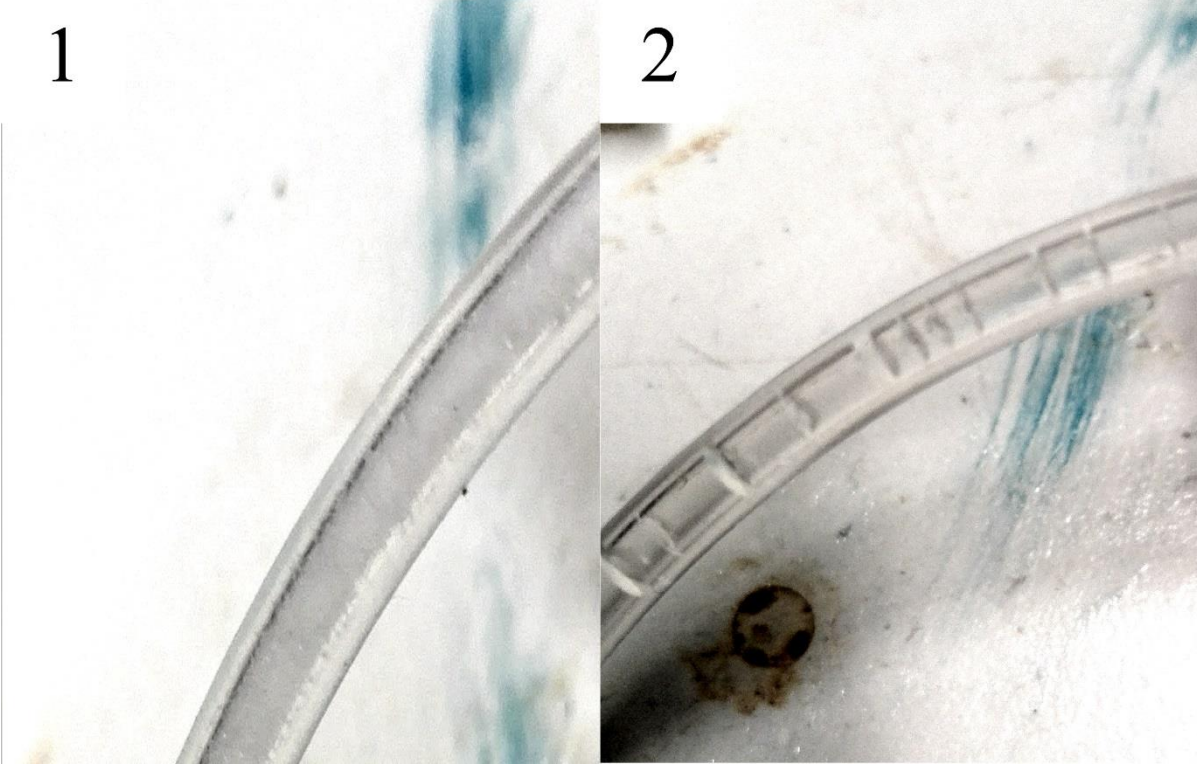
Figure 11-9: 1) Fine textured foam seen in the production tubing during experiments in tight fractures. This foam is similar to foam produced during experiments conducted in sand packs by fellow master student Solberg (2017). 2) Large bubbles are seen during experiments on open and partially open fractures. During baseline and experiments in smooth fractures, no bubbles were seen.

Due to the high pressure at inlet, during foam experiment in tight fractures, a reduction in the volumetric injection rate was necessary. The injection rate was change to 10 ml/h and a co-injection which started at gas fraction $f_g = 1.0$ was performed. The gas fraction was reduced in increments of 0.1 until it reached 0 (100% liquid injection). The differential pressure measured is shown in **Figure 11-10**.

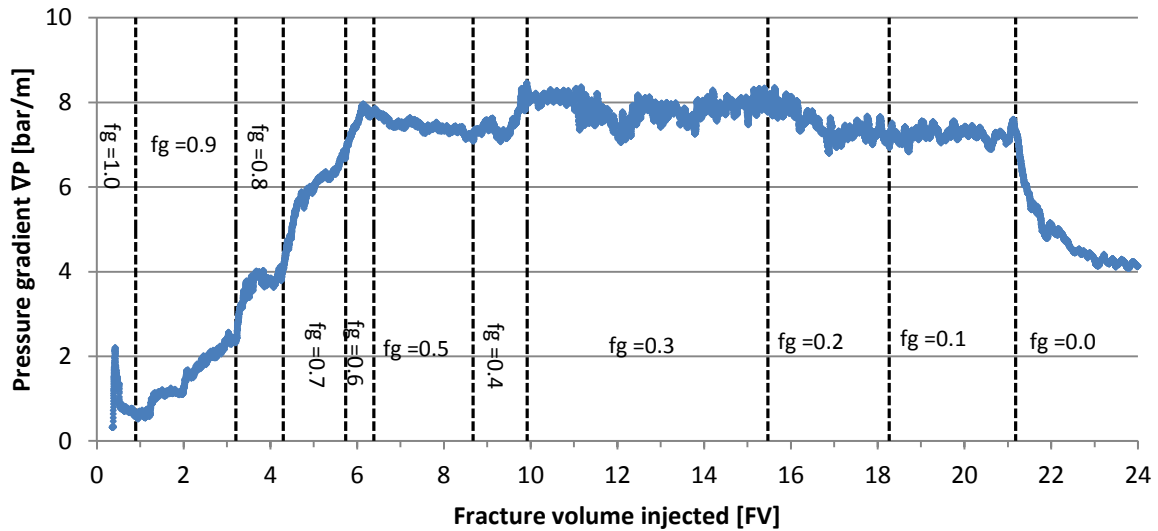**Figure 11-10: Pressure gradient measured during a co-injection of surfactant and N2 in core 2i-4. A total volumetric rate of 10ml/h was used. Core 2i-4 has tight fractures and permeability 0.1[D]. To focus on the gas fractions, the tail production of 100% water injection is cut short. The final pressure gradient of 100% water saturation ended at approximately 1 bar/m, see Figure 0-1 in Appendix C for complete measurements.**

The differential pressure increased as gas fraction decreased until gas fraction 0.6 was reached. The differential pressure between f_g 0.6 and 0.9 exhibit small-scale variations, but is rather stable. However, a slight increase followed with slightly larger variations in the pressure measurements occur at gas fraction 0.4. The reason behind this increase is not understood. A possibility may be the change from high-quality foam to low-quality foam. On the other hand the gas fraction 0.4 seems to low, and foam flow should already be of low-quality foam. In chapter **11.2** the change from high- to low-quality foam in fractures were found to be between gas fraction 0.82 and 0.89.

The stable differential pressure through several different gas fractions can be caused by two different mechanisms. The first possibility is that foam properties are equal for gas fraction 0.6 through 0.1, and foam of the same apparent viscosity is generated. Foam in porous media is found to experience the greatest apparent viscosity at gas fractions around 0.9 and decrease at both higher and lower gas fractions (Patton et al., 1983). This can, however, be different in fractures. Another possibility is foam generated at gas fraction 0.6 settles in part of the fracture as a stagnant foam, hence blocking flow paths. The abrupt decrease in differential pressure as gas fraction 0.0 is reached indicate that there is some kind of equilibrium inside the fractured network which no longer is sustained. The differential pressure at pure surfactant injection needed roughly 25 fracture volumes to stabilize; this can strengthen the theory of stagnant foam. If there is stagnant foam generated inside the factures, this could take numerous fracture

volumes of liquid to flush out. After 25 fracture volumes, the pressure gradient was 0.9 bar/m, compared to baseline at 0.3 bar/m. This is a clear hysteresis effect and can possibly be caused by stagnant foam or trapped gas in some other way. Capillary trapped gas, however, is not likely due to the low capillary pressure in fractures.

Previous master students Johansen (2016) and Vasshus (2016) conducted a similar experiment in a marble network with open fractures. The results obtained can be seen in **Figure 11-11**.
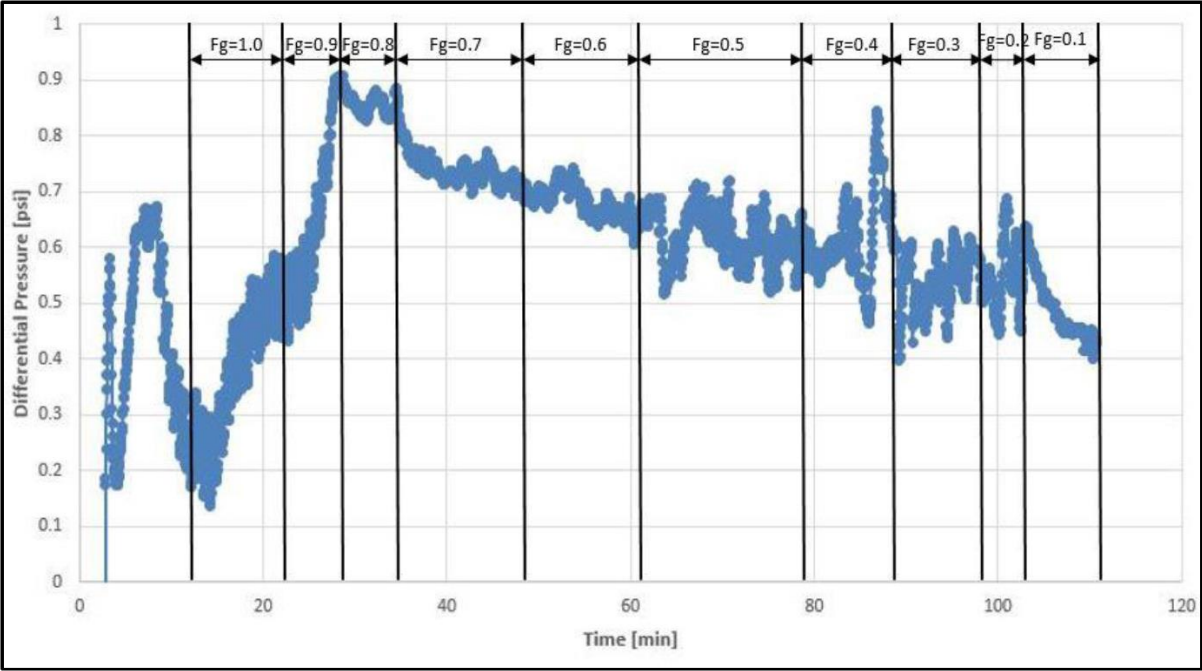

Figure 11-11: Pressure gradient during a co-injection of surfactant and air in fractured marble network. Total volumetric rate was 180ml/h. From gas fraction 1.0 to 0.8 there is an increasing trend in the pressure drop. From gas fraction 0.7 to 0.3 a steady decrease is seen in pressure gradient before it stabilizes at fraction 0.3 to 0.1. The experiment was conducted by precious master student Johansen (2016) and Vasshus (2016).

Although absolute pressures are significantly higher in the tight fractured system, due to lower fracture conductivity, the pressure trends can be compared. The pressure trend in the open fractured network (**Figure 11-11**) compared to the tight fractured network (**Figure 11-10**) show distinct differences. The open fractured network achieved the maximum differential pressure at gas fraction 0.9. After gas fraction 0.8, a steady decrease in the differential pressure was observed. This indicates that there are different mechanisms occurring in fractured networks of different aperture. The pressure trend in the open fractured network correlates with the apparent viscosity of foams described in literature. This difference could be explained by stagnant foam in tight fractures, and no stagnant foam in open fractures.

11.5. Foam Evaluation by MRF and Apparent Viscosity

The mobility reduction factor (MRF) and apparent viscosity are often used to quantify foams ability to reduce gas mobility. In this sub chapter the results from the open, tight and smooth fractures will be correlated by using MRF and apparent viscosity. The partially open fractures will not be correlated. This is because these cores were used to generate the L-plot and a different injection strategy was used. The necessary data to generate MRF curves and properly correlate the behavior is therefore not present.

Mobility reduction factor

The MRF and apparent viscosity were calculated from the experiments conducted with varying gas fractions. The mobility reduction factor was calculated using equation (2). MRF is a good indicator of how effective the foam is as a mobility reduction agent. However, instead of using single phase gas as the reference, the pressure during foam experiment was divided by the baseline study. The reason behind this decision is to focus on foam generation and mobility reduction in fractures. Differential pressure at two phase flow will be higher than single phase gas; regardless if the liquid is brine or surfactant. As described in theory two phase flow will reduce the conductivity of each fluid, due to relative permeability. By dividing the results by baseline, reduced mobility due to foam generation will be emphasized. The calculated mobility reduction is shown in **Figure 11-12**.
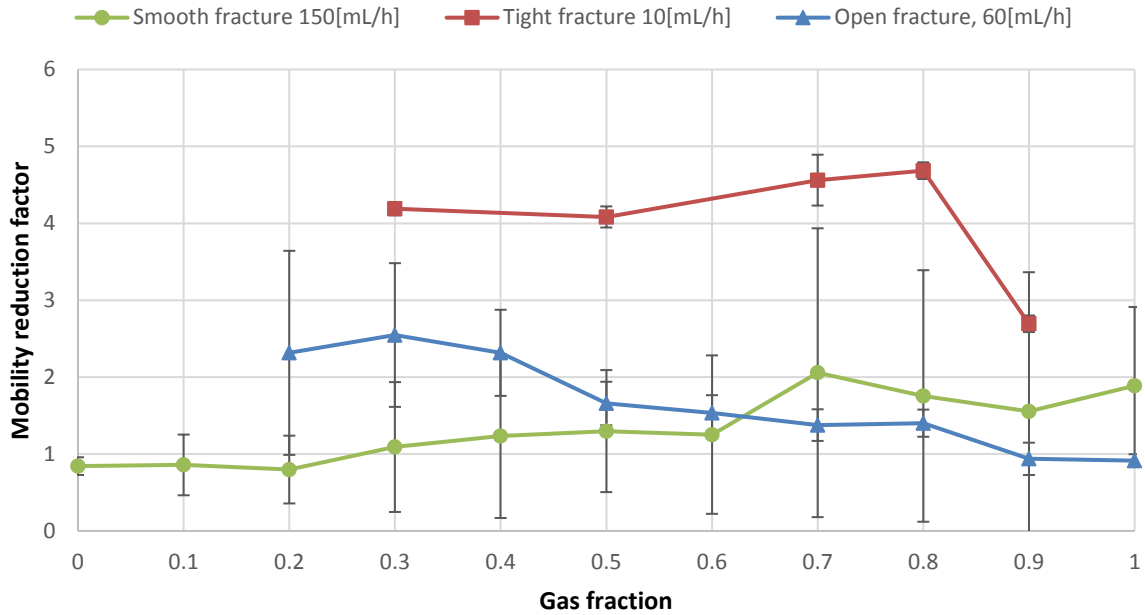
Figure 11-12: Mobility reduction factor was calculated for experiments in open, smooth and closed fractures. The measurements of co-injection in open fractured network (core 2i-1) were taken from previous master student Johansen (2016). A significantly higher MRF is observed in the tight fracture. Experiment on core 2i-1 by Johansen (2016) started at gas fraction 0.2 with increasing gas fraction. Experiments done on smooth and tight fractures started at gas fraction 1.0 and with reducing gas fractions. This is believed to impact the results due to hysteresis.

The MRF show a clear indication that foam has generated, and significantly reduced the mobility of gas in tight fractures. The reduction varies with f_g, but is as high as 4.7 at $f_g = 0.8$. The MRF calculated for smooth and open fractures is not as significant, but show an increase in the mobility reduction of 2.0 and 2.5, respectively, at maximum value. The smooth fractures exhibit an increased mobility reduction as gas fractions decrease, while the mobility reduction in the open fracture has the highest value at low gas fractions. Two explanations are proposed to explain these results. A significant difference between the two experiments is the difference in gas fraction direction. The open fracture experiment was started at gas fraction 0.2 and had an increasing gas fraction, while the smooth fracture was started at gas fraction 1.0 with decreasing gas fraction. Due to hysteresis effect, this can have a significant impact on the pressure trend. Because the mobility reduction factor takes the baseline study into consideration the behavior of the baseline could possibly impact the result as well.

Apparent viscosity

Another method for investigating the effect of foam is investigating the apparent viscosity of the foam. Apparent viscosity is a measurement of how the pseudo phase, foam, behaves by

measuring its artificial viscosity. This is calculated by equation (4) by treating foam as a single phase; results are plotted in **Figure 11-13**.
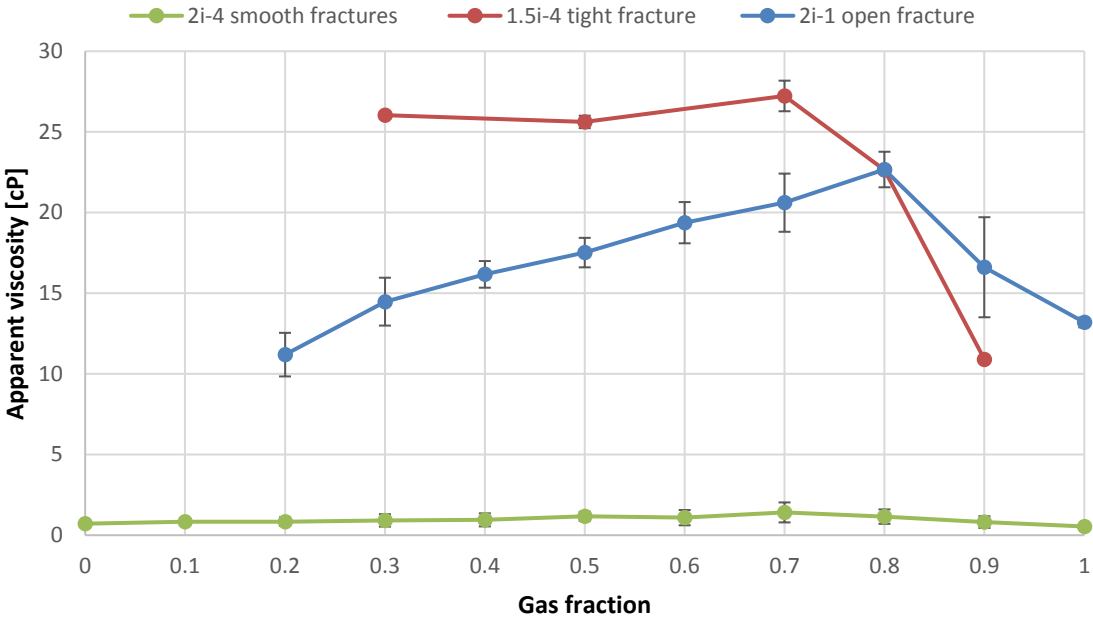

Figure 11-13: Apparent viscosity [cP] was calculated for experiments in open, smooth and closed fractures. Measurements of core 2i-1 were done by previous master student Johansen. A significantly higher MRF is observed in the tight fracture. Experiment on core 2i-1 by Johansen started at gas fraction 0.2 with increasing gas fraction. Experiments done on smooth and tight fractures started at gas fraction 1.0 and with reducing gas fractions. This is believed to impact the results due to hysteresis.

By studying the apparent viscosity for the different fracture system a few clear trends occur. The most significant result is the lack of increase in viscosity in the smooth fracture. This clearly shows that there is no foam generation in smooth fractures. This could be due to several reasons, including insufficient mixing and lack of foam generation sites; discussed in chapter **11.3 Foam Generation in Smooth Fractures**. In **Figure 11-13** the difference between the open and closed fracture is not as significant as when investigating the mobility reduction factor. The apparent viscosity trend is however quite different. The difference could in large parts be due to the different direction the experiments was performed in, hence hysteresis. The experiments in open and tight fractures were performed with increasing and decreasing gas fraction respectively.

There is a clear difference between the mobility reduction results (**Figure 11-12**) and the apparent viscosity (**Figure 11-13**). This is because the baseline was used as a reference when calculating MRF. When calculating the apparent viscosity the pressure measurements from the co-injection are used directly, and do not take the increased differential pressure of two phase

flow into consideration. This have both positive and negative aspects. As seen the apparent viscosity is a god way of assessing if foam is generated or not. However, MRF is more useful when considering implementing foam as an EOR method. By calculating the MRF with respect to a baseline study the effect, and gain, compared to water alternating gas (WAG) injection is clearer.

From the result above it is obvious that stronger foams were generated in tight fractures. A significant visual difference between the fluids produced from tight and open fractures is seen in the outlet tubing, as shown in **Figure 11-9**. The stronger foam, generated in tight fractures, is believed to be generated by a combination of several mechanisms, the main mechanisms are likely to be the two following. Tight fracture will experience numerous contact points; i.e. more snap-off sites. For foam generation to occur at snap-off sites, a certain capillary pressure is necessary (Ransohoff and Radke, 1988). Experimental measurements performed by Reitsma and Kueper (1994) found that capillary pressure in fractures increased as the normal pressure across the fracture increased. This can be correlated to open and closed fracture, where a tight fracture will have a higher capillary pressure. These effects are likely to produce stronger foams in tight fractures than open.

11.6. Co-Injection Applying PET/CT Imaging

11.6.1. Foam Stability Results

Experiments conducted on opaque core samples are usually analyzed based on measurements of differential pressure and effluents with few or no visual indications of flow. The measurements are then used to discuss the mechanisms causing the results. Foam behavior in core plugs is often correlated to experiments conducted on transparent models of other materials, hence surface properties differ. Experiments performed by Buchgraber et al. (2012) in silicon micro models are a good example of this. To further quantify the experimental results on foam behavior in fractures, co-injections were conducted in a PET/CT scanner at MIC. The experiments performed utilizing PET/CT imaging were comparable to the experiments so far on tight fractures; co-injection of N_2 gas and liquid. Two experiments were conducted; a baseline and a foam experiment. A total volumetric rate of 10ml/h was used with varying gas fractions. The fractured core (saturated by brine) was initially flushed with gas before co-injection begun. Due to short half-life of FDG, $t_{1/2} = 109\ min$, $f_g = 0.9, 0.8, 0.7, 0.5$ and 0.3 (in that order) were used. The same core was subjected to a full f_g cycle ($f_g = 1 \rightarrow 0$ with

increments of 0.1) outside of the PET/CT scanner to verify the behavior. The results from core 1.5i-4 are shown in **Figure 11-14**.
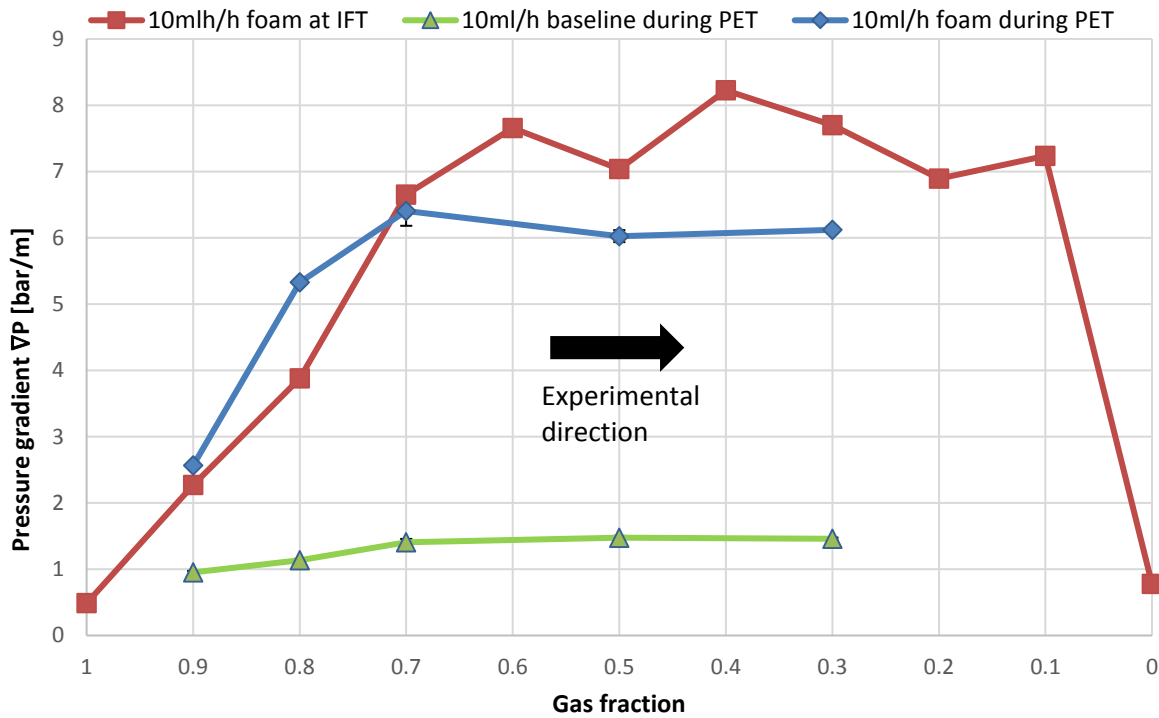

Figure 11-14: Co-injection of surfactant and N2 in core 1.5i-4. Total velocity of 10ml/h. The experiments during PET were not ran at all gas fractions due to time limitations at the Bergen University Hospital. The experiment with all gas fractions (red) was run at IFT at the same conditions as the experiments during the PET scan at MIC.

A significant increase in differential pressure during foam experiments compared to baseline were observed. At gas fraction 0.7 to 0.3 the differential pressure is approximately four times higher during foam experiment compared to baseline. This is a clear sign of foam generation *in-situ*, during *in-situ* imaging of flow in tight fractures. Investigation of the outlet tubing showed a fine bubbled gas dispersion as seen in **Figure 11-9**.

The experimental results obtained at MIC are almost identical to the experiment performed at IFT. Some minor differences are observed, and this can be caused by several reasons. Foam is not static and completely equal results cannot be expected. The room where the PET/CT scanner is placed is a few degrees warmer than the laboratory at IFT; this could potentially impact the experiment. However, foam experiments conducted at MIC and IFT show the same pressure trend; the results at MIC are therefore believed to be representative of foam experiments conducted at IFT.

11.6.2. Visualization of Foam Flow in Tight Fractures

Before co-injections a baseline was performed. During PET scanning radioactive brine was injected into the fractured network, which was saturated with non-radioactive brine. This was done to investigate the main flow path for liquid inside the fractured core. An image of the injection of radioactive brine is shown in **Figure 11-15**.
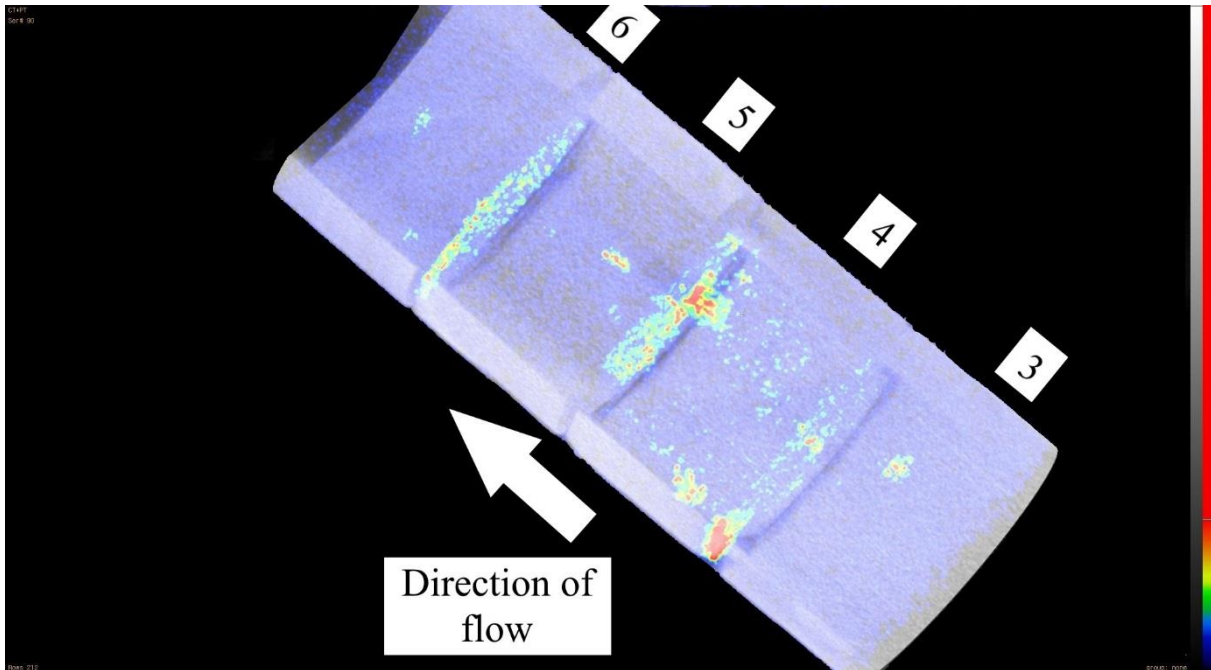

Figure 11-15: Injection of radioactive brine into a tight fractured network. This was done to investigate the main flow paths of liquid. In this picture, core segment 3, 4, 5 and 6 are seen. Two inlet core segments are outside the PET scanner range (field of view = 10 cm). The image is a tilted 3D projection of the PET/CT results. Imaged at MIC, Dept. of Biomedicine, UoB.

In **Figure 11-15** and **Figure 11-16** core segment 3, 4, 5 and 6 from **Figure 7-7** is scanned. Core segment 1 and 2 are outside the PET scanners field of view, which is 10 cm. The decision to focus on segment 3 to 6 was due to possible inlet effects in the first segments. It is possible that a certain length to generate foam is necessary. By focusing on the last part of the fractured network the possible inlet effect is avoided in the images.

During the injection of radioactive brine, **Figure 11-15**, some very distinct signals can be seen. Strong signals are especially observed in the cross-sectional fractures between the core segments. These fractures are most likely larger than the fractures in each core segments, because they were cut and not fractured. In the core segments, where the tight fractures are located, the signal varies. In segment 4 there is a wider distribution than what is observed in segment 3, 5, and 6; where the signal is localized in narrow flow paths, i.e. poor sweep.

After injecting 3.8 fracture volumes of radioactive brine, non-radioactive brine was injected. This was to remove all radioactivity from the fractured core before the baseline co-injection. When the radioactive brine was removed, a co-injection of brine and N_2 were performed. The co-injection were performed with decreasing gas fractions from 0.9 to 0.3 in pre-defined increments, using a total volumetric flow rate of 10 ml/h. Due to short half-life of FDG, $t_{1/2} = 109\ min$, the radioactive signal from the baseline co-injection decayed overnight, and foam co-injection could be performed with a new dose of FDG the next day. PET scans were continuously acquired during both the baseline and foam co-injection. Images locating the radioactive signal in the fractured network were reconstructed during stable pressures at each gas fraction. The location of radioactive signal during baseline and foam floods at f_g 0.9, 0.7, 0.5 and 0.3 can be seen in **Figure 11-16**, and the time of each reconstruction and volume injected during that time can be seen in Table 11-1.

Table 11-1: An overview of the reconstructed intervals from the PET/CT acquisition. These are the background for the following images and measured data.

Gas fraction	Baseline/Foam	Time reconstructed [s]	Radioactive liquid injected [ml]
0	Baseline	120	1.667
0.9	Baseline	420	0.117
0.8	Baseline	240	0.133
0.7	Baseline	240	0.200
0.5	Baseline	660	0.917
0.3	Baseline	660	1.283
0.9	Foam	660	0.183
0.8	Foam	660	0.367
0.7	Foam	660	0.550
0.5	Foam	660	0.917
0.3	Foam	660	1.283
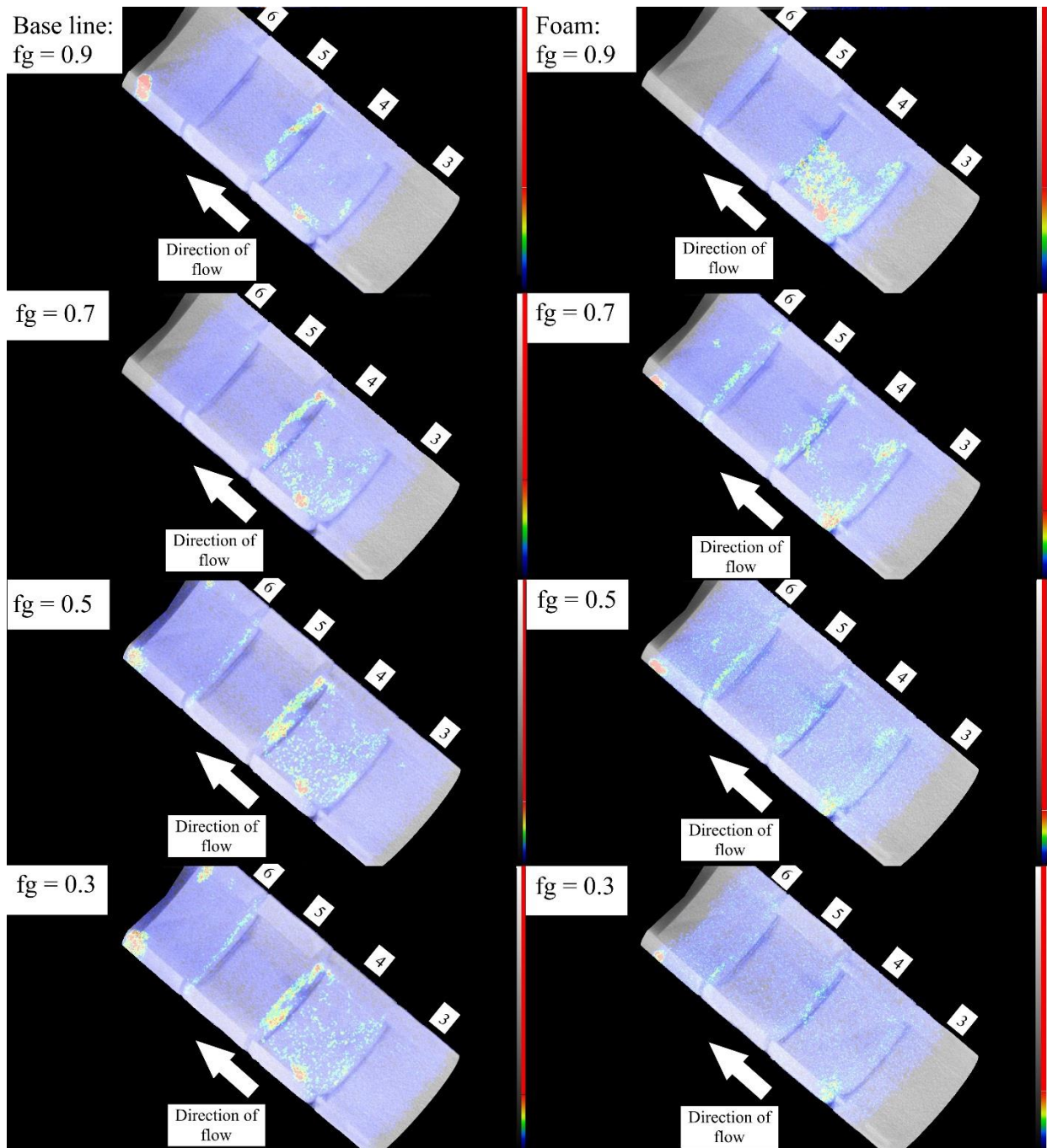
Figure 11-16: PET data on top of a CT image of core 1.5i-4 during co-injection. The baseline and the foam experiment is shown on the left and right side respectively. The colored signal shows the location of radioactivity. Significant differences between the baseline and the foam experiment are seen, indicating foam generation *in-situ*. The PET scanner can measure signals in a length of approximately 10 cm. The images above show core segment 3 to 6, as indicated. The images are tilted 3D projections of the PET/CT results. Imaged at MIC, Dept. of Biomedicine, UoB.

Baseline co-injection

By investigating the images of baseline and foam injection (**Figure 11-16**), differences between the two experiments were found. A trend during the baseline is increasing signals as the gas fraction decreases, as expected due to larger fractions of liquid injected. Another observation is strong signals in the cross-sectional fractures between the core segments during the baseline; which may indicate an accumulation of brine in the cross-sectional fractures. These cross-sectional fractures are most likely larger than the tight fractures. In the tight fractures (in each core segment) the signal is in general weaker and varied. In some areas, there are no signal, whereas other areas have strong signal. The signals mainly occur at the same places during baseline as during the radioactive brine injection (**Figure 11-15**). However, in the first cross-sectional fracture (between segment 3 and 4), there is a strong signal during the radioactive brine injection which does not occur during the baseline co-injection. A strong signal during the radioactive brine injection, which disappears during the baseline co-injection, is most likely caused by gas accumulation. This signal is in the upper part of the core and can possibly show vertical segregation, which is a major challenge in gas injection.

Surfactant co-injection

During the surfactant co-injection some significant differences are observed, compared to the baseline co-injection. A larger distribution in the signal is seen, and the strong signal in the cross-sectional fractures between the core segments appears to be gone. During gas fraction 0.9 the foam experiment shows a broader distribution inside the tight fracture in core segment 4. During baseline co-injection gas fraction 0.9 do not show the same distribution in the tight fracture. The main signal (i.e. liquid flow) in segment 4 during the baseline seems to follow the edge of the core during $f_g = 0.9$. This is a clear indication that sweep in tight fractures is greatly increased during foam injections. The same trend continues during the other gas fractions, but is not as clear. Due to increased liquid rates as gas fraction is reduced more FDG is being injected. This should result in a stronger signal at low gas fractions, due to more injected radioactive liquid. During the baseline co-injection an increase in signal is seen as the gas fraction decreases, however this is not observed during the foam injection. The reason behind this is not fully understood but may be caused by a different gas fraction *in-situ* than what is being injected; according to Martinez (1998) the limiting capillary pressure could change gas/liquid fraction *in-situ*. Improved sweep could lead to a wide spread liquid saturation and no

preferred flow path. If there is no main flow path for the liquid, this can also result in widespread signals without accumulation of signals at certain localization.

11.6.3. Measured Activity Through the Fractured Network

By using the software InterView Fusion a Region of Interest, ROI, can be generated, where the activity within is measured. By making several cross sectional regions of interest along the fractured network an overview of the activity *in-situ* can be made.
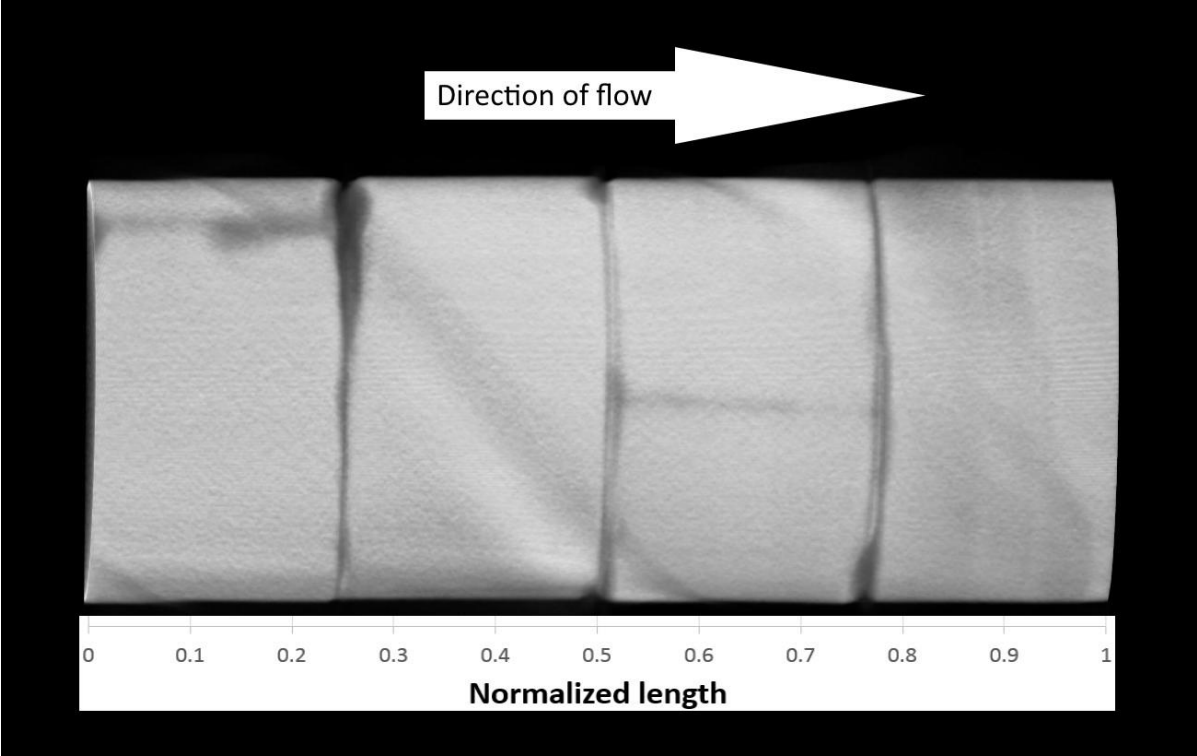

Figure 11-17: Side view of core 1.5i-4 where core segment 3 to 6 are seen. The normalized length of the core used in Figure 11-18 and Figure 11-19 is shown. Imaged at MIC, Dept. of Biomedicine, UoB.

The measured activity is proportional to the liquid fraction inside the fractured network. However, because no measurements were done at 100% radioactive brine saturation exact saturation is impossible to calculate. By plotting the measured activity in each ROI against the normalized length of the core, the variations in saturation for each gas fraction can be seen. Due to the fact that it is the liquid which is labeled with FDG an increase in liquid fraction will increase the radioactive concentration *in-situ*. To account for this, each signal has been scaled to an injection of 0.5 ml of liquid. By doing this, the different gas fractions should be directly comparable. Another experimental artifact can be differences in the radioactive concentration in the liquid each day. To account for the differences, the activity in the production tubing were measured each day at the same gas fraction. The measured activity was then used to correlate

the difference in activity, this way the baseline and foam experiment should be directly comparable. The plotted results can be seen in **Figure 11-18**, **Figure 11-19** and **Figure 11-20**.
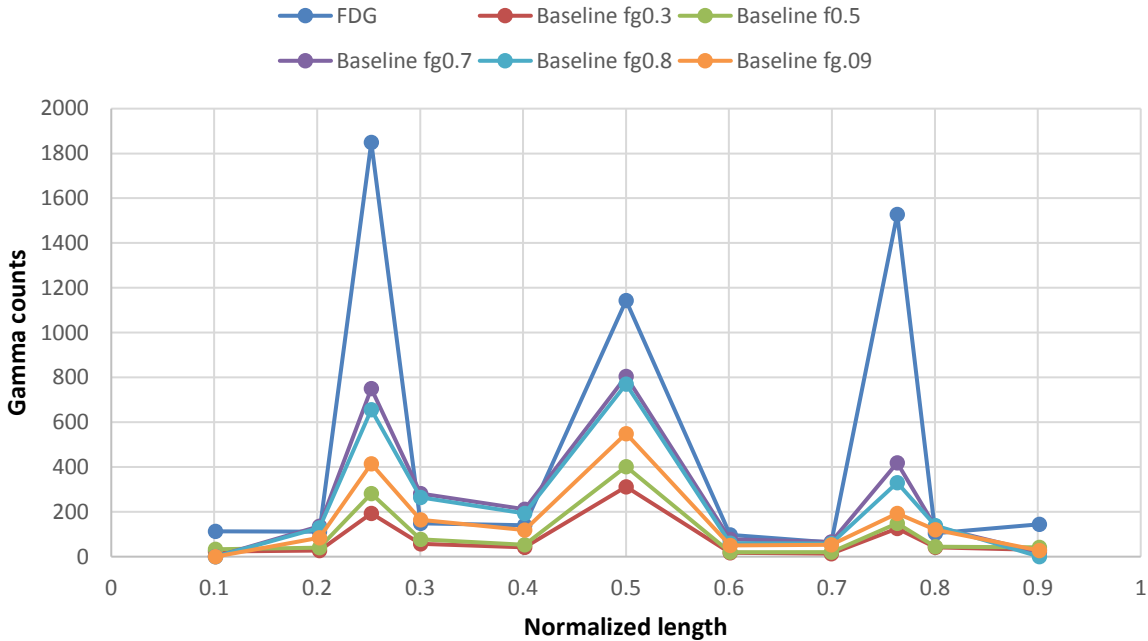

Figure 11-18: Measured activity along the fractured network at each gas fraction during baseline in addition to the radioactive brine – non radioactive brine displacement, labeled "FDG". Each gas fraction has been scaled to represent an injection of 0.5ml brine.

In **Figure 11-18** the measured activity through the fractured core for the different gas fractions can be seen. The three cross-sectional fractures between the core segments show a considerable increase in the measured activity compared to the tight fractures. This further indicate that these fractures have larger aperture than the fractures in the core segments. All gas fraction sow a considerable lower saturation in the cross-sectional fractures than the pure brine injection. This show that there is most likely an accumulation of radioactive brine during the radioactive brine injection, which does not occur (at the same amount) during co-injection. Between the co-injections it is gas fraction 0.7 and 0.8 which have the highest liquid saturations *in-situ*, whereas gas fraction 0.3 has the lowest saturation *in-situ*. The reason behind this is not fully understood, however it could be caused by vertical segregation at high gas fraction or relative permeability effects.
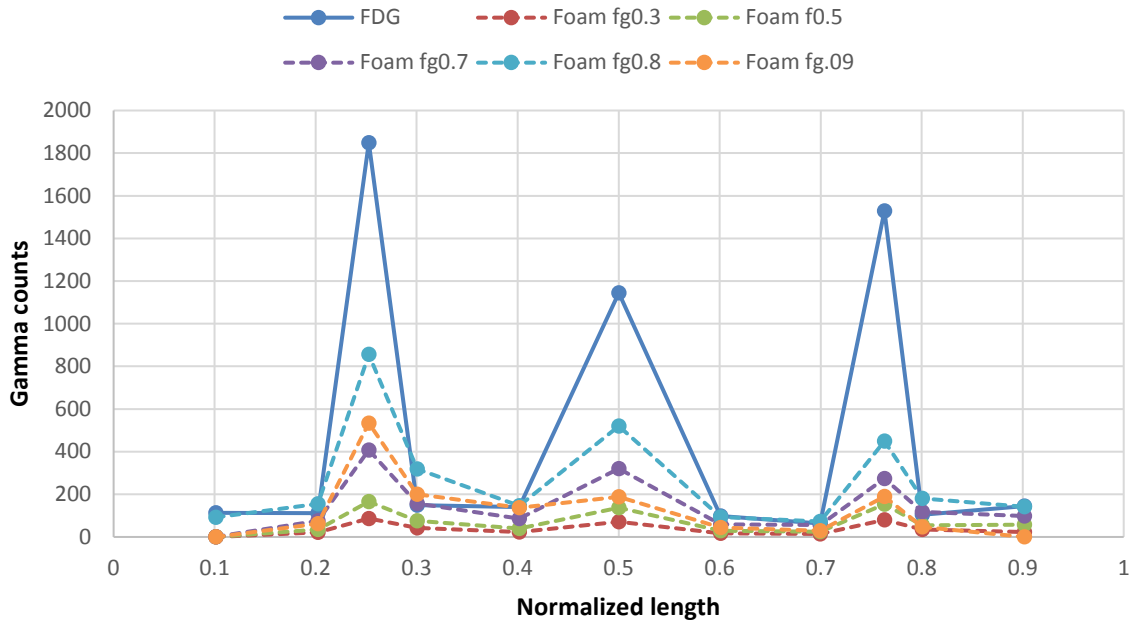
Figure 11-19: Measured activity along the fractured network at each gas fraction during foam experiment. Each gas fraction has been scaled to represent an injection of 0.5ml surfactant.

In **Figure 11-19** the same measurements have been done during foam injection. The peaks at the three cross-sectional fractures between the segments seems to be significantly reduced. This can be explained by the foam *in-situ*. If all fractures are filled with foam, no accumulation of liquid should occur. Without accumulation of liquid, a low saturation is expected. This is a clear indication of improved sweep in the fractured network during foam injection.

Between the surfactant co-injection it is gas fraction 0.8 which shows the highest saturation *in-situ*, while gas fraction 0.3 and 0.5 have the lowest saturation. The reason behind this is not understood. However it could be caused by stagnant foam. The co-injections started at gas fraction 0.9 and were reduced until gas fraction 0.3 was reached. As seen from the pressures the differential pressure did not decrease as the gas fraction decreased. If this is caused by stagnant foam the saturation *in-situ* could differ from that being injected.
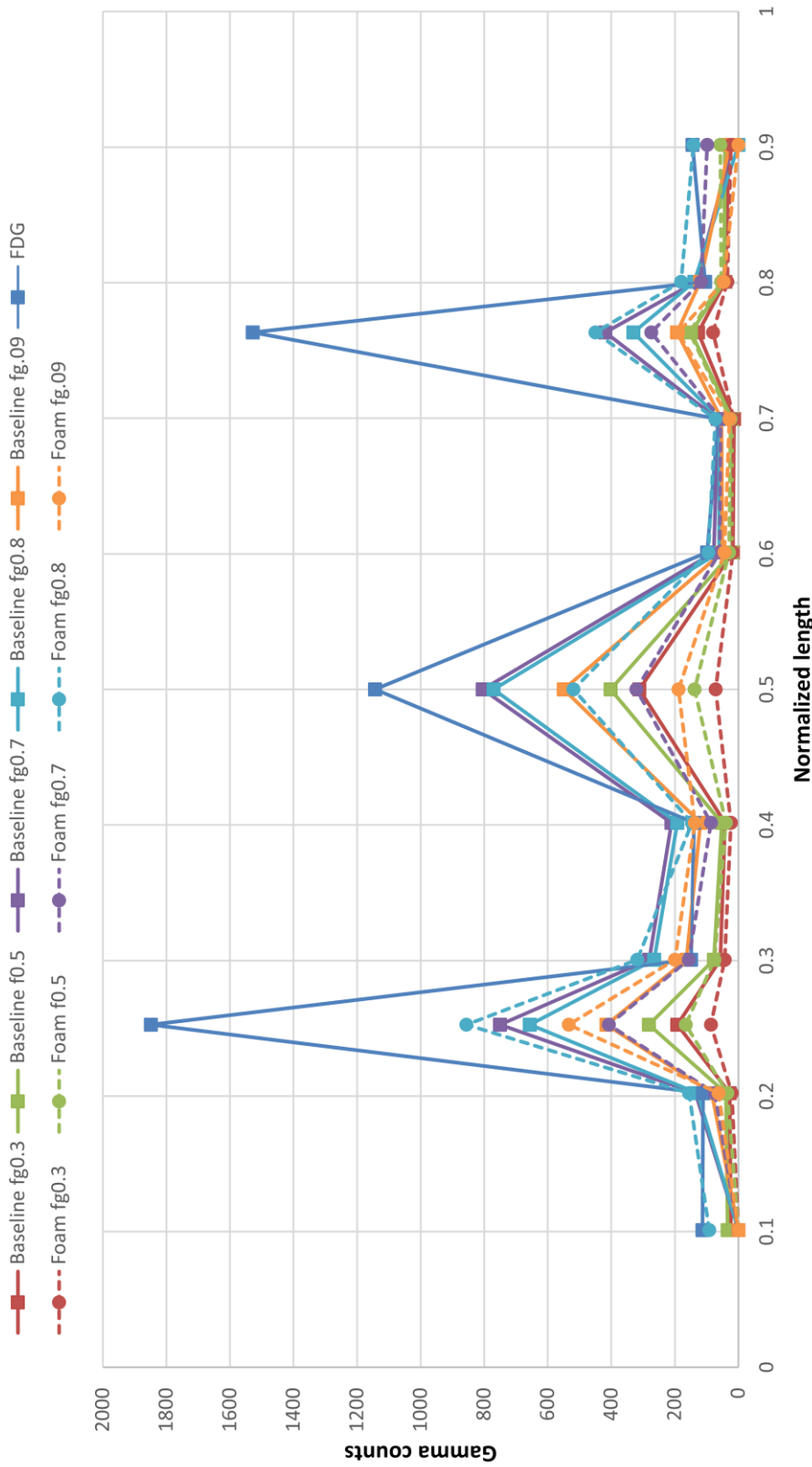
Figure 11-20: All measured saturations (gamma counts) during the PET/CT scanning on core 1.5i-4. Baseline co-injection is marked by solid lines whereas foam co-injection is marked as dotted lines. All gas fractions have been scaled to represent 0.5 ml liquid injection to comparable.

By plotting all the measurements in one plot the foam experiment is easily compared to the baseline co-injection. In general the trend is lower counts for the surfactant co-injection than the baseline. This indicate increased sweep during foam in fractures. However there are some exceptions, in the first cross-sectional fracture gas fraction 0.8 and 0.9 show a higher concentration during foam than baseline. The same is observed in the last cross-sectional fracture for gas fraction 0.8. In the cross-sectional fracture in the middle it is however significantly lower saturation during the foam surfactant co-injection. The reason behind this is not understood. It may be caused by an increased volume resulting in coalescence and liquid accumulation at high gas fractions.

11.7. Experimental Challenges and Uncertainties

11.7.1. Precipitation

Previous master student Vasshus (2016) observed precipitation in the effluents from foam study on fractured marble while using sandstone brine. To investigate if there is a reaction between sandstone brine and marble a continuous flooding of a fully saturated fractured core (core 2i-2) was performed. The differential pressure measured during constant rate injection of sandstone brine had a significant increase, as seen in **Figure 11-21**. This is a clear indication that there is some kind of interaction between the solid and brine, however further investigations were necessary to confirm this theory.
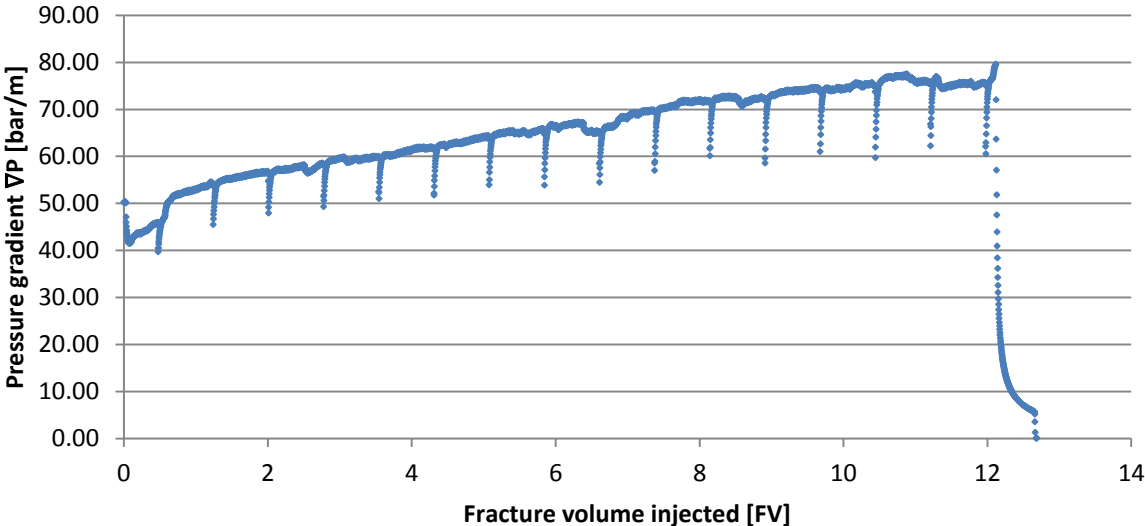
Figure 11-21: Due to experimental results defying Darcy's law the pressure drop across core 2i-2 was measured during several fracture volumes of brine injection at a constant rate of 60ml/h. It was believed that there might be a reaction between the brine and rock surface. The trend of increasing differential pressure at constant liquid rate is a clear indication of a reaction. The reduction in differential pressure at constant intervals is an artifact caused by the pump changing piston.

To quantify a possible reaction between the sand stone brine and rock surface pH measurements of brine at inlet and outlet were found to be a good method. Dissolution of calcium carbonate (the main component in marble) in water will generate free OH- ions, hence generate a basic solution. If a change in pH is measured this will prove that there is some kind of reaction between the brine and rock surface. Measurements were conducted by pH strips, and the measured pH at inlet and outlet was 6.75 ± 0.25 and 9.0 ± 1 respectively. Proving a reaction between the sand stone brine and the marble surface. To avoid the reaction between brine and rock surface the brine was changed to chalk brine. Chalk brine is already saturated with Ca-ions which could prevent reaction between brine and marble. The pH was measured at inlet and outlet after changing to chalk brine; pH was measured at 6.75 ± 0.25 at both inlet and outlet, after several fracture volumes had flushed the fractured core. After changing the brine no further increase in differential pressure over time was seen. Concluding with none or very low reaction between chalk brine and marble. The reason why chalk brine was not used from the beginning was due to previous Ph.D. student Haugen had experienced problems with precipitation when the chalk brine was used in surfactant solutions (Haugen et al., 2012). No precipitation was seen during any of the studies were Huntsman SURFONIC® L24-22 was used together with chalk brine. This is good news regarding the field pilot in East Seminole.

11.7.2. Other Uncertainties

- Varying differential pressure

  In some experiments, especially in smooth and open fractures, severe fluctuations were seen in differential pressure during co-injections. After processing the experimental data, the average pressure during the stable period is found. The cause of these fluctuations are thought to be gas slippage and/or gas compressibility effects (Rossen, 1990, Prud'homme, 1995)

- Identifying stable regions

  Due to fluctuations in measured differential pressure identifying the stable region of a gas fraction could be challenging. Especially in tight fractures where both increasing, decreasing and stable pressure could be observed. Reasons for this change could be bubble trains changing flow paths, or other redistributions of fluids *in-situ*.

- Temperature

  The gas volume is highly dependent on temperature. The experiments were conducted at room temperature, and some fluctuations in temperature are unavoidable in a room.

- Concentrations

  When mixing brine and surfactant solution, a scale was used to weigh the individual components.

- System pressure

  All experiments were conducted at elevated pressures. Most experiments were conducted at 1 bar back pressure. However some experiments were conducted at 4 bar. All experiments were produced into a closed container, and a small pressure increase (approximately 0.05 bar) during the experiments were observed. This could potentially influence the results.

- Different core size

  Different core sizes could impact results. However, this is not thought to be significant because the most conductive fracture dictates the fluid flow. This is seen by imaging.

- Effect of confinement pressure

  During permeability measurements of core 2i-2, a very high confinement pressure (26 bar) was used, to investigate the effect of high stress on the fractures. Significantly reduced permeability was measured (0.30 ± 0.01D), similar cores (2i-3 and 2i-4) had permeabilities ranging from 6.8 to 7.1D with confinement pressures of approximately 10 bar. This indicates a large impact on fracture conductivity from confinement pressure.

Part IV – Conclusions and Future Work

12. Conclusions

Foam generation and foam behavior were studied in fractures of varying aperture and surface roughness. The foam performance was investigated by both measurements of differential pressure, visual investigation of the production tubing and utilization of PET/CT scanner. Experiments were compared to baseline studies to quantify the effect of using surfactant solution.

- Fracturing and reassembling of marble cores to represent real rough-walled fractures of apertures varying from open, partially open to tight fractures were found to be successful.

- By investigating mobility reduction factor and apparent viscosity, both open, partially open and tight fractures indicate foam generation *in-situ*; co-injection of gas and surfactant is found to greatly reduce gas mobility compared to baseline. Smooth fractures, however, did not generate foam, and no reduction in gas mobility was observed.

- Foam generated in tight fractures are found to be stronger than foam in open and partially open fractures. By investigating the production tubing foam in tight fractures is found to have bubbles several magnitudes of order smaller than those generated in open and partially open fractures.

- Foam behavior of low-quality foam behaves differently in fractures compared to porous media. In porous media low-quality foam is only dependent on gas velocity. In fractures low-quality foam is found to be dependent on both liquid and gas velocities.

- By utilizing PET/CT scanning, saturation *in-situ* can be measured. A significant reduction in liquid saturation is seen during co-injection of gas and surfactant. This is found to be due to increased sweep.

- A critical velocity for foam generation in fractures is found to exist.

- A significant hysteresis effect is seen during foam experiments. Significant differences in results on experiments performed from $f_g = 0$ to $f_g = 1$ compared to experiments performed at the opposite direction. Hysteresis is also found to keep the differential pressure constant during several different gas fractions in tight fractures.

13. Future Work

To further understand foam generation and behavior in fractures the following work is suggested based on results from this thesis.

- Further investigate the critical velocity for foam generation in fractures, and examine the influence of different fracture apertures.

- Reproduce the experiments conducted in this thesis at different flow conditions, e.g. at high pressure and temperature to investigate foam generation and behavior at reservoir conditions.

- Perform co-injections in oil saturated water-wet fracture networks to investigate the impact the presence of oil has on foam in fractures.

- Perform co-injection in oil saturated oil-wet fracture networks to investigate the impact of oil-covered surfaces on foam behavior, and investigate possible wettability changes due to the presence of surfactants.

Part V – References and Appendixes

References

AHR, W. M. 2011. *Geology of carbonate reservoirs: the identification, description and characterization of hydrocarbon reservoirs in carbonate rocks*, John Wiley & Sons.

ALVAREZ, J. M., RIVAS, H. J. & ROSSEN, W. R. 2001. Unified Model for Steady-State Foam Behavior at High and Low Foam Qualities. *SPE Journal,* 6**,** 325 - 333.

ANDERSON, W. G. 1987. Wettability literature survey part 5: the effects of wettability on relative permeability. *Journal of Petroleum Technology,* 39**,** 1453-1468.

BAILEY, D. L., TOWNSEND, D. W., VALK, P. E. & MAISEY, M. N. 2005. *Positron emission tomography,* Berlin, Springer.

BARNES, H. A., HUTTON, J. F. & WALTERS, K. 1989. *An introduction to rheology*, Elsevier.

BOAS, F. E. & FLEISCHMANN, D. 2012. CT artifacts: causes and reduction techniques. *Imaging in Medicine,* 4**,** 229-240.

BRATTEKÅS, B. & FERNØ, M. A. 2016. New Insight from Visualization of Mobility Control for Enhanced Oil Recovery Using Polymer Gels and Foams. *In:* ROMERO-ZERÓN, D. L. (ed.) *Chemical Enhanced Oil Recovery (cEOR)-a Practical Overview.* InTech.

BROWN, H. W. 1951. Capillary Pressure Investigations. *Journal of Petroleum Technology,* 3**,** 67 - 74.

BUCHGRABER, M., CASTANIER, L. M. & KOVSCEK, A. R. Microvisual investigation of foam flow in ideal fractures: role of fracture aperture and surface roughness. SPE Annual Technical Conference and Exhibition, 8-10 October 2012 San Antonio, Texas, USA. Society of Petroleum Engineers.

CASTEEL, J. & DJABBARAH, N. 1988. Sweep improvement in CO2 flooding by use of foaming agents. *SPE reservoir engineering,* 3**,** 1,186-1,192.

CHEN, J.-D. & WILKINSON, D. 1985. Pore-scale viscous fingering in porous media. *Physical review letters,* 55**,** 1892.

CHOU, S. Conditions for generating foam in porous media. SPE Annual Technical Conference and Exhibition, 6-9 October 1991 Dallas, Texas. Society of Petroleum Engineers.

CRAIG, F. F. 1971. *The reservoir engineering aspects of waterflooding,* New York, HL Doherty Memorial Fund of AIME.

DAVID, A. & MARSDEN JR, S. S. The rheology of foam. Fall Meeting of the Society of Petroleum Engineers of AIME, 28.10.1969 1969 Denver, Colorado, USA. Society of Petroleum Engineers.

DICKSEN, T., MILLER, C. A. & HIRASAKI, G. J. 2002. Mobility of Foam in Heterogeneous Media: Flow Parallel and Perpendicular to Stratification. *SPE Annual Technical Conference and Exhibition.* Dallas, Texas.

DONALDSON, E. C., CHILINGARIAN, G. V. & YEN, T. F. 1989. *Enhanced oil recovery, II: Processes and operations*, Elsevier.

EXEROWA, D. & KRUGLYAKOV, P. M. 1998. *Foam and foam films : theory, experiment, application,* New York, Elsevier.

FALLS, A., MUSTERS, J. & RATULOWSKI, J. 1989. The apparent viscosity of foams in homogeneous bead packs. *SPE Reservoir Engineering,* 4**,** 155-164.

FARAJZADEH, R., LOTFOLLAHI, M., EFTEKHARI, A. A., ROSSEN, W. R. & HIRASAKI, G. J. H. 2015. Effect of Permeability on Implicit-Texture Foam Model Parameters and the Limiting Capillary Pressure. *Energy & Fuels,* 29**,** 3011-3018.

FERNØ, M., EIDE, Ø., STEINSBØ, M., LANGLO, S., CHRISTOPHERSEN, A., SKIBENES, A., YDSTEBØ, T. & GRAUE, A. 2015a. Mobility control during CO 2 EOR in fractured carbonates using foam: Laboratory evaluation and numerical simulations. *Journal of Petroleum Science and Engineering,* 135**,** 442-451.

FERNØ, M., GAUTEPLASS, J., HAUGE, L. P., ABELL, G. E., ADAMSEN, T. & GRAUE, A. 2015b. Combined positron emission tomography and computed tomography to visualize and quantify fluid flow in sedimentary rocks. *Water Resources Research,* 51**,** 7811-7819.

FERNØ, M. A. 2015. Does foam work in fractured systems? *Complex Fluids in Porous Media.* Bordeaux, France.

FIROOZABADI, A. & HAUGE, J. 1990. Capillary Pressure in Fractured Porous Media (includes associated papers 21892 and 22212). *Journal of Petroleum Technology,* 42**,** 784-791.

HALDAR, S. K. 2013. *Introduction to Mineralogy and Petrology,* Saint Louis, UNITED STATES, Elsevier Science.

HAUGEN, Å., FERNØ, M. A., GRAUE, A. & BERTIN, H. J. 2012. Experimental study of foam flow in fractured oil-wet limestone for enhanced oil recovery. *SPE Reservoir Evaluation & Engineering,* 15**,** 218-228.

HICKS JR, P. J. 1996. X-ray computer-assisted tomography for laboratory core studies. *Journal of Petroleum Technology,* 48**,** 1,120-1,122.

HIRASAKI, G. J. & LAWSON, J. B. 1985. Mechanisms of Foam Flow in Porous Media: Apparent Viscosity in Smooth Capillaries. *Society of Petroleum Engineers Journal,* 25**,** 176-190.

HOLDITCH, S. A. 2003. The increasing role of unconventional reservoirs in the future of the oil and gas business. *Journal of petroleum technology,* 55**,** 34-79.

HOMSY, G. M. 1987. Viscous fingering in porous media. *Annual review of fluid mechanics,* 19**,** 271-311.

HUBBERT, M. K. Nuclear energy and the fossil fuel. Drilling and production practice, 1956. American Petroleum Institute.

JOHANSEN, S. A. 2016. *An Experimental Study of Foam Flow in Fractured Systems of Increasing Size.* MSc, University of Bergen.

KAHROBAEI, S., BONNIEU, S. V. & FARAJZADEH, R. Experimental Study of Hysteresis Behavior of Foam in Porous Media. IOR 2017-19th European Symposium on Improved Oil Recovery, 2017 Stavanger, Norway.

KETCHAM, R. A. & CARLSON, W. D. 2001. Acquisition, optimization and interpretation of X-ray computed tomographic imagery: applications to the geosciences. *Computers & Geosciences,* 27**,** 381-400.

KHATIB, Z. I., HIRASAKI, G. J. & FALLS, A. H. 1988. Effects of Capillary Pressure on Coalescence and Phase Mobilities in Foams Flowing Through Porous Media. *SPE Reservoir Engineering,* 3**,** 919-926.

KOVSCEK, A., TRETHEWAY, D., PERSOFF, P. & RADKE, C. 1995. Foam flow through a transparent rough-walled rock fracture. *Journal of Petroleum Science and Engineering,* 13**,** 75-86.

LAKE, L. W. 2010. *Enhanced oil recovery,* Richardson, Tex Society of Petroleum Engineers

LIEN, J. R., JAKOBLSEN, M. & SKAUGE, A. 2011. *Introduksjon til petroleums- og prosessteknologi,* Universitet i Bergen.

LOTFOLLAHI, M., KIM, I., BEYGI, M. R., WORTHEN, A. J., HUH, C., JOHNSTON, K. P., WHEELER, M. F. & DICARLO, D. A. 2017. Foam Generation Hysteresis in Porous Media: Experiments and New Insights. *Transport in Porous Media,* 116**,** 687-703.

LYONS, W. C. & PLISGA, G. J. 2006. *Standard Handbook of Petroleum & Natural Gas Engineering*, Gulf Professional Publishing.

MARTINEZ, J. M. A. 1998. *Foam-Flow Behavior in Porous Media: Effects of Flow Regime and Porous-Medium Heterogeneity.* University of Texas.

MARTINS, A., LOURENCO, A., SA, C. & SILVA JR, V. Foam rheology characterization as a tool for predicting pressures while drilling offshore wells in UBD conditions. SPE/IADC drilling conference, 27 February-1 March 2001 Amsterdam, Netherlands. Society of Petroleum Engineers.

MAUČEC, M., DUSTERHOFT, R., RICKMAN, R., GIBSON, R., BUFFLER, A., STANKIEWICZ, M. & VAN HEERDEN, M. Dynamic Imaging of Fluid Mobility in Low-Permeability Matrices Using Positron Emission Tomography. Unconventional Resources Technology Conference, 2013 Denver, Colorado. Society of Exploration Geophysicists, American Association of Petroleum Geologists, Society of Petroleum Engineers, 1587-1596.

MELLOR, M. & HAWKES, I. 1971. Measurement of tensile strength by diametral compression of discs and annuli. *Engineering Geology,* 5**,** 173-225.

NELSON, R. 2001. *Geologic analysis of naturally fractured reservoirs*, Gulf Professional Publishing.

OMAMI, G., TAMIMI, D. & BRANSTETTER, B. F. 2014. Basic principles and applications of 18F-FDG-PET/CT in oral and maxillofacial imaging: A pictorial essay. *Imaging science in dentistry,* 44**,** 325-332.

OSTERLOH, W. T. & JANTE, M. J., JR. 1992. Effects of Gas and Liquid Velocity on Steady-State Foam Flow at High Temperature. *SPE/DOE Enhanced Oil Recovery Symposium.* Tulsa, Oklahoma: Society of Petroleum Engineers.

PANCHAROEN, M., FERNØ, M. A. & KOVSCEK, A. R. 2012. Modeling foam displacement in fractures. *Journal of Petroleum Science and Engineering,* 100**,** 50-58.

PATTON, J., HOLBROOK, S. & HSU, W. 1983. Rheology of mobility-control foams. *Society of Petroleum Engineers Journal,* 23**,** 456-460.

PRUD'HOMME, R. K. 1995. *Foams: Theory: Measurements: Applications*, CRC Press.

RANSOHOFF, T. & RADKE, C. 1988. Mechanisms of foam generation in glass-bead packs. *SPE reservoir engineering,* 3**,** 573-585.

REITSMA, S. & KUEPER, B. H. 1994. Laboratory measurement of capillary pressure-saturation relationships in a rock fracture. *Water Resources Research,* 30**,** 865-878.

ROEHL, P. O. & CHOQUETTE, P. W. 1985. *Carbonate petroleum reservoirs,* New York, Springer Science & Business Media.

ROMERO-ZERÓN, L. 2012. Advances in Enhanced Oil Recovery Processes. *Introduction to Enhanced Oil Recovery (EOR) Processes and Bioremediation of Oil-Contaminated Sites.* INTECH Open Access Publisher.

ROSSEN, W. R. 1990. Theory of mobilization pressure gradient of flowing foams in porous media: I. Incompressible foam. *Journal of Colloid and Interface Science,* 136**,** 1-16.

SANI, A. M., SHAH, S. N. & BALDWIN, L. Experimental investigation of Xanthan foam rheology. SPE Production and Operations Symposium, 24-27 March 2001 Oklahoma City, Oklahoma. Society of Petroleum Engineers.

SCHRAMM, L. L. 2000. *Surfactants : fundamentals and applications in the petroleum industry,* Cambridge, Cambridge University Press.

SEETHEPALLI, A., ADIBHATLA, B. & MOHANTY, K. K. 2004. Physicochemical interactions during surfactant flooding of fractured carbonate reservoirs. *SPE journal,* 9**,** 411-418.

SHENG, J. J. 2013. *Enhanced oil recovery : field case studies,* Waltham, Mass, Gulf Professional Publishing.

SOLBERG, P. 2017. *Polymer Enhanced Foams and Flow Regimes in Unconsolidated Sand.* MSc MsC, University of Bergen.

SPEIGHT, J. G. 2009. *Enhanced Recovery Methods for Heavy Oil and Tar Sands,* Houston, Texas, Gulf Publ. Co.

STEVENSON, P. 2011. *Foam engineering: fundamentals and applications,* Hoboken John Wiley & Sons.

TSANG, Y. 1989. On two-phase relative permeability and capillary pressure of rough-walled rock fractures. *Lawrence Berkeley National Laboratory*.

UREN, L. C. 1946. *Petroleum production engineering : oil field development,* New York, McGraw-Hill.

VAN GOLF-RACHT, T. D. 1982. *Fundamentals of fractured reservoir engineering,* Amsterdam, Netherland, Elsevier.

VASSHUS, S. 2016. *Experimental Study of Foam Generation and Flow in Carbonate Fracture Systems.* MSc, University of Bergen.

YAN, W., MILLER, C. A. & HIRASAKI, G. J. 2006. Foam sweep in fractures for enhanced oil recovery. *Colloids and Surfaces A: Physicochemical and Engineering Aspects,* 282–283**,** 348-359.

ZOLOTUKHIN, A. B. & URSIN, J.-R. 2000. *Introduction to petroleum reservoir engineering*, Norwegien Academic Press (HóyskoleForlaget).

Appendix A – Nomenclature

M	Mobility ratio
λ	Mobility
k_r	Relative permeability
µ	Viscosity
$µ^{app}$	Apparent viscosity
N_c	Capillary number
σ	Interfacial tension
u	Velocity
P	Pressure
ΔP	Pressure drop
∇P	Pressure gradient
L	Length
q	Flux
K	Absolute permeability
P_c	Capillary pressure
P_c^*	Limiting capillary pressure
ρ	Density
V	Volume
w	Weight
r	Radius
f_g	Gas fraction
f_g^*	Gas fraction dividing strong-foam and weak-foam region
wt%	Weight percent
$t_{1/2}$	Half-life

Appendix B – Abbreviations

MRF	Mobility reduction factor
SAG	Surfactant alternating gas
PET	Positron Emission Tomography
FDG	^{18}F-fluorodeoxyglucose
CT	X-ray Computed Tomography
UoB	University of Bergen
HuH	Haukeland university Hospital
MIC	Molecular Imaging Center
IFT	Institute of Physics and Technology
EOR	Enhanced Oil Recovery
FV	Fracture volume
ROI	Region of Interest
WAG	Water Alternating Gas

Appendix C - Uncertainty calculations

Measurements and calculated measurements, y, in this thesis is generally a function of different measurements $x_1, x_2, x_3, \ldots, x_i$ with an uncertainty $\delta_{x_1}, \delta_{x_2}, \delta_{x_3} \ldots, \delta_{x_i}$ which gives:

$$y = f(x_1, x_2, x_3, \ldots, x_i)$$

Calculating mean value with uncertainty:

For a dataset containing the measured values $x_1, x_2, x_3, \ldots, x_N$ the mean value $\bar{x}$ can be calculated by:

$$\bar{x} = \frac{(x_1 + x_2 + x_3 \pm \cdots + x_N)}{N} = \frac{1}{N} \sum_{i=1}^{N} x_i \qquad (A1)$$

Where N is the number of measurements.

From the dataset which the mean, $\bar{x}$, is calculated the standard deviation $\sigma_{\bar{x}}$, can be calculated as:

$$\sigma_{\bar{x}} = \sqrt{\frac{1}{N-1} \sum_{i=1}^{N} (x_i - \bar{x})^2} \qquad (A2)$$

From the standard deviation the uncertainty, δx, of the mean can be calculated:

$$\delta x = \sigma_{\bar{x}} = \frac{1}{\sqrt{N}} \sigma_x = \sqrt{\frac{1}{N(N-1)} \sum_{i=1}^{N} (x_i - \bar{x})^2} \qquad (A3)$$

The final value with uncertainty then becomes:

$$y = \bar{x} \pm \delta x \qquad (A4)$$

Uncertainty of adding and subtracting:

When a value R is calculated by adding or subtracting independent values $x, y, z, \ldots, i$ where each independent value has a known uncertainty $S_x, S_y, S_z, \ldots, S_i$ then the uncertainty for the calculated value R, denoted S_R, can be calculated by:

$$S_R = \sqrt{\left(\frac{\delta R}{\delta x} S_x\right)^2 + \left(\frac{\delta R}{\delta y} S_y\right)^2 + \left(\frac{\delta R}{\delta z} S_z\right)^2 + \cdots + \left(\frac{\delta R}{\delta i} S_i\right)^2} \qquad (A5)$$

By partially deriving equation (A5) with respect to $x, y, z, \ldots, i$ the result is the simplified version:

$$S_R = \sqrt{(S_x)^2 + \left(S_y\right)^2 + (S_z)^2 + \cdots + (S_i)^2} \qquad (A6)$$

Calculating the uncertainty of quotient or product:

If a value R is calculated as either a quotient or product of independent values $a^2 x, b^2 y, c^2 z, \ldots, n^2 i$, given that $a, b, c, \ldots, n$ are constants and $x, y, z, .., i$ are independent variables, where each independent variable has a known uncertainty $S_x, S_y, S_z, \ldots, S_i$ then the uncertainty of the calculated value R, denoted S_R, is calculated by the following formula:

$$\frac{S_R}{R} = \sqrt{\left(a\frac{S_x}{x}\right)^2 + \left(a\frac{S_y}{y}\right)^2 + \left(a\frac{S_z}{z}\right)^2 + \cdots + \left(a\frac{S_i}{i}\right)^2} \qquad (A8)$$

An overview of the known uncertainties in this experiment can be seen in Table 0-1.

Table 0-1: Instrumental uncertainties provided by the manufacture of the instruments.

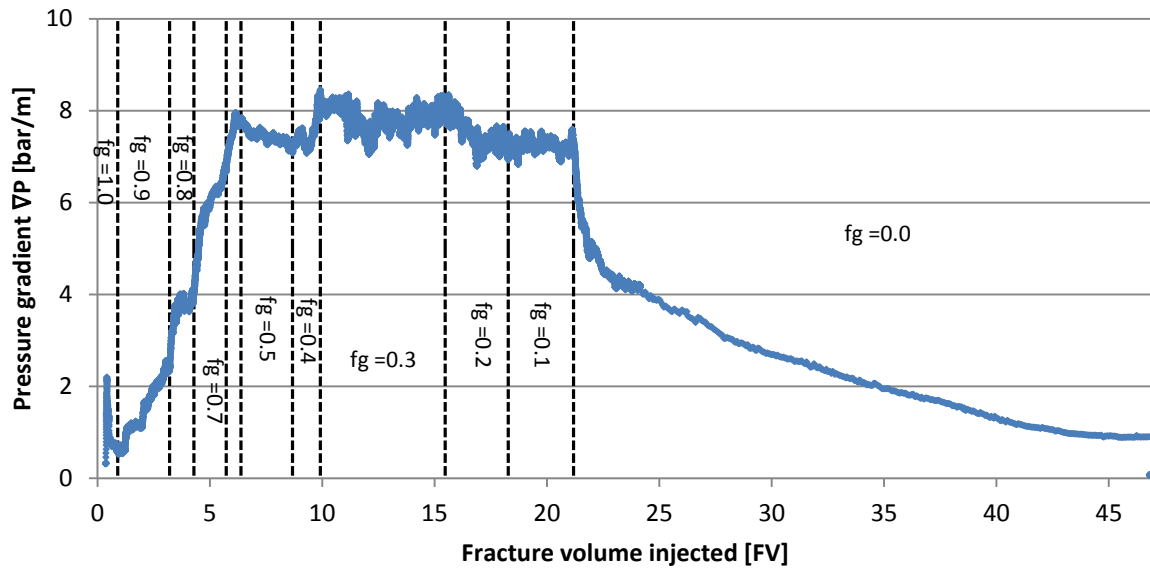| Instrument	Parameter	Uncertainty	Unit
Pressure transducer	Pressure	±0.01	bar
Mass flow controller	Volume	±0.02	ml/min
Pump	Volume	±1ml/h or 0.15% of rate	ml/h
Weight	Mass	±0.01	Gram
Caliper	Length	±0.02	mm

Appendix D - Experimental results

Figure 0-1: Differential pressure with varying gas fraction during a foam experiment on core 1.5i-4. The foam experiment was done by co-injection of surfactant and N2 gas at a constant volumetric rate of 10ml/h. Core 1.5i-4 had a tight fracture with permeability 0.1D. This plot is equal to Figure 11-10 except that it show the complete tail production.
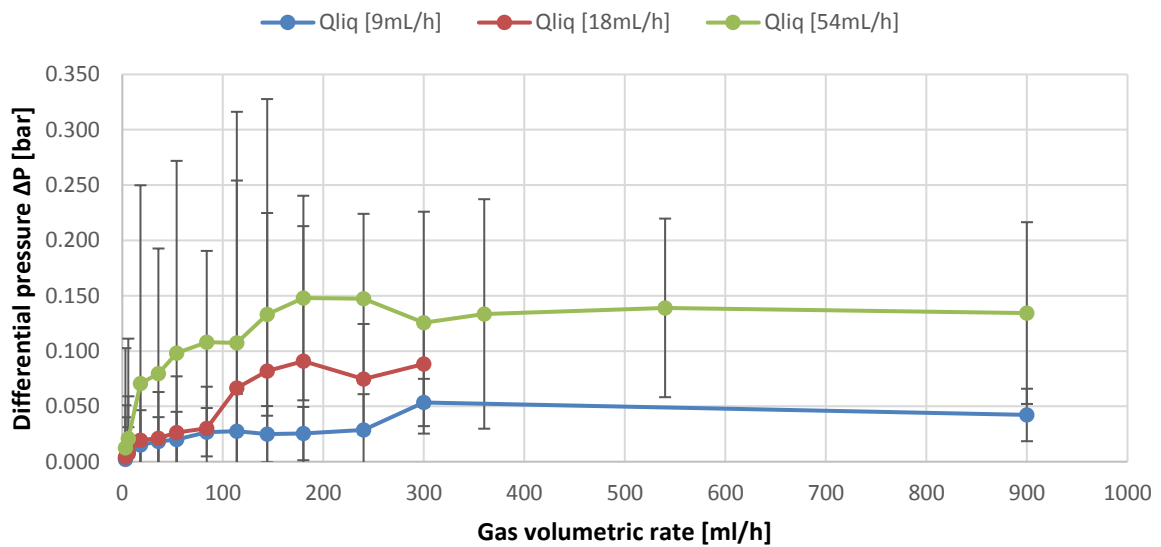

Figure 0-2: The differential pressure measured at constant liquid rate with increasing gas rate. This plot is the raw, and un-altered data behind Figure 11-3 and Figure 11-4.
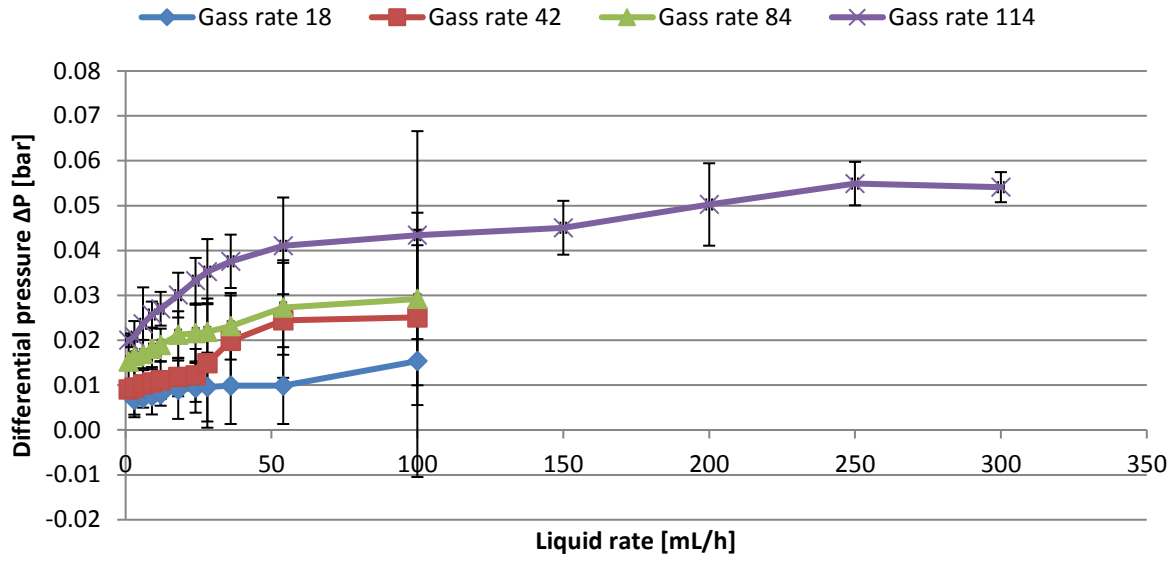
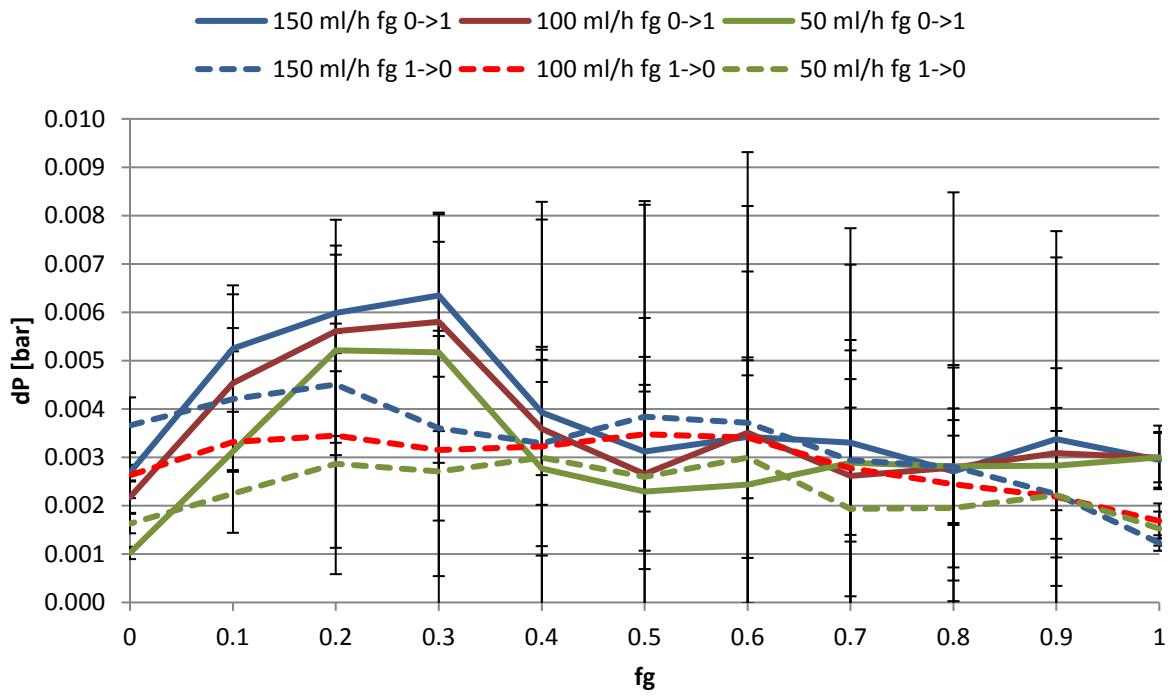**Figure 0-3: Increasing liquid rate at constant gas rate. Conducted on core 2i-3**

Figure 0-4: Differential pressure measured for baseline in smooth fractures. Conducted on core 2i-4
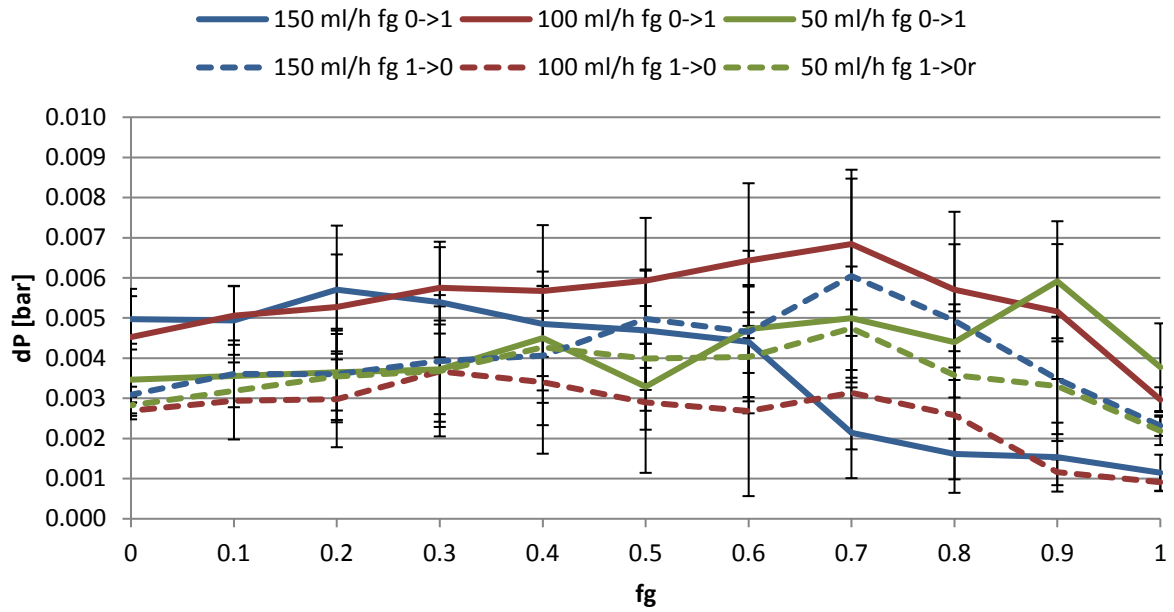
Figure 0-5: Differential pressure measured for foam experiment in smooth fractures. Conducted on core 2i-4
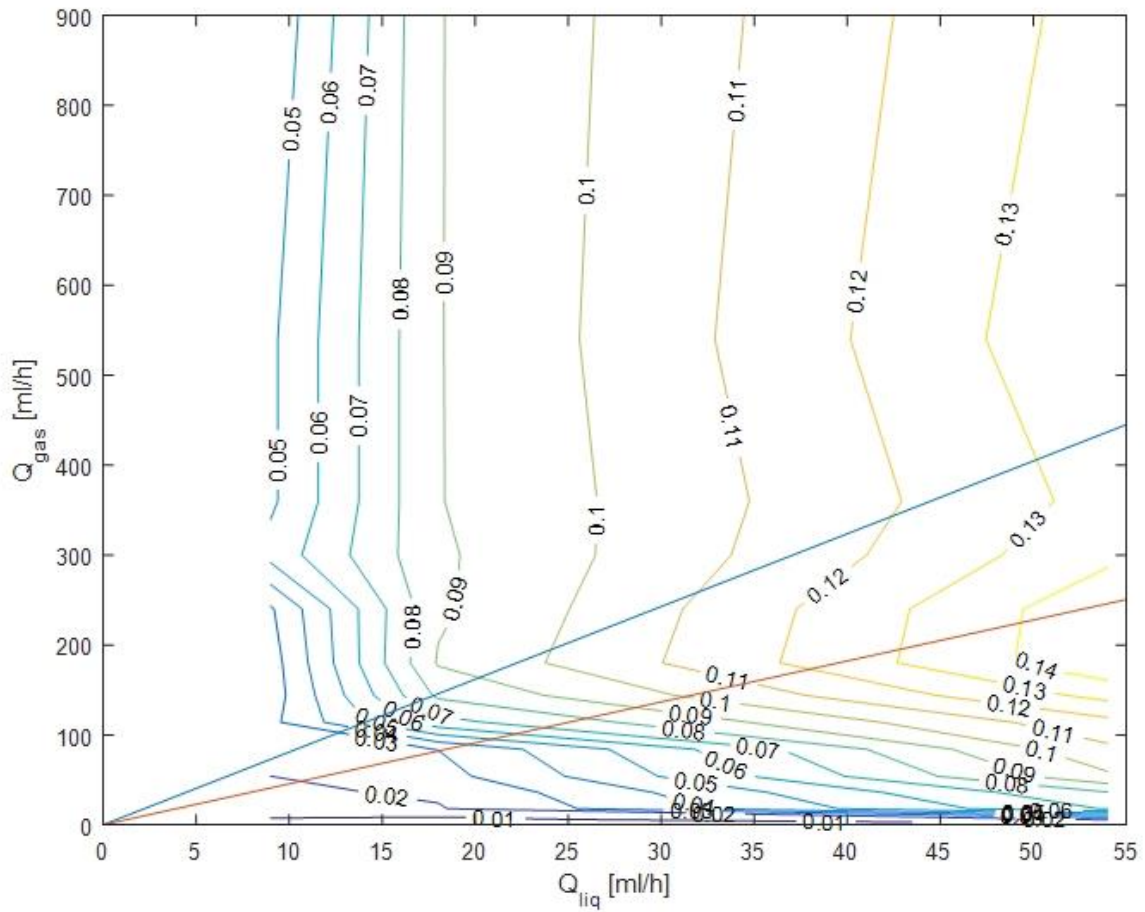

Figure 0-6: Same contour plot as in section 11.2 but it starts in liquid rate 0

100